Christoph Url, BSc

Eco-friendly routing based on current air quality sensor data

MASTER'S THESIS

to achieve the university degree of

Master of Science

Master's degree programme: Geospatial Technologies

submitted to

Graz University of Technology

Supervisor

Ass.Prof. Dipl.-Ing. (FH) Dr.techn. Johannes Scholz

Institute of Geodesy

Graz, December 2019

AFFIDAVIT

I declare that I have authored this thesis independently, that I have not used other than the declared sources/resources, and that I have explicitly indicated all material which has been quoted either literally or by content from the sources used. The text document uploaded to TUGRAZonline is identical to the present master‘s thesis.

Date

Signature

Abstract

Nowadays, almost every major city has to deal with air pollution. One of the main causes is the transport sector, which is increasing from year to year. In addition to pollutants, this sector also contributes significantly to greenhouse gases, with CO_2 taking over the largest share. A solution to alleviate this problem is offered by the environmentally friendly routing approach, which does not search for the fastest or shortest route, but for the most fuel-efficient one. In the present thesis, an eco-friendly routing based on the GIP (Graphenintegrations-Plattform) data is carried out. For this purpose, theoretical foundations are first determined from the literature in order to implement them in a routing experiment. On the basis of the driving dynamics and the elaborated essential road, vehicle, and traffic characteristics an eco-routing model is created and subsequently implemented for the city of Graz using an A-star algorithm.

The aim of the model is that the route does not lead through areas with high air pollution. On this account, current pollutant data are integrated into the routing with the focus on the particular matter (PM) pollutant. For this purpose, both data from fixed measuring stations and simulated data from air quality sensors of vehicles, which measure the pollutants directly on the road, transmit standardized observations to a web server. These data are queried before each routing to determine the current pollution on the roads. By using an air quality index, these measurements are evaluated and weighted corresponding to the pollution. The differences between the routes according to time, distance, fuel consumption and CO_2 are illustrated using several scenarios. Furthermore, the effects of the implementation of the PM values are shown, thereby the routes lead around the areas with high pollution. It should be emphasized that the weighting of the PM values plays an essential role, since if the values are too low, areas with high pollution are still traversed and the routes become uneconomic if the weighting is too high. By means of various hotspot analyses it is indicated how far the routes are from the focus of the pollution, taking into account and without taking into account the PM values.

Zusammenfassung

Heutzutage hat nahezu jede größere Stadt mit den Problemen der Luftverschmutzung zu kämpfen. Eine der Hauptursachen dafür ist der von Jahr zu Jahr wachsende Verkehrssektor. Neben den Schadstoffen trägt dieser Sektor erheblich zu den Treibhausgasen bei, wobei CO_2 den größten Anteil übernimmt. Einen Lösungsansatz zur Minderung dieses Problems, bietet das umweltfreundliche Routing, bei dem nicht die schnellste oder kürzeste, sondern die energieeffizienteste Route ermittelt wird. In der vorliegenden Arbeit wird ein umweltfreundliches Routing auf Basis der GIP (Graphenintegrations-Plattform) - Daten durchgeführt. Hierfür werden zunächst theoretische Grundlagen aus der Literatur ermittelt, um diese in einem Routing-Experiment umsetzen zu können. Auf der Grundlage der Fahrdynamik und der ausgearbeiteten wesentlichen Straßen-, Fahrzeug- und Verkehrseigenschaften wird ein Eco-Routing-Modell erstellt und in weiterer Folge für die Stadt Graz mittels A-Stern-Algorithmus umgesetzt.

Ziel des Modells ist es, dass die Routen nicht durch Gebiete mit hoher Luftverschmutzung durchgeführt werden. Aus diesem Grund werden aktuelle Schadstoffdaten in das Routing einbezogen, mit dem Fokus Feinstaub PM. Zu diesem Zweck übermitteln sowohl Daten von fixen Messstationen als auch simulierte Daten von Luftgütesensoren von Fahrzeugen, die die Schadstoffe direkt auf der Straße messen, standardisierte Beobachtungen an einen Webserver. Diese Daten werden vor jedem Routing abgefragt, um die aktuelle Luftqualität der Straßen ermitteln zu können. Unter Anwendung eines Luftqualitätsindex werden diese Messungen ausgewertet und gewichtet. Die Unterschiede zwischen den Routen nach Zeit, Entfernung, Kraftstoffverbrauch und CO_2 werden anhand mehrerer Szenarien ermittelt. Darüber hinaus werden die Auswirkungen der Implementierung der PM-Werte näher erläutert, wenn Routen durch Gebiete mit hoher Verschmutzung umfahren werden. Ein Augenmerk liegt auf der speziellen Rolle der Gewichtung der PM-Werte, da bei zu geringen Werten stark belastete Gebiete durchfahren und bei zu hoher Gewichtung die Routen unwirtschaftlich werden. Anhand verschiedener Hotspot-Analysen wird veranschaulicht, wie weit die Routen unter Berücksichtigung und ohne Berücksichtigung der Schadstoffwerte vom Verschmutzungsschwerpunkt entfernt sind.

Acknowledgements

With the following lines I would like to thank all those who have supported and motivated me during this thesis.

My special thanks go to Ass.Prof. Dipl.-Ing.(FH) Dr.Techn. Johannes Scholz from the Institute of Geodesy, for the supervision of this thesis and the numerous discussions. Thank you for the content support, the constructive feedback and the scientific inputs.

I would also like to thank Mag. Andreas Schopper from the State of Styria (Air Pollution Control Unit) for the additional information and assistance regarding particulate matter in the city of Graz.

A big thank you also applies to my friends and fellow students who motivated me and brought me to other thoughts. You made my student days to an unforgettable time.

Finally, I would like to express my special thanks to my parents, brother and close family members who have given me backing and invaluable support for the whole academic studies. Your patience, mental support and motivating words helped me to achieve my goals. Thanks a lot!

Contents

List of Figures

List of Tables

List of Abbreviations

ADAC	Allgemeine Deutsche Automobil-Club
API	Application Programming Interface
CAN	Controller Area Network
CAQI	Common Air Quality Index
CO	Carbon Monoxide
CO_x	Various Carbonyl Compounds
CO_2	Carbon Dioxide
CS_2	Carbon Disulphide
C_6H_6	Benzene
C_6H_{14}	Hexane
C_7H_{16}	Heptane
ECU	Electronic Control Unit
EEA	European Economic Area
EPA	Environmental Protection Agency
EPSG	European Petroleum Survey Group Geodesy
EU	European Union
GHG	Greenhouse Gas
GIP	Graphenintegrations-Plattform
HC	Hydrocarbon
HTTP	Hypertext Transfer Protocol
H_2S	Hydrogen Sulphide
IRI	International Roughness Index
NEDC	New European Driving Cycle

NO	Nitric Oxide
NO_x	Nitrogen Oxide
NO_2	Nitrogen Dioxide
OGC	Open Geospatial Consortium
O&M	Observations & Measurements
ORS	OpenRouteService
OSM	OpenStreetMap
O_3	Ozone
PM	Particulate Matter
RMS	Route Mean Square
SensorML	Sensor Model Language
SOS	Sensor Observation Service
SO_x	Sulphur Oxide
SO_2	Sulphur Dioxide
SWE	Sensor Web Enablement
VOC	Volatile Organic Compounds
WGS-84	World Geodetic System 1984
WHO	World Health Organization
WLTP	World Harmonized Light Vehicle Test Procedure
XML	Extensible Markup Language

Chapter 1

Introduction

"Air pollution represents the biggest environmental risk to health" (World Health Organization, 2016, p. 15). Every year, approximately 4.2 million people worldwide die from heart disease, lung cancer, strokes, lung disease and respiratory problems caused by poor air pollution (World Health Organization, n.d.c). One of the main causes of the threat to human health is road traffic, which in addition to harming people also damages the environment (Transport & Environment, n.d.). Moreover to pollutants, vehicles cause greenhouse gas (GHG) emissions, of which CO_2 is the most important source (Umweltbundesamt, n.d.e). Air pollution limits have been determined within the EU, but above all the urban population is affected by exceedances of the limit values, which are particularly caused by passenger cars and delivery vans (Transport & Environment, n.d.). Diesel and petrol vehicles make up the largest share of passenger cars, with diesel vehicles producing fewer GHGs due to their lower fuel consumption, whereas petrol vehicles spread fewer air pollutants. Alternative drive systems and fuels such as biomass, hydrogen, electricity are on the rise, but the processes are not yet fully developed (Umweltbundesamt, n.d.b).

Based on sustainable and smart technologies, cities are trying to counteract the problems of the future. These technologies are usually associated with high investment and expenditure of time. One solution that does not require many additional resources and can therefore be implemented without high costs and time, is eco-friendly routing. Eco-friendly routing does not consider the shortest or fastest route but the most environmentally friendly. Different aspects of eco-friendly routing are considered in the literature. In most cases, the route with the lowest CO_2 emissions is to be determined. In addition, the route with the lowest fuel consumption or pollutants is also detected.

Air quality in cities is monitored using a wide variety of air quality sensors, which can be mobile or stationary. On the basis of air quality indexes, it is possible to assess the air quality in order to make statements about which limit values apply to good or bad air. In the meantime, vehicles already have such sensors so that when the outside air is bad, the fresh air flaps are closed and no more air is drawn in from the outside (Gevatter &

Grünhaupt, 2006).

As part of the master's thesis, simulated data are generated to determine the current air quality on the roads. Based on these data, roads with good and poor air quality are evaluated. Furthermore, an eco-friendly routing is performed, which is linked to the evaluations of air quality. Thus, several scenarios are developed in which pollution-free routes are carried out on roads with good air quality. The use case is to be treated in Graz.

1.1 Scientific issues and goals of the thesis

Because traffic produces greenhouse gases as well as pollutants, CO_2 is considered on the one side and PM on the other. CO_2 is taken into account when creating the environmentally friendly route, as this is directly related to fuel consumption. The city of Graz has to deal with particulate matter problems and that's why the work is focused on the PM areas.

The influences of fuel consumption and CO_2 on the vehicle, road and traffic characteristics is considered. In particular, the intersections and turning behaviour are also be taken into account. Before an own model is to be created, other eco-friendly routing models from the literature are presented. In addition, the driving dynamics are also discussed, with particular attention being paid to driving resistance. Based on these factors, a model is developed in which the fuel consumption and the CO_2 is minimal. The model is applied to the road network of Graz.

One further point which is considered is the air quality in Graz. With the help of the measuring stations, current PM data are simulated and a separate air quality index is created. Using the index, nearly each edge in the road network of Graz is assigned a value about the air pollution. All this data are sent to a server using the SOS standard from OGC and are queried in a standardized manner.

Finally, the eco-routing model is combined with the result of air quality. The aim is to avoid routes through areas of poor air quality in order not to cause even higher air pollution there. Therefore, routes are only developed through areas with good air quality.

Based on these assumptions, a research question compares the shortest, fastest and most environmentally friendly route. The parameter distance, time, fuel consumption and CO_2 are considered. The first research question is therefore:

- What are the significant differences between shortest, fastest routes

(distance, time, CO_2, fuel consumption) and eco-friendly routes?

The second research question is dealing with the areas of air pollution and is directed to the following question:

- Is it possible to calculate (near) real-time eco-friendly routes based on air quality sensor measurements, avoiding currently air-polluted areas?

Additional, the effects of these eco-friendly routes are also examined, as traffic is diverted from currently polluted areas to areas with less air pollution. What are the effects of that traffic "re-routing"?

1.2 Methodical approach

In the first step, the focus is on literature research. The mainly factors, which are essential for an eco-friendly routing, are determined. A model is developed based on driving resistance and the influences of road, traffic and vehicle characteristics on fuel consumption and the greenhouse gas CO_2. So that the main goal of the routing, which is a minimum of fuel consumption and CO_2, can be reached. Data needed for the model are a road network with turning behaviour, locations and type of intersections of Graz and district boundaries of Styria. In the next step, it is necessary to combine the calculated model with the road network of Graz. According to the previous terms, each edge of the network gets a value. This value presents the cost, which emits a vehicle of pollutants on this edge.

Furthermore, it is identified which roads in Graz have a good or a poor air quality. For this purpose, it is necessary to declare the current air quality on each edge. With the aid of the measuring stations, comprehensive data can be generated by interpolation. In order to understand better the pollutant concentrations, it is necessary to develop an air quality index. Compared to other evidence from the literature, a suitable index is created for Graz. Using the SOS, the data can be integrated into the routing. Finally, the current air quality and the exhaust pollutants of the vehicles are weighted in the road network. According to this evaluation, the shortest path algorithm A-star is used. In total, three scenarios with different air quality data are developed to answer the research questions. In order to better emphasize the differences between the routes, hotspot analyses are carried out. Furthermore, an attempt is made to compare the results obtained with other approaches.

The following diagram (Figure 1.1) gives a rough overview of the most important workflows, which were previously mentioned.

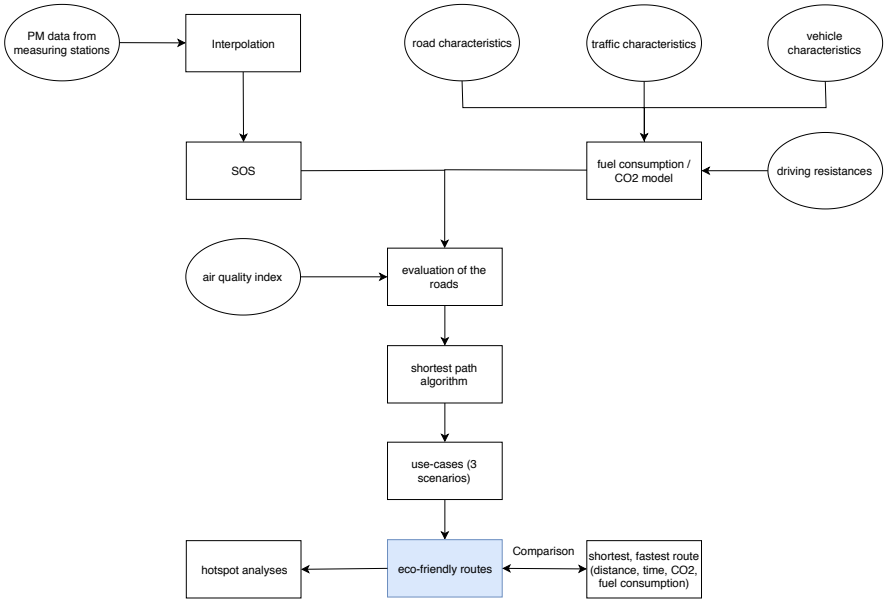

Figure 1.1: Workflow of the thesis

1.3 Literature survey

The following chapter gives a small selection of the literature used in this thesis, with a brief look at the most important topics. In general, the sources of literature mainly refer to papers on which chapter 2 is particularly based.

In most of these, a wide variety of CO_2 models are created, which are finally used for an eco-friendly routing. These models take into account a wide variety of factors. Pandian, Gokhale, and Ghoshal give a good review of the key characteristics that affect the emission rates of a vehicle. These factors include road characteristics, traffic characteristics and vehicle characteristics. Road characteristics include, for example, traffic junctions or intersections. The traffic density or the queue length are among the traffic properties. Vehicle characteristics, such as vehicle age, fuel types or engine types, additionally affect CO_2 emissions. Fontaras, Zacharof, and Ciuffo provide another good overview of the various factors that influence fuel consumption and CO_2 emissions of vehicles in Europe. Among other things, these compare the analyses carried out in the laboratory with those under real conditions.

- Pandian, S., Gokhale, S., & Ghoshal, A. K. (2009). Evaluating effects of traffic and vehicle characteristics on vehicular emissions near

traffic intersections. Transportation Research Part D: Transport and Environment, 14, 180-196. https://doi.org/10.1016/j.trd.2008.12.001

- Fontaras, G., Zacharof, N.-G., & Ciuffo, B. (2017). Fuel consumption and CO2 emissions from passenger cars in Europe – Laboratory versus real-world emissions. Progress in Energy and Combustion Science, 60, 97–131. https://doi.org/10.1016/j.pecs.2016.12.004

Technical backgrounds, which lead from the calculation of driving resistance to the track-specific fuel consumption, are evident in the following papers:

- Ersoy, M., & Gies, S. (2017). Fahrwerkhandbuch: Grundlagen - Fahrdynamik - Fahrverhalten - Komponenten - Elektronische Systeme - Fahrerassistenz - Autonomes Fahren - Perspektiven (5. Auflage). Wiesbaden: Springer Fachmedien Wiesbaden.
- Haken, K.-L. (2011). Grundlagen der Kraftfahrzeugtechnik: Mit 36 Tabellen sowie 20 Übungsaufgaben (2., aktualisierte und erw. Aufl.). Fahrzeugtechnik. München: Hanser. Retrieved from `http://www.hanser-elibrary.com/isbn/9783446426047`

An important point of the topic is the development of an air quality index, which is suitable for the city of Graz. The literature describes several approaches to calculating indices that differ depending on the considered pollutants or the raw data. The two papers by Ramos et al. and Plaia & Ruggieri present a variety of methods for calculating the air quality index. Shooter and Brimblecombe give on the one hand a good overview of the definition of an air quality index and on the other hand they mention the reasons for creating an index.

Since 2006 the CAQI (Common Air Quality Index) exists in Europe, which was developed to compare the air pollution in the cities of Europe. The index is divided into a roadside index and a background index, which are calculated hourly, daily and annually to make cities more comparable (van den Elshout, 2012) The pollution load in Austria is processed by the ZAMG (Zentralanstalt für Meteorologie und Geodynamik), which also refers to the CAQI (Umweltbundesamt, n.d.h). Further topics about the CAQI can be found in the following papers:

- Van den Elshout, S. (2012). CAQI Air quality index: Comparing Urban Air Quality across Borders - 2012.

- Van den Elshout, S., Léger, K., & Heich, H. (2014). Caqi Common Air Quality Index–update with PM(2.5) and sensitivity analysis. The Science of the Total Environment, 488-489, 461–468. https://doi.org/10.1016/j.scitotenv.2013.10.060

In literature, the CO_2 models are subdivided into macroscopic, mesoscopic or microscopic models, depending on the level of detail of the model. The models presented in the thesis are based on the following sources:

- Elbassuoni, S., & Abdel-sRahim, A. (2013). Modeling Fuel Consumption And Emissions At Signalized Intersection Approaches: A Synthesis Of Data Sources And Analysis Tools. 54th Annual Transportation Research Forum, Annapolis, Maryland, March 21-23, 2013. (206953).
- Faris, W. F., Rakha, H. A., Kafafy, R. I., Idres, M., & Elmoselhy, S. (2011). Vehicle Fuel Consumption and Emission Modelling: An In-Depth Literature Review. International Journal of Vehicle Systems Modelling and Testing, 6(3/4), 318–395.
- Yue, H. (2008). Mesoscopic fuel consumption and emission modeling (Doctor thesis). Virginia Polytechnic Institute and State University, Blacksburg, USA. Retrieved from `https://www.researchgate.net/publication/228999987_Mesoscopic_fuel_consumption_and_emission_modeling`

Chapter 2

Theoretical Part

This chapter contains the most important theoretical foundations which are relevant for the thesis. First, an insight into the emissions and pollutants caused by the vehicles is given. Furthermore, the most important factors that influence fuel consumption are mentioned. Since the model for calculating fuel consumption is based on driving dynamics, especially on driving resistance, these are considered in more detail. The main facts about air quality, CAN-Bus, SOS and air quality indexes are dealt with. In addition, an overview of the existing eco-friendly routing models is presented.

2.1 Exhaust emissions of vehicles

The following section describes in more detail the pollutants and emissions caused by vehicles. In particular, the spatial distribution and development of the greenhouse gas CO_2 and the pollutant PM are discussed.

On the one hand, GHGs are enormously increasing climate change and the resulting extreme weather events and weather anomalies, and on the other hand, air pollutants are endangering human health (Umweltbundesamt, n.d.f; World Health Organization, n.d.a). One of the main causes of both emissions and pollutants is the transport sector (Umweltbundesamt, n.d.g; Umweltbundesamt, n.d.e). The pollutants and emissions are emitted by vehicles as exhausted gases. Although technological advances in the vehicle and fuel subjects have made improvements, increasing traffic and a growing number of miles driven offset the positive development (Umweltbundesamt, n.d.e). Among the most important emissions the vehicles emit include nitrogen oxides (NO_x), particulate matter (PM), volatile organic compounds (VOCs), carbon monoxide (CO) and sulphur dioxide (SO_2) (International Organization of Motor Vehicle Manufacturers [OICA], n.d.). The transport sector accounts for more than 50 % of NO_x emissions and has a strong impact (about 10 % or more) on the other air pollutants. In particular, road traffic causes significant emissions of all pollutants, with the exception of SO_x. The emissions from road traffic are mainly derived from the combustion of fuel. Non-exhaust emissions contribute to VOCs because

of fuel evaporation and PM due to brake- and tire wear and attrition (European Environment Agency, 2018).

In order to counteract the rising emissions, the EU has set the average CO_2 emissions at 130 g/km for new European passenger vehicles since 2012 and at 95 g/km for 2020 (Verordnung (EG) Nr. 443/2009 des Europäischen Parlaments und des Rates vom 23. April 2009 zur Festsetzung von Emissionsnormen für neue Personenkraftwagen im Rahmen des Gesamtkonzepts der Gemeinschaft zur Verringerung der CO2-Emissionen von Personenkraftwagen und leichten Nutzfahrzeugen, 2009). In Austria, the average CO_2 emission rates for new vehicles in 2017 were 120.7 g/km (Bundesministerium für Nachhaltigkeit und Tourismus, 2019). In order to be able to compare the fuel consumption and the CO_2 emission rates of vehicles, these are evaluated under standardized laboratory conditions (ÖAMTC, n.d.). The WLTP (World Harmonized Light Vehicle Test Procedure), which replaces the NEDC (New European Driving Cycle), has been in use mandatory since 1. September 2018 in the EU-28 (Porsche Austria GmbH & Co OG, n.d.b; Volkswagen AG, n.d.). Based on realistic test conditions, the WLTP provides more life-like information on fuel consumption and CO_2 emission rates, compared to the NEDC (Porsche Austria GmbH & Co OG, n.d.b). In addition, depending on the emission levels, the vehicles are divided into emission classes. The classes range from Euro 1 to Euro 6, with class 6 (since 2014) having the lowest and class 1 the highest exhaust pollutants (AllSecur Deutschland AG, n.d.).

2.1.1 Carbon dioxide

Carbon dioxide is the most important greenhouse gas, which accounts in 2015 for more than two thirds of total GHG emissions (International Energy Agency, 2018). The CO_2 emission levels are influenced by the factors fuel, distance covered, specific energy consumption of a vehicle and driving style. On the one hand improved technological developments, such as combustion technology, reduce the CO_2 emissions (for more information about the influence of vehicles on CO_2 see chapter 2.2). But on the other hand, an increase in weight and in performance of vehicles as well as additional equipment such as air conditioning systems lead to a rise in fuel consumption (Umweltbundesamt, n.d.e).

Due to these factors and a growing economic output, CO_2 emissions have increased significantly over the years. Overall, global CO_2 emissions from fuel combustion in 2016 were around 32.31 GtCO2. Compared to the early 1970s, the share has almost doubled and since 2000 it has even increased by 40 % (see figure 2.1). Around a quarter (24 %) of CO2 emissions from

2016 are attributable to the transport sector, which has increased by 71 % compared to 1990. Road traffic recorded the strongest absolute growth of +2.5 GtCO2, which is attributable to 74 % of road transport. However, the shares of emissions of the sub-sectors remained unchanged (see Figure 2.2) (International Energy Agency, 2018). A similar picture emerges for the greenhouse gases in Austria, where the transport sector is responsible for around 29 % of the total GHGs in 2016. About 99 % of this share is attributable to road traffic. For the distribution of CO_2 emissions by sector, no current data could be found, but these are with about 84 % of the main cause of greenhouse gases in Austria and therefore it can be assumed that the above mentioned values also approximately represent the CO_2 emissions (Anderl et al., 2018).

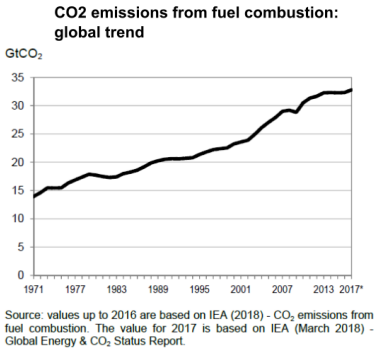

Figure 2.1: CO_2 emissions from fuel combustion: global trend 1971 to 2017 (International Energy Agency, 2018, p.9)

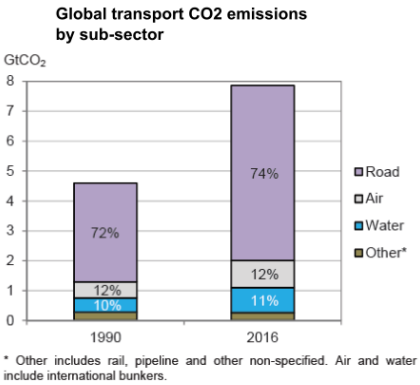

Figure 2.2: Global transport CO_2 emissions by sub-sector 1990 vs. 2016 (International Energy Agency, 2018, p.15)

2.1.2 Particulate matter

One of the most important pollutants in the air is particulate matter, which has the greatest impact on humans (Filip & Brezoczki, 2017; World Health Organization, n.d.b). According to the WHO, traffic in European cities accounts for around 30 % of particulate matter emissions (World Health Organization, n.d.a). PM consists of the integral part of sulphate, nitrates, ammonia, sodium chloride, black carbon, mineral dust and water. It contains of a mixture of liquid and solid particles of inorganic or organic substances that occur in the air (World Health Organization, n.d.b). The particles can be distinguished by size. The particulate matter PM10 consists of 50 % particles with a diameter of 10 μm, a lower proportion of larger particles and a higher proportion of smaller particles. Due to this size, the particles

can reach deep into the lungs and have negative effects on human health (Umweltbundesamt, n.d.c). Another subdivision is the particulate matter PM2.5, which consists of the subset of PM10. The particles are similar in composition to PM10 except that they have a diameter of 2.5 μm. These particles can even reach the alveoli (Umweltbundesamt, n.d.d). Especially particulate matter is produced by diesel vehicles (Umweltbundesamt, n.d.e).

Due to the decrease in national and international emissions, a reduction in pollutant transport and more favourable dispersion conditions, the particulate matter in Austria declined since the year 1990 (Umweltbundesamt, n.d.c). As shown in figure 2.3, the traffic causes about 18 % of the total PM10 (also for PM2.5), which is the main cause in metropolitan areas. In particular, the transport sector is experiencing the largest decline of around 37 % (55 % for PM2.5) because of improved technologies in the field of propulsion and exhaust aftertreatment (figure 2.4) (Buxbaum et al., 2018).

Due to the development of particulate diminution technologies for vehicles which reduce exhaust emissions, the importance of non-exhaust emissions has increased. The non-exhaust emissions share of PM2.5 of the EEA-33 countries in the road transport sector increased from 17 % in the year 2000 to 42 % in 2016. The proportion of PM10 also rise from 30 % to 60 % within those years (European Environment Agency, 2018).

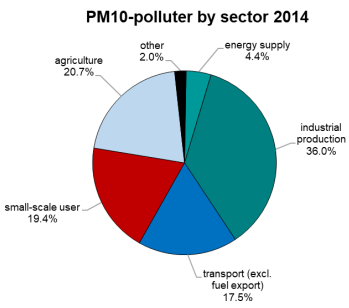

Figure 2.3: PM10 polluter in Austria by sector in 2014 (Buxbaum et al., 2018, p.12)

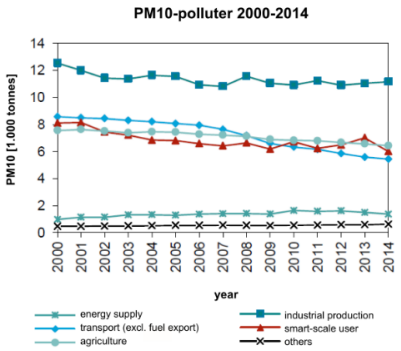

Figure 2.4: PM10 polluter from 2000 to 2014 in Austria (Buxbaum et al. ,2018, p.12)

2.2 Factors of influence

In principle, it is important to know which factors are responsible for high vehicle emissions and their fluctuations (Rouphail, Frey, Colyar, & Unal,

2001). Therefore, in the following chapter, the most important factors influencing fuel consumption and emissions are given for the vehicle, road and traffic sectors. The selection of the factors was made on the basis of the parameters found in the literature, which are necessary for the practical part (chapter 3). It should be mentioned that due to the complexity of weather conditions and individual driving behaviour, these were not explicitly dealt with.

2.2.1 Road characteristics

The characteristics morphology, road shape and road surface influence the world-wide CO_2 emissions, but none of them are described in vehicle certification tests. The morphology represents the geomorphological properties of the road. The road parameters include altitude, road shape, road grade and road surface, which greatly affect the fuel consumption of vehicles (Fontaras et al., 2017). At higher altitudes, aerodynamic resistance is lower due to lower air density, but fuel consumption will increase with curves and altitude differences (Pavlovic et al., 2016). The effects of curve analyses on fuel consumption, is not taken into account in this thesis, as they extend beyond the horizon and are not essential for the urban area. The road surface is characterized by structural requirement and building material (Pavlovic et al., 2016). The structural conditions distinguish between roughness and texture, with the building materials mostly being cement and asphalt (Fontaras et al., 2017). In the following paragraph the parameters road grade, road surface, road shape and speed are described in more detail.

Road grade

One of the most important factors for both fuel consumption and exhaust emissions from the vehicle is road grade. A vehicle uses more power when driving uphill than when driving in the plain, but it consumes the least when driving downhill (Fontaras et al., 2017). If road grades are not taken into account, it can lead to over or underestimating of the performance of the vehicles, whereby the emissions are evaluated imprecisely (Wyatt, Li, & Tate, 2014). Road grades have especially an influence on CO_2 emissions (Pavlovic et al., 2016).

Wyatt et al. conducted a study examining the effects of road grade on CO_2 emissions while assessing the sensitivity of emissions. They found that estimating emissions at the microscale level requires a road grade profile for every second of test data. It was also shown that when modelling emissions,

even a small proportion of non-compliance with the road grade is enough to achieve large inaccuracies in the estimation of emissions. Therefore, traffic management and urban planning projects should include the calculation of vehicle emissions in their analyses (Wyatt et al., 2014).

In a study in Naples (Italy), two Euro 5 diesel vehicles were used to determine the effects of road gradient on CO_2 and NO_x emissions using the Vehicle Specific Power (VSP) analysis. The research was conducted along a mixed route consisting of urban, extra-urban and highways. The results show that there is a linear correlation between road grade and CO_2 emissions from -4 to 5 % road grade, with the exception of flat routes. By contrast, the NO_x emissions are very much dependent on the vehicle and can be declared by the second-order polynomial equation (Costagliola, Costabile, & Prati, 2018).

A study by Park and Rakha depicts that fuel consumption increases by 9 % due to 1 % rise in road grade. The research was conducted for three traffic control scenarios using the INTEGRATION software. One scenario was driving at a constant speed, the second along a main road with stop signs and the third in network with traffic signals (Park & Rakha, 2006).

Furthermore, it should be noted that additional fuel consumption by driving uphill cannot be compensated by driving downhill. This means driving in hilly areas costs more power than in flat areas and should therefore be considered in every routing, so that the driver is prevented from steep roads (Boriboonsomsin & Barth, 2009; Fontaras et al., 2017). This thesis is also confirmed by Boriboonsomsin and Barth, which compared in a study a flat route with a hilly route. The results indicate that fuel consumption at hilly routes is 15 to 20 % higher than on flat routes and that from -2 to 2 % there is a linear correlation between road grade and fuel consumption (Boriboonsomsin & Barth, 2009; Pavlovic et al., 2016). Similar results were obtained in the study by Park and Rakha as well, which was mentioned before. The road grade yielded on average 4 %, reaching a maximum of 6 % (see figure 2.5) (Pavlovic et al., 2016).

Road surface

As mentioned before, the road surface is characterized by structural conditions and construction material. The following section gives an overview of the roughness and texture as well as the building materials cement and asphalt.

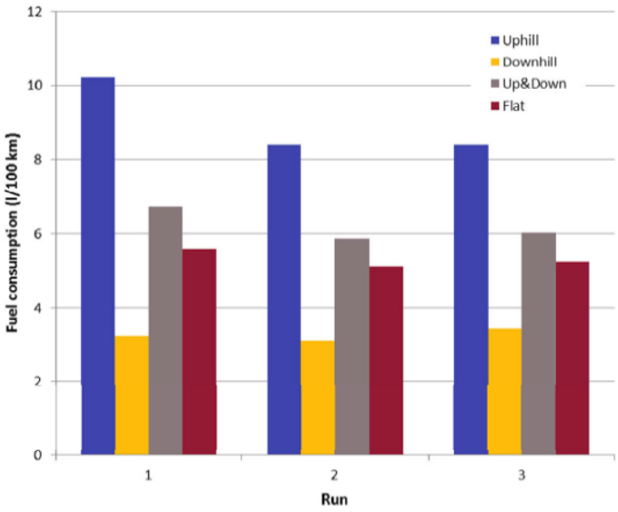

Figure 2.5: Fuel consumption for different routes depending on road grade (Pavlovic et al. ,2016, p.116)

Roughness Road roughness is determined as aberration from the vertical profile of a road surface, which affect the drive quality (Local Government & Municipal Knowledge Base, n.d.; Pavement Interactive, n.d.). In addition, the roughness has a significant influence on the noise, fuel consumption, dynamic pavement loading and vehicle dynamics (Beuving, Jonghe, Goos, Lindahl, & Stawiarski, 2004; Local Government & Municipal Knowledge Base, n.d.). Roughness is an important indicator of road condition assessment used for maintenance and reconstruction (Greene, Akbarian, Ulm, & Gregory, 2013). Roughness is measured by an index, the most commonly used one is the international roughness index IRI. The IRI is calculated based on the filtered ratio of the accumulated suspension motion of a generic vehicle (in mm, inches, etc.) and the distance the vehicle has covered (in m, km, etc.) (Pavement Interactive, n.d.). Values range mostly from 2 to 16 mm/m, with values of 2 high quality surfaces, such as airways or superhighways, while values above 12 mm/m of unpaved roads with depressions are mentioned. The most European streets have an IRI value between 3 and 7 mm/m (Fontaras et al., 2017).

According to a study by Ko et al., it was found that at a speed of 60 km/h and an IRI of 3.5 m/km the fuel consumption is lowest (Ko et al., 2009). The figure 2.6 represent the positive relationship between fuel consumption and IRI. It is obvious that an increase in the IRI from 2 m/km to 5 m/km also means an increase of 3 % of fuel consumption for a medium car (Greene et al., 2013).

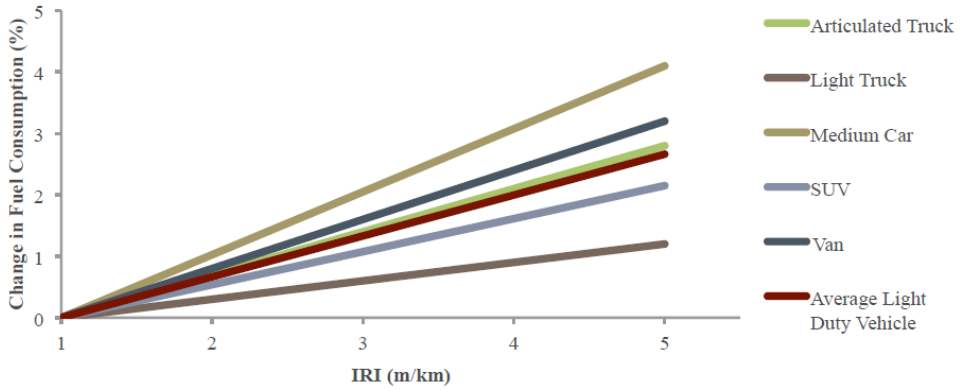

Figure 2.6: Dependence between road roughness and fuel consumption (Greene et al. ,2013, p.12)

Texture The condition of the road surface is determined by the texture, which influences driving comfort, traffic safety, quality of construction and road user costs. The road texture is determined as the vertical deviation from an even flat surface and is distinguished by wavelength (Aavik, Kaal, & Jentson, 2013). So the texture influences the correlation between tyre footprint and road surface (Fontaras et al., 2017). To render the texture depth measurement in a single value, the root mean square RMS is used (Lopez Arteaga, 2010). Depending on the size, the textures are divided into micro-, macro-, megatexture or unevenness. These have an influence on rolling resistance, friction, noise, tire wear, vehicle wear, ride quality and splash depending on the wavelength (Aavik et al., 2013). In general, the smaller the wavelengths, the better the effects are for the vehicles (Fontaras et al., 2017). The RMS has a linear relationship with the rolling resistance coefficient, where an increase in texture is accompanied by an increase in rolling resistance (Lopez Arteaga, 2010). Increasing textures by 0.5 mm results in an increase in rolling resistance of 10 % (Willis, Robbins, & Thompson, 2015). In addition, due to different textures the fuel consumption of the vehicles can be increased by up to 10 %.

For fuel economy, it is essential that the road surface offers a good condition regarding to roughness and texture. Therefore, it is important that the roads are constantly maintained. In addition, it should be noted that the roads should reduce traffic noise and should ensure driving safety and comfort (Beuving et al., 2004).

Construction Construction is responsible for the texture and roughness of the roads. In general, asphalt pavements consume less emissions than concrete roads for construction, operation and maintenance. However, these

only account for 2 to 5 % of total emissions, the remaining share being caused by road traffic. For road traffic, the differences between asphalt and concrete pavements are marginal. A study in the Netherlands has shown that at a speed of 90 km/h, fuel consumption is 2.7 % higher on concrete pavement than on asphalt (Beuving et al., 2004).

Road shape

Furthermore, the road shape plays an important role for the exhaust emissions and fuel consumption. Depending on the road class, different emission rates are achieved. The highest values are reached by local roads, since the vehicles in these have a high proportion in the acceleration mode with low speed (Nesamani & Subrahmanian, 2006). The different driving modes are described in chapter 2.2.2. Similar emission levels include arterial and sub-arterial roads, with the exception of NO_x. These are higher in arterial roads, presumably due to strong accelerations. CO_2 emissions also reflect high emissions in local roads, while lower ones in arterial roads (see figure 2.7). In addition, in the figure 2.7 the Indian Driving Cycle (IDC) is shown, which does not represent the real-world driving and is therefore not considered (Nesamani & Subrahmanian, 2006). Another study carried out by Rosqvist confirms these assumptions. In this study, roads in residential areas were examined and showed that lower emissions are produced on larger roads than on smaller ones (Rosqvist, 2007).

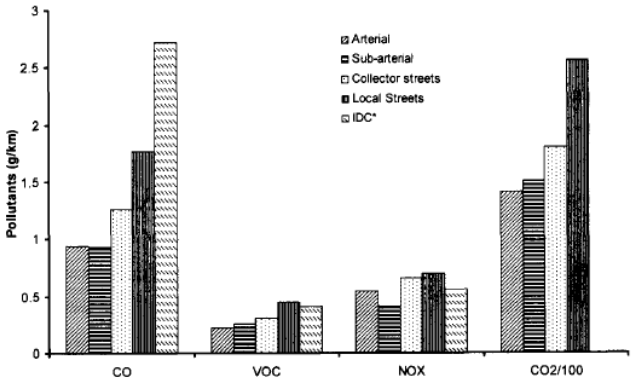

Figure 2.7: Emission rates for different road classes. *CO_2 emission rate is not estimated in the case IDC (Nesamani & Subrahmanian, 2006, p.24)

In addition, humps and junctions reduce fuel consumption and most emissions in residential areas. Especially the humps have an enormous impact, which have ten times the effect of junctions. The emission savings are equated when a vehicle drives 100 m in a residential street. Based on

the results it is shown that a driving pattern is developing at junctions and humps that reduces fuel and emissions. These theses are presented in the following figure 2.8 (Rosqvist, 2007).

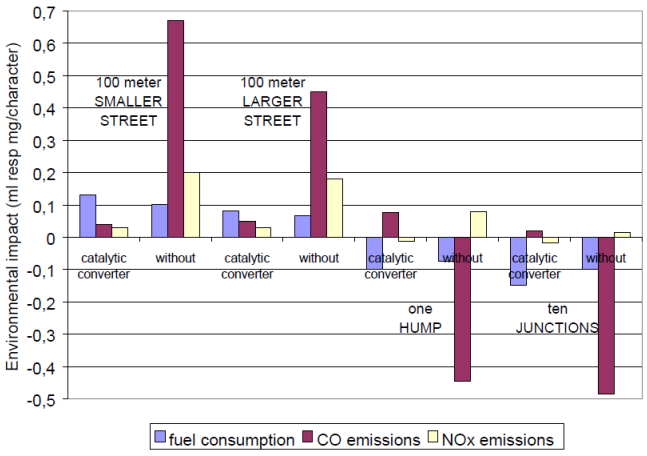

Figure 2.8: Influences of different road characteristics on fuel consumption and emissions CO,NO_x (Rosqvist, 2007, p.7)

Effects of the speed reduction equipment depend on the traffic intensity. A study in Sweden shows that at high traffic intensity, the lowest emissions could be achieved on major roads with humps at a speed of 50 km/h. On the other hand, the best results on semi-central roads could be achieved with high traffic intensity without humping at a speed of 30 km/h. Even by medium and low traffic on semi-central roads proved to be the best solution, a speed of 50 km/h without humps (Höglund & Niittymäki, 1999).

Another point to consider is the road intersection. Intersections reduce the constant flow of traffic and slow down the cruising speed. The longer the vehicle stops, the more fuel and emissions are consumed (Mandavilli, Russell, & Rys, 2003). More details about delays due to intersections can be found in chapter 2.2.2.

Studies have shown that roundabouts can reduce exhaust emissions and fuel consumption of vehicles compared to controlled intersections, depending on the traffic. Due to the improved traffic flow and the resulting reduced idle time, roundabouts offer these environmentally friendly advantages (Mandavilli et al., 2003). In the study by Várhelyi the use of roundabouts instead of signalized intersections decreased on average 29 % CO, 21 % NO_x and 28 % fuel consumption per vehicle. The influenced area concerns 100 m before the junction and 50 m beyond the junction. Moreover, the deceleration per vehicle is reduced on average by 11 seconds. Therefore roundabouts reduce not only emissions but also save time. In addition, the roundabouts

were compared with yield sign intersections, where roundabouts showed on average slightly higher emissions (CO increased by 4 %, NO_x by 6 % and fuel consumption by 3 %) (Várhelyi, 2002). The study by Mandavilli et al. also confirms that roundabouts significantly reduce emissions over stop controls. It was discovered that roundabouts especially in the afternoons and evenings, when there is more traffic than in the morning, have enormous positive influences. On average, CO are 42 % (21 %), CO_2 59 % (16 %), NO_x 48 % (20 %) and HC 65 %(18 %) lower than at stop controls (Mandavilli et al., 2003). The percentages in parenthesis represent the values in the morning.

However, on the other hand, another study by Kakooza, Luboobi, and Mugisha shows just the opposite in high traffic. It was found out that, roundabouts with high traffic volumes have disadvantages compared to signalized and non-signalized intersections. This disadvantage is due to the geometry of the intersections. The fact that the vehicles have to drive slower to overcome the intersection and then accelerate again, leads to problems at high arrival rate. In contrast, the vehicles only have to drive straight ahead at signalized or unsignalized intersections. The shortest waiting time could be achieved at signalled intersections. Due to the cyclic operation at signalized intersections, the traffic for each approach road is resolved at certain intervals with high traffic density. This inevitably leads to both fewer vehicles and less waiting time. On the other hand, at roundabouts or unsigned intersections, the vehicles cross the give-way line by random. For the light traffic, however, it has been shown that the roundabout has the least waiting times compared to signalized and unsignalized intersections (Kakooza, Luboobi, & Mugisha, 2005).

In summary, it can be explained that roundabouts have advantages, especially in light traffic conditions, however in the case of heavy traffic volume, this cannot always be clearly evaluated. In high traffic, signalized intersections are probably the best solution.

A precise statement on how intersections affect fuel consumption and emissions is relatively difficult to achieve, as each study focuses on different fields with different conditions and therefore provides different results. A study by Wu, Ci, Chu, and Zhang examined a distance of about 4.3 km, which included ten intersections, of which were nine signalized intersections and one a stop intersection. It was found that on average about 50 % of the fuel consumption is due to the intersections (Wu et al., 2015). Similar values were also obtained from the study of Dobre et al., which analysed only one intersection with traffic lights. A vehicle with 40 km/h approaches a traffic light, which will soon switch to red. On the one hand, a scenario was investigated in which a vehicle accelerates to get over the green traffic light, and on the other a scenario in which a vehicle slows down and waits

until the red traffic light turns to green. The CO_2 emissions for the first scenario were around 54 g of CO_2, for the second scenario around 96 g of CO_2. This means that CO_2 emissions are about 43 % higher for the second case, where the vehicle has to wait at the intersection (Dobre et al., 2012).

Speed-limit

Another important aspect concerns the cruising speed. Automotive engineers have proven that gas engines consume the lowest fuel at a speed of 50-70 km/h and petrol engines of 50-80 km/h. Figure 2.9 represents the relationship between fuel consumption and vehicle speed. The two green arrows limit the range of the optimal ratio between speed and fuel consumption. If the speed is lower or higher that the limits (green arrows), more fuel is consumed (Nasir, Md Noor, Kalam, & Masum, 2014). Due to the high fuel consumption in the acceleration mode (see chapter 2.2.2) and the enormous engine power at higher speeds, a parabolic shape of the curve results (Barth & Boriboonsomsin, 2009). Curve C illustrate the positive effects for fuel consumption of reduction aerodynamic resistance at higher speeds. The dot-dash line represents the relationship between fuel consumption and speed of electric and hybrid cars (Nasir et al., 2014).

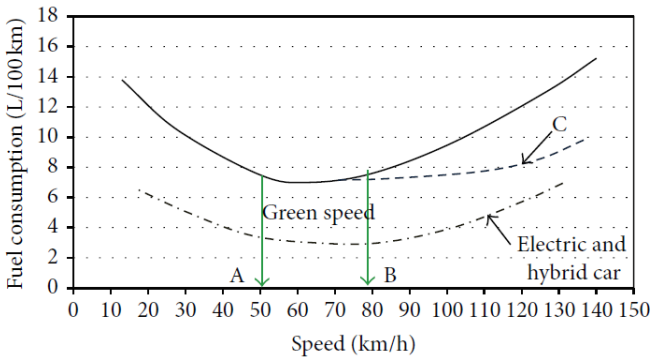

Figure 2.9: Influence of vehicle speed on the fuel consumption (Nasir et al., 2014, p.2)

The course of the curve for the relationship between exhausted emissions and speed looks the same as the fuel consumption. The study from Tong, Hung, and Cheung shows that the emissions CO, HC and NO_x as well as fuel consumption up to 70 km/h decrease as speed increases (see figure 2.10) (Tong et al., 2000). The CO_2 emissions also show a similar course of the curve (Schäfer & Basshuysen, 1995). For instance, instead of driving at 80 mph (∼130 km/h), a vehicle would travel 70 mph (∼110 km/h), reducing CO_2 emissions by up to 14 % (Commission for Integrated Transport, 2007).

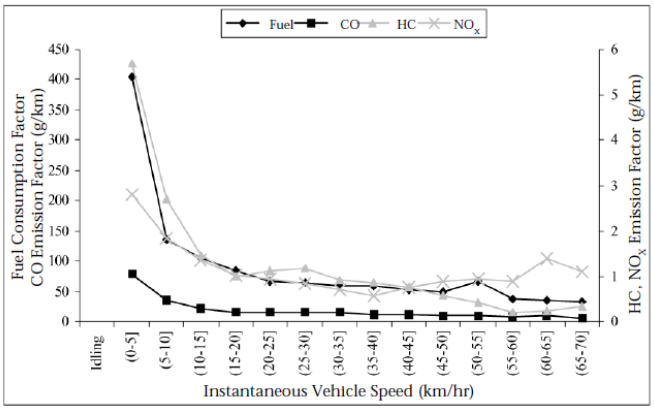

Figure 2.10: Fuel consumption and emissions depending on the vehicle speed (Tong et al., 2000, p.549)

2.2.2 Traffic characteristics

The following section presents the main traffic conditions affecting emissions and fuel consumption. Especially the topics congestion, control delays, driving modes and traffic control are considered.

Congestion

Traffic conditions affect a variety of factors, with congestion having the biggest impact (Pavlovic et al., 2016; The Public Sector Digest, INC., n.d.). Traffic congestion is ubiquitous in urban areas, which is driven on the one hand by immigration into the cities and by spreading the vehicle as a primary means of transport (The Public Sector Digest, INC., n.d.). Compared to the late 20th century, people spend about three times as much time in congestion in the 21st century (Rodrigue, Comtois, & Slack, 2017). Congestion has a huge effect on economic activity and transport costs (Bundesministerium für wirtschaftliche Zusammenarbeit und Entwicklung, Referat Wasser, Stadtentwicklung, Mobilität, 2016). In Cairo, for instance, around 8 billion USD (year 2010) are wasted every year due to high traffic, even more than 17 billion USD by 2030 (The World Bank Group, 2014).

For the road user congestion has an influence on travel time, vehicle operating costs (VOC) and on emissions of the vehicle (Errampalli, Senathipathi, & Thamban, 2015). Therefore, changes in fuel consumption are reflected especially (Pavlovic et al., 2016). An increase in traffic means a reduction in the average speed and a rise in the frequency and magnitude of vehicle accelerations and decelerations (Greenwood & Bennett, 1996). Thus,

Table 2.1: Comparison of emissions and fuel consumption of two routes under normal traffic conditions and with congestion (Vlieger et al., 2000, p.4654)

Route (length)	**Traffic condition**	**Travelling time [min]**	**FC [l]**	**CO [g]**	**HC [g]**	**NO_x [g]**
1 (35 km)	Normal	43	2.7	69	5.3	4.8
	Congested	103	3.8	112	6.6	5.2
2 (20 km)	Normal	49	2.8	80	6.7	8.9
	Congested	76	3.4	135	9.4	10

the driving behaviour is influenced by changing traffic conditions (Fontaras et al., 2017). In addition, psychological impact should also be included. It was found out that congestion is reflected in some drivers with anger, stress, lack of sleep and reduced performance (Caldow, 2008). These factors can affect driving behaviour and safety (Pavlovic et al., 2016).

In general, it is difficult to define a common number by how much fuel consumption increases in congestion, as they are different for each vehicle and depending on the driving behaviour. However, a study by Vlieger, Keukeleere, and Kretzschmar has shown that an increase in traffic leads to a fuel consumption between 20 and 45 % depending on the driving behaviour. Based on two routes in Antwerp (Belgian), which are composed of parts of ring, rural and urban streets were once driven under normal driving conditions in the forenoon and one at peak time in the morning under normal driving behaviour. For these two routes, the fuel consumption increases by not quite 30 or 20 %, respectively. The emissions rates of CO, HC, NO_x also grow up to 40 %, where NO_x have the lowest rates (see table 2.1) (Vlieger et al., 2000).

Among other things, it should be noted that highway congestion can even reduce fuel consumption in certain cases, as low speed is maintained, and driving is adjusted to the leading vehicle, thereby reducing variability in fuel consumption (Pavlovic et al., 2016).

On roads with high traffic vehicle downtime leads to even linger idle times, which negatively impacts fuel economy (Fontaras et al., 2017). If vehicles have integrated a start-stop system, the engine is automatically switched off at standstill and only starts again when the clutch is actuated (Porsche Austria GmbH & Co OG, n.d.a). According to measurements by the NEDC, emissions can be reduced up to 8 %, in urban traffic even up to 15 % (Bosch Robert GmbH, n.d.).

Control delays

The following section presents an approach for quantifying control delays, which are generated by control devices such as traffic lights or a stop sign. Basically, emissions are higher for vehicles with delays than when they are in motion. Delay events consist of the driving modes idling, acceleration and deceleration, which are mentioned in chapter 2.2.2 (Mathew, 2014; Pandian et al., 2009). In general, identifying delays is a difficult process because there are many different approaches that often lead to different results. Therefore, it is important to develop a predictive model that can estimate delays (Mathew, 2014). The basic principle is described in more detail on the basis of figure 2.11, in which time is firstly compared with distance and second with speed. Additionally, the trajectory of a vehicle in free flow against a trajectory with disabilities due to control delay is illustrated. At time t1 the vehicle slows down and approaches the intersection, coming to a standstill between t2 and t3. From time t3, the vehicle begins to accelerate again and crosses the intersection at time t4. After all, the vehicle has the same speed again at time t5 as without the control delay. The points L1 and L5 symbolize the position of the vehicle at time t1 and t5, respectively (Othayoth & Rao, 2018).

Among the most important parameters of the control delay count approach delay and stopped delay. The stopped delay occurs when the vehicle is completely stopped, that is, when it is idling and ends when the vehicle accelerates . The approach delay contains the stopped delay and starts from the instant of time when a vehicle slows down and ends when the vehicle has achieved the cruising speed again (Mathew, 2014; Rouphail et al., 2001). It is *"the horizontal (time) difference between the hypothetical extension of the approaching velocity slope and the departure slope after full acceleration is achieved"* (Othayoth & Rao, 2018, p.6).

The control delay is the time difference between a vehicle that passes unobstructed (free-flow) through an intersection and one which is hindered due to control devices. Thus, this results from the stopped delay, the deceleration delay and the acceleration delay and represents the total delay at the intersection (Othayoth & Rao, 2018; Pandian et al., 2009).

Basically, there are two ways to measure delays. Firstly, the delay for a single vehicle, which is the average of all vehicles for a certain time period, can be calculated. The individual delay is given in seconds per vehicle for a time interval. On the other hand, the delay can also be stated as the aggregate value for all vehicles over a certain period of time. The total delay is given in hours, minutes or seconds for all vehicles in a time interval (Mathew, 2014).

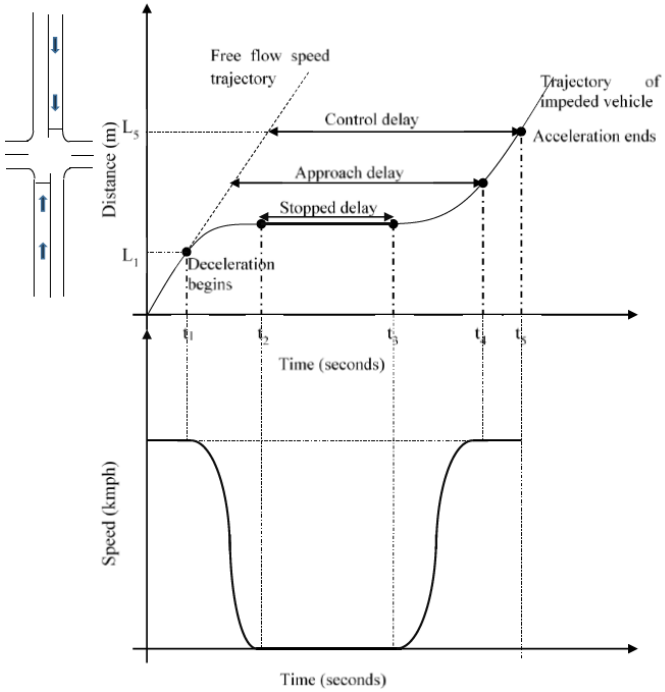

Figure 2.11: Distance-time and speed-time diagramm of a stopped vehicle at the signalized intersection (Othayoth & Rao, 2018, p.7)

Driving Mode

As mentioned before, in the case of delays the four driving modes, acceleration, deceleration, idling and cruising occur. The effects of these modes on the emissions NO, HC, CO and CO_2 were clarified in a study by Frey, Unal, Rouphail, and Colyar. The study tested ten vehicles in three different roads near the city of Cary, in North Carolina. It turned out that the driving mode acceleration has the highest rates for all emissions, especially after idling (Frey et al., 2003; Rouphail et al., 2001). This mode is followed by the cruising mode, which has the second highest emission rates on average. The third highest emissions has the deceleration mode, followed by the idling, which has the lowest values. On average, the pollutants CO and NO are ten times higher in the acceleration mode than in the idling mode. The same applies to the pollutants HC and CO_2 in which the acceleration mode is higher by a factor of five (see figure 2.12). In addition, the time was taken into account, in which the vehicle is in each mode. It should be emphasized the acceleration mode in which the residence time is only less than 20 %, but this has a fuel consumption and emissions of 35 to 40 %. The biggest contributor is the cruising mode, which consumed on average more than 40 % of the time (see figure 2.13) (Frey et al., 2003).

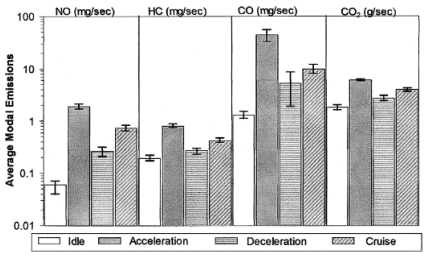

Figure 2.12: Effects of driving modes on emissions (Frey et al., 2003, p.998)

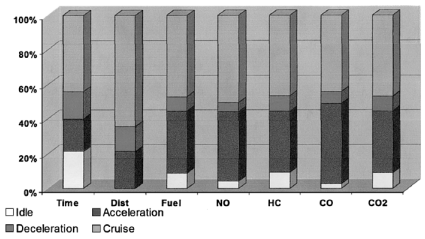

Figure 2.13: Influence of driving modes on travel time, distance travelled, fuel use and emissions (Frey et al., 2003, p.1000)

Furthermore, the emissions were examined in relation to the control delay. It was found that the emissions at control delay are twice as high compared to no obstacles. This is because with a control delay, accelerations always occur, which is the main cause of high emission rates (Rouphail et al., 2001).

In conclusion, the study showed that acceleration and cursing modes have a significant impact on vehicle emissions, whereas deceleration and idling have less impact (Frey et al., 2003).

Traffic control

In addition, it is important to link vehicle emissions with traffic measurements to determine the effects of emissions due to road design and traffic control (Rouphail et al., 2001). A study carried out in the city of Phoenix, in Arizona, shows the effects of traffic signal control on vehicle delays, fuel, and emissions (figure 2.14). Based on three intersections on an arterial road, the study was conducted with only one direction taken into account. It is to mention that the results would not be so clear if both directions were modelled. However, the three models implemented (poor coordination, good coordination, real-time coordination) show how clearly, in the scope of 50 %, the level of signal coordination contributes to the reduction of delay, fuel and emissions (Rakha, van Aerde, Ahn, & Trani, 2000).

2.2.3 Vehicle characteristics

The literature mentions various factor that influence the emissions and fuel consumption of vehicles. An insight about the vehicle characteristics in

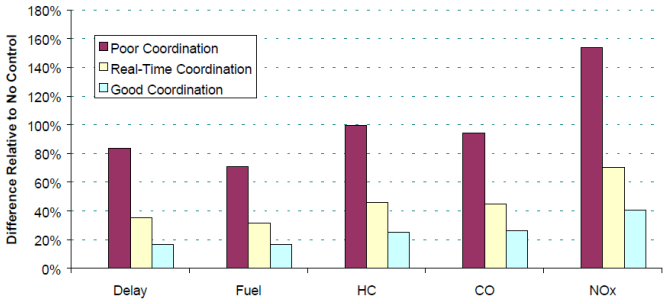

Figure 2.14: Influence of the type of signal control on delay, fuel consumption and emissions (Rakha et al., 2000, p.26)

Europe is give in the table 2.2. The properties CO_2, mass, capacity and power of the vehicles are listed by fuel.

Table 2.2: Characteristics of European passenger cars ordered by fuel (European Environment Agency, 2016b)

Fuel	**CO2 [g/km]**	**Mass [kg]**	**Capacity [cc]**	**Power [kW]**
All	120.7	1380	1600	66
Diesel	119.2	1526	1811	71
Petrol	122.7	1214	1358	59

A good overview of the large number of affecting fields is provided by Guensler. Vehicle parameter, fuel parameter, vehicle operating conditions and vehicle operating environment are mainly responsible for the emissions of the vehicles. These as well as the most important associated variables are shown in Table 2.3 (Guensler, 1993).

The following section describes the most important vehicle parameter found in the current literature. First of all, general factors influencing fuel consumption are mentioned. Subsequently, the focus will be on the vehicle weight, auxiliary systems, aerodynamic resistance and rolling resistance, as these strongly influence fuel consumption and the exhausted emissions. In general, 53 % from the engine power is used to conquer the aerodynamic drag. The remaining energy is applied for rolling resistance (32 %), auxiliary equipment (9 %) and drive train (6 %) (Sudin, Abdullah, Shamsuddin, Ramli, & Tahir, 2014).

Table 2.3: Parameters and conditions that influence the emission rates of vehicles (Guensler, 1993, p.5)

Vehicle Parameters:	Fuel Parameters:
• Vehicle class [weight, engine size, HP, etc.]*	• Fuel type
• Model year	• Oxygen content
• Accrued vehicle mileage	• Fuel volatility
• Fuel delivery system (e.g. carbureted or fuel injected)	• Sulfur content (SOx precursor)
• Emission control system	• Benzene content
• Onboard computer control system	• Olefin and aromatic content
• Control system tampering	• Lead and metals content
• Inspection and maintenance history	• Trace sulfur (catalyst effects)*

Vehicle Operating Conditions:	Vehicle Operating Environment:
• Cold or hot start mode (unless treated separately)	• Altitude
• Average vehicle speed	• Humidity
• Modal activities that cause enrichment*	• Ambient temperature
• Load (e.g. A/C, heavy loads, or towing)	• Diurnal temperature sweep
• Trip length and trips/day*	• Road grade*
• Influence of driver behavior*	

* These components are not explicitly included in the USEPA or CARB emission rate models.
Source: Guensler, 1993

General factors

In general, most studies show a significant correlation between vehicle age and vehicle mileage relative to the emissions (Pandian et al., 2009). Both factors lead to an increase of the exhaust emissions, which depict a moderate rise in properly functioning vehicles, but a huge increase in the case of defect emissions controls. Especially the pollutants CO and HC are affected (Wenzel, Singer, & Slott, 2000).

The emissions rise significantly with an increasing age of the vehicles (Harrington, 1997), because newer vehicle models use improved technologies

and less deterioration of the engine and emission control devices (Beydoun & Guldmann, 2006). In addition, the average emissions increase with the mileage, because more vehicle mileage lead to more wear on mechanical and emission-reducing devices (Beydoun & Guldmann, 2006; Wenzel & Ross, 1997). Furthermore, the size of the displacement has a negative effect on the exhaust emissions of the vehicle, but the number of cylinders has a positive one (Beydoun & Guldmann, 2006).

Another aspect that influences emissions is the fuel type. Whether diesel or gasoline is more environmentally friendly depends on the emissions considered. Basically, the combustion of one litre of diesel produces around 2.66 kg of CO_2, and around 2.29 kg CO_2 for gasoline (Natural Resources Canada, 2014). However, if the same type of vehicle with the same engine power is compared, then the gasoline engine consumes more fuel and therefore more CO_2 than diesel vehicles (Umweltbundesamt, n.d.a). This is also confirmed by the study of O'Driscoll, Stettler, Molden, Oxley, and ApSimon, which compared 149 Euro 5 and 6 vehicles based on CO_2 and NO_x emissions. The gasoline vehicles showed between 13 to 66 % higher CO_2 emissions than diesel vehicles. In the urban area, the average CO_2 emissions for gasoline vehicles were around 210.5 g/km, whereas for diesel vehicles around 170.2 g/km. However, if the NO_x emissions are considered, the result is reversed. Gasoline vehicles achieve 86 to 96 % lower emission rates than diesel vehicles. The average emissions were eleven times larger for diesel vehicles in the urban area. Thus, diesel vehicles have lower CO_2 emissions, whereas gasoline vehicles have lower NO_x emissions. The study came to the conclusion that one possible solution would be hybrid vehicles that would reduce both CO_2 and NO_x emissions (O'Driscoll et al., 2018). Especially in urban areas, an Otto-hybrid engine would compensate for the excess emissions (Umweltbundesamt, n.d.a).

The vehicle model is another relevant aspect of the emissions. Due to different manufacturing and different design, the emissions vary depending on the model. In addition, emission control systems that have differences in efficiency and lifetime affect emission levels. Thus, every vehicle has model-specific emission rates (Wenzel et al., 2000).

Another factor that increases fuel consumption is the horsepower (hp) of the engine. In general, more power means more consumption. For instance, a vehicle with standard engine consumes 6.4 l/100km on highways and in urban areas with 140 hp, whereas the vehicle in sport variation with 200 hp consumes 5 l/100km (Natural Resources Canada, 2018). Among other things, it should be considered that regular maintenance reduces the emissions of vehicles. This is applied for both older and newer vehicles, but for the last one it does not have that much impact (Wenzel & Ross, 1997).

Vehicle mass

One of the main factors affecting the fuel consumption is the vehicle mass. The more weight the vehicle has, the more expenditure of energy is required to get it moving (Natural Resources Canada, 2018). The weight of the vehicle comprises of the empty vehicle, the occupants, the load and the fuel (Fontaras et al., 2017). Mickānaitis, Pikānas, and Mackoit found out that with an increase by 100 kg of the vehicle mass, CO_2 emissions and fuel consumption raised by 6.5 % for petrol cars and 7.1 % for diesel cars (Mickānaitis et al., 2007). However, CO_2 emissions could decrease between 1.3-1.8 % and 2.7-3.6 % if the weight of the vehicle reduced by 5 or 10 % (Fontaras & Samaras, 2010). In general, a vehicle consumes 0.4 l/100km more fuel when it is 100 kg heavier (Dudenhöffer & John, 2009). The exhaust emissions of the vehicles could be reduced by 40 % by 2050 if the fleet weight of passenger cars would be reduced from 1380 kg to 1000 kg (FIA, n.d.).

In addition to the weight of the vehicle is still the weight of the occupants to consider. This is expressed by the occupant rate, which is composed of the occupants per vehicle (including driver) (Pavlovic et al., 2016). The average occupant rate in the EU-15 is 1.6 (2008), or 120 kg, as the average occupant weight is assumed to be 75 kg (European Environment Agency, 2009; Pavlovic et al., 2016). In addition, another 5 to 10 kg of extra weight for the equipment should be assumed. To determine the CO_2 emissions per passenger, the total value of emissions is divided by the number of passengers. This method is widely used to evaluate the environmental impact of various passenger transport systems. Overall, a high occupant rate is preferable, because although the weight and thus the fuel consumption of the vehicle is increased, but the CO_2 emissions per passenger are reduced. Initiatives like car-sharing or carpooling should support to reduce the occupant rate (Pavlovic et al., 2016). The two factors roof box and trailer additionally influence the weight, but are not taken into account in this thesis, as these are hardly used for everyday trips in the city.

On the one hand, automobile manufacturers use lightweight materials such as aluminium or advanced composites, and on the other hand, they make improvements in the design to counteract the excess weight of the car. This allows smaller engines to be used as less energy is needed to move the vehicle (Natural Resources Canada, 2018). A reduction in weight also leads to positive drivetrain changes, such as engine performance (Fontaras et al., 2017). Thus, lighter vehicles and more efficient components could reduce the peak performance of the powertrains, resulting in lower fuel consumption (Elgowainy et al., 2013; Fontaras et al., 2017). However, a reduction of the vehicle weight is always in a conflict with the comfort as well as the safety of the occupants against the increase in pollutant emissions (Pandian et al.,

2009). The figure 2.15 gives an overview of the influence of the weight of the vehicle on the fuel consumption, which were find by Pavlovic et al. in the literature.

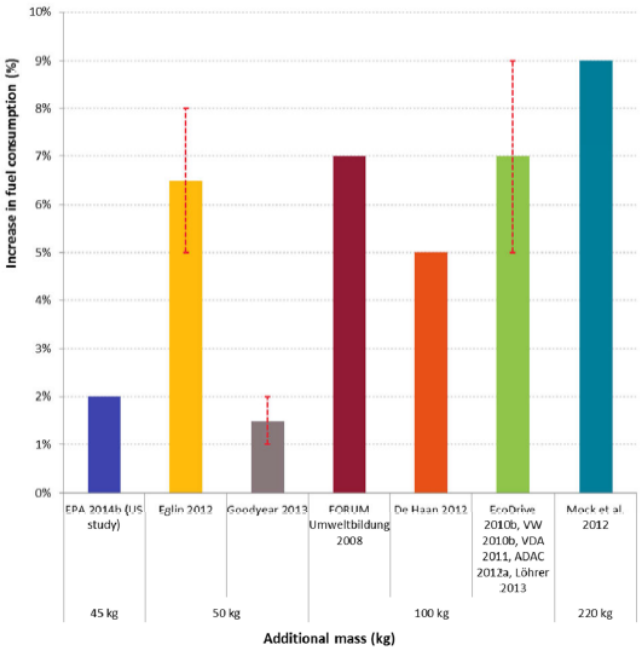

Figure 2.15: Increase in fuel consumption due to additional mass as reported in different sources (Pavlovic et al., 2016, p.92)

Auxiliary systems

Basically, auxiliary systems are used to support a comfortable and safe driving in the vehicle (Fontaras et al., 2017). However, these systems require energy and thus also cause a higher fuel consumption (U.S. Department of Energy, n.d.). Among the most important auxiliary systems count air conditioning systems, heating systems, steering assist systems and other electrical consumers and auxiliaries such as windscreen wipers or heated seats (Fontaras et al., 2017). Especially the new accident avoidance systems like adaptive cruise control, lane-keeping assist, park assistant, or backup camera are mostly present in today's vehicles (Consumer Reports, n.d.; Pavlovic et al., 2016). The total electrical energy requirement of an average vehicle in Europe is appreciated to 750 W (European Commission, 2013). Both electrical and mechanical auxiliaries affect fuel consumption. Mechanical devices obtain the energy directly from the engine, for electrical devices, the alternator operation must be increased, which increases the engine performance

(Pavlovic et al., 2016). The following section focus on air conditioners as they have the biggest impact. Furthermore, control systems are mentioned, which occur today in all vehicles. In addition, an overview of the energy consumption of various comfort and safety features is provided.

Air Condition The air condition system has the greatest effect on the fuel consumption of the additional systems. Overall, a vehicle can consume up to 20 % more if the air conditioner is used (Natural Resources Canada, 2018). The ambient temperature determines the energy consumption of the air conditioning system. The greater the difference between the desirable indoor temperature and the ambient temperature, the more power is needed to achieve this. Different weather conditions can also influence the power consumption of the air conditioning system (Pavlovic et al., 2016).

In a study by De Moura and Tribess, the three conditions of city traffic condition, road conditions at 80 km/h and constant speed at 120 km/h were simulated by means of dynamometers. Research shows that on average, fuel consumption increased by 16 % in the urban area, 11 % on highways, and 13 % in combined areas using an A/C control system (De Moura & Tribess, 2007).

The amount of fuel consumption depends almost entirely on the desired performance, which depends on the required interior temperature, the outside temperature, the air humidity and the solar radiation. By contrast, the speed of the vehicle does not matter much. Basically, it is irrelevant for the air condition, whether the vehicle is at 2 km/h in a traffic congestion or driving at 120 km/h on a road, provided that the ambient conditions are constant. However, if the proportion of air conditioning in the total fuel consumption is considered in relation to the distance travelled, this increases at low speed and higher ambient temperatures (Kemle, Manski, Harald, & Weinbrenner, 2008). The study from Roujol and Joumard also supports previous assumptions that speed and traffic situation do not have a significant impact on fuel consumption (Roujol & Joumard, 2009). The ADAC (Allgemeine Deutsche Automobil-Club) emphasizes, that the additional consumption by an air conditioner depends on the duty cycle. The fact that the data are usually made in litres per kilometre, the consumption is higher at lower speed than at higher speeds. Instead of a belt drive, modern vehicles often have electrical air-conditioning compressors, which contribute to fuel reduction through situational and intelligent interventions (ADAC e.V., n.d.).

However, other researchers came to the conclusion that traffic conditions have an impact on fuel consumption and CO_2 emissions, but this is justifiable due to differences in distance travelled. The relative difference in ambient

temperature of 13 °C and a desired cabin temperature of 23 °C is 4 %, 2.5 %, and 1 % on urban, rural, and highway rides. In general, fuel consumption increases with ambient temperatures (13 °C, 23 °C, 30 °C, 37 °C), with the highest in the urban area and the lowest on the highways. This is because it takes longer in urban areas to reach a certain distance. From 23 °C to 37 °C, CO_2 emissions increase approximately linearly (Weilenmann, Alvarez, & Keller, 2010). The relative difference can be explained by the fact that higher engine power is required at higher speeds, which in turn leads to higher fuel consumption. As a result, the relative fuel loss for the air condition at higher speed is lower (Pavlovic et al., 2016).

Also, the type of air conditioning, whether manual, semi-automatic or fully automatic affects fuel consumption. In a study by the ADAC, it was found from a middle-class vehicle that 0.48 l of manual equipment, 0.49 l for semi-automatic systems and 0.36 l for automatic systems was more used for 100 kilometres, compared to a deactivated air conditioning system. The ambient temperature was assumed to be 25 °C and the desired interior temperature 22 °C (ADAC e.V., n.d.).

However, the positive effect of saving fuel on new vehicles also has a disadvantage. Due to the lower heat output of the engine to the coolant, the heating power is reduced. Therefore, often additional heating systems are integrated in the vehicles. Basically, A/C systems can be deployed to heat the cabin, but these systems are used very rarely. The additional fuel consumption was determined in a study by Feuerecker, Schafer, and Strauss in Frankfurt. The use of heating systems consumes on average between 0.15 to 0.25 l per 100 km more fuel, depending on the type of system and its performance (Feuerecker et al., 2005).

Steering assistance system Another factor that requires additional energy is the steering assistance system. In comparison to the total operating time of the vehicle, steering actions rarely occur, but these will often come into use in future due to modern systems such as lane keeping, parking, collision avoidance, side wind compensation or congestion assistance. Therefore, these become more important for fuel consumption. On average, vehicle consume up to 4.5 % more fuel through the use of steering assistance systems, with modern systems consuming 1 to 2 % (Pavlovic et al., 2016).

Other auxiliaries There are also other systems that are responsible for higher fuel consumption and CO_2 emissions, whose impact in the real world is either hard to measure or very low (Pavlovic et al., 2016). For instance, devices such as fuel pumps or fuel injection systems influence the fuel consumption, which is proven in certification tests, but not under real driving

conditions (Arthur D. Little, 2006; Pavlovic et al., 2016). A factor that has only a small influence on the fuel consumption, are headlights (Pavlovic et al., 2016). Headlights require about 144 W, which results to an additional fuel consumption of 0.14 l/100km, according to the study by Huhn. In addition, the daytime running light was analysed and found to cause increased fuel consumption of up to 0.28 l/100km. However, the use of LED (Light-emitting Diode) light sources can significantly reduce fuel consumption (Huhn, 2008).

Table 2.4 gives an overview of the energy requirements and fuel consumption of the auxiliary systems of European vehicles (Dudenhöffer & John, 2009). The fuel consumption in l/100km refers to the average speed in the NEDC of 33.6 km/h (Schmidt & Johannsen R., 2011). Although air conditioners, heating systems and electric motors for windows, sunroof or seat adjustment increase fuel consumption, and are increasingly installed in vehicles, these are not taken into account in the European driving cycles (Dudenhöffer & John, 2009). It should also be taken into account that with a large number of optional extras, the weight can rise well by 150 kg, resulting in additional consumption of 0.6 l/100km (Dudenhöffer & John, 2009). Based on these results, a vehicle would have consumed 1.5 l/100km additional fuel on a rainy winter night, assuming that windscreen wipers, headlamps, heated rear windows and wipers, and electric booster heater are used (Pavlovic et al., 2016). A previous study has shown, that the use of air conditioning, dipped beam and radio increases CO_2 emissions by up to 16 % (Schmidt & Johannsen R., 2011).

Aerodynamic resistance

Another important factor influencing the consumption of fuel is the aerodynamic resistance, which is especially at higher speeds the main fuel consumer for vehicles (Ersoy & Gies, 2017). Due to ineffective aerodynamic shapes of the vehicles enormous drag develops, which boost the fuel consumption. The pressure or shape drag have the greatest influence on the aerodynamic resistance of the vehicle (Sudin et al., 2014). For the total aerodynamic drag the main responsible with 80 % is the pressure drag. The remaining 20 % is due to frictional drag (Wood, 2004). Therefore, a reduction of the aerodynamic drag is for the fuel consumption rate essential (Sudin et al., 2014).

The aerodynamic resistance consists of the product of the frontal area A of the vehicle, the aerodynamic drag coefficient c_w, the air density ρ and the square of the driving speed (Fontaras et al., 2017). A more detailed explanation of the aerodynamic resistance is given in chapter 2.3.1. An in-

Table 2.4: Increased fuel consumption due to comfort and safety features (Dudenhöffer & John, 2009, p.15)

	continuous consumption [W]	**consumption in l/h**
headlights	150	0.150
fog lights	100	0.100
electric window lift	300	0.300
electric sunroof	200	0.200
rear window heating	120	0.120
rear window wiper	70	0.070
electric seat adjustment	150	0.150
electric mirror adjustment	20	0.020
seat heating	400	0.400
electric auxiliary heater	1000	1.000
front window heating	500	0.500
electric steering wheel heater	50	0.050
air conditioning	1500	1.500
wiper	150	0.150
heated windscreen washer	80	0.080
navigation system	15	0.015
sum	**4805**	**4.805**

crease in drag due to changing vehicle shape or size and aerodynamic design increases aerodynamic resistance, resulting in higher CO_2 emissions and fuel consumption (Fontaras et al., 2017). This results in a close relationship between the cruising speed and the fuel required to conquer the drag (Auto Research Center, n.d.). Although the air density has no direct influence on the aerodynamic properties of the vehicle, but this affects fuel consumption. Depending on the altitude and the ambient conditions, the air density varies. Because the air density is lower in higher areas, its impact on altitude can be determined. On the other hand, it is difficult to calculate the effect of weather conditions on air density and fuel consumption (Pavlovic et al., 2016). Basically, there is almost always an ambient wind, with the strength and the local wind direction diversify due to different landscape along a road (Hucho & Sovran, 1993).

Even small changes in aerodynamic resistance lead to higher fuel consumption (Pavlovic et al., 2016). Van Mensch, Ligterink, and Cuelenaere found out that when the driver side mirror is folded, the passenger side mirror is removed, the windscreen wiper blades and antenna are taken off, and the wheel caps are closed, 4 % of aerodynamic drag can be reduced (van Mensch et al., 2014). In addition to the reduction of drag, the lift and side forces are for vehicle stability enormously important (Crolla, 2009). Al-

though the drag coefficient has decreased in recent years due to improved design and high developed manufacturing engineering, the increasing vehicle size has compensated the benefit (Fontaras & Dilara, 2012; Pavlovic et al., 2016).

A decrease in aerodynamic resistance of 5 and 10 % for NEDC, respectively, leads to a reduction in CO_2 emissions of 0.6 to 1.2 % and 1.2 to 2.4 %. In general, smaller vehicles have advantages over larger ones. Due to the cube-like geometry, the aerodynamic properties of smaller vehicles are worse, however, these have lower fuel consumption and therefore the absolute CO_2 savings are equal or even lower to the larger vehicles (Fontaras & Samaras, 2010).

On average, the c_w value is 0.30, and since 1960 this has fallen by 40 % (Pischinger & Seiffert, 2016). In the future, a drag coefficient of 0.24 is to be achieved, which reduces the fuel consumption by 1.6 l/100km at a speed of 130 km/h. In this context, according to NEDC, the CO_2 value would decrease by 7 g/km (Gilliéron & Kourta, 2008).

Among other things, attempts are being made to improve the drag coefficient and the lift coefficient by means of structures such as vortex generators, spoilers or tail plates. Although these add-on devices do not lead to significant improvements, but it is on the one hand, the resistance and fuel consumption (up to 7 %) a little reduced and on the other hand improves the stability of the vehicle (Bansal & Sharma, 2014; Sudin et al., 2014).

In addition, other factors such as roof add-ons, open windows or wind conditions have an influence on the aerodynamic resistance, which is not discussed in detail in the work.

Rolling resistance

Due to the fact that about 30 % of the vehicle's CO_2 emissions are due to rolling resistance, this is an important component of fuel consumption (European Commission, 2006). The energy dissipation in the tire due to the damping properties of the rubber and the deformation of the tire contact patch is called rolling resistance (Crolla, 2009). About 90 % of the rolling resistance is due to the energy loss of the deformation (Michelin, 2003).

The rolling resistance is influenced by the parameters load, tyre pressure, surface texture of the road, temperature and speed (Michelin, 2003). The vehicle weight is proportional to the rolling resistance of the tire (Fontaras et al., 2017). The rolling resistance of the tire is described by the rolling resistance coefficient, which is dimensionless and is assumed to be either

constant or proportional to the vehicle speed (Fontaras et al., 2017; Michelin, 2003). The rolling resistance of the vehicle can be improved between 5 and 30 %, resulting in a reduction in fuel consumption of 1-3.5 % (Fontaras et al., 2017).

Tyres Due to the influence of the tyres on the fuel consumption of the vehicle, these are briefly mentioned. The rolling resistance depends on the type of tire and the size, which is particularly important at low speeds and influences urban fuel consumption (Crolla, 2009; Fontaras et al., 2017).

Tyres are classified into different energy efficiency classes depending on the value of the rolling resistance coefficient (Fontaras et al., 2017). The classes range from A to G, where A has the highest efficiency with a coefficient less than 6.5 and G the lowest efficiency with a coefficient greater than 12.1 (Verordnung Nr. 1222/2009 des Europäischen Parlaments und des Rates vom 25. November 2009 über die Kennzeichnung von Reifen in Bezug auf die Kraftstoffeffizienz und andere wesentliche Parameter (Text von Bedeutung für den EWR), 2009). Fuel consumption can be reduced by up to 9 % when class A tires are used instead of class G. For instance, if a vehicle uses a new tire for 65.000 km and has a fuel consumption of 8 l/100km, a total of up to 440 l of fuel could be saved. Therefore, it should be noted that although more efficient tires have higher acquisition costs, but they are compensated by fuel economy (European Commission, n.d.). On average, fuel consumption can be reduced by 2.1 % when tires with a lower rolling resistance are used instead of a tire with higher rolling resistance (Pavlovic et al., 2016). Generally, the value of the rolling resistance is higher, the broader the tire (Fontaras et al., 2017).

In addition to the tire category, tire condition and maintenance are also very important. Although the tire wear can reduce the rolling resistance coefficient, it leads to loss of grip and poor tire characteristics, causing unsafe and dangerous driving. Exact effects of the tire under poor properties on the fuel consumption are not known and are also to be avoided for safety reasons. The most important tire maintenance is tire pressure monitoring (Pavlovic et al., 2016). In general, rolling resistance rise as tire pressure is reduced, whereas at low tire pressure, the rolling resistance is increased due to less compression of the tread in the contact area. Reducing the tire pressure by 1 bar results in an increase in rolling resistance of 30 %, which in turn increases fuel consumption by between 3 and 5 %. However, with an increase in tire pressure of 1 bar, while the rolling resistance is reduced by about 20 %, it should be noted that due to the manufacturer's deviation, this may have an effect on durability, grip or safety (Michelin, 2003; Pavlovic et al., 2016).

Reducing the rolling resistance coefficient by 10 and 20 %, respectively, would reduce the fuel consumption of an NEDC by an average of 1-1.25 and 2-2.5 % (Fontaras & Samaras, 2010). In addition to the tire pressure the misaligned tires, suspension losses and air filters should also be checked during maintenance to save fuel (Pavlovic et al., 2016).

2.2.4 Overview

In Table 2.5, all the factors mentioned above, which have an influence on fuel consumption and emissions, are presented in an overview. Depending on the positive or negative influence on the consumption, the factors are marked with a red up-pointing or a green down-pointing arrow. For instance, a higher number of cylinders, regular maintenance, wider roads and increased use of traffic control means lower emissions. The black-marked arrows pointing in both directions symbolize emission increases as well as reduced emissions, depending on the situation. For example, a higher speed of over 80 km/h and a lower speed of less than 50 km/h provide for higher fuel consumption. Humps can bring both advantages and disadvantages for emissions, depending on the traffic situation. The emissions also vary in the driving modes, depending on which is in use. The remaining factors cause an increase in emissions and therefore have a red arrow pointing upwards.

2.3 Driving dynamics

Driving dynamics is understood to mean the *"movement of the vehicle in space as well as the forces and moments acting on the vehicle"* (Ersoy & Gies, 2017, p.52). Driving speeds, distances, accelerations, angles, etc. characterize the vehicle movements to which belong the straight driving, cornering, acceleration, braking, etc.. In addition, vibrations and forces act, which make the system to a complex dynamic one. On the one hand, the vehicle weight with load and on the other hand, the inertia forces generated by acceleration, braking and cornering, affect directly the vehicle. In addition, aerodynamic forces and engine drive torques still occur, which are transmitted to the road surface via the tire contact surfaces.

The driving dynamic is subdivided into longitudinal dynamics, vertical dynamics and lateral dynamics. Movements in the vehicle longitudinal direction, which are caused by the driving and braking, are referred to as longitudinal dynamics. An essential role plays the driving resistances and the power requirements, which are described in more detail in the following chapter 2.3.1. In addition, braking and traction characteristics are still part

Table 2.5: Overview of the factors used to influence the emissions and fuel consumption of vehicles

Category	Factor	Influence
Vehicle characteristics	age	⇑
	mileage	⇑
	displacement	⇑
	cylinder	⇓
	mass	⇑
	auxiliary systems	⇑
	aerodynamic resistance	⇑
	rolling resistance	⇑
	maintenance	⇓
	HP	⇑
road characteristics	grade	⇑
	roughness	⇑
	texture	⇑
	road class	⇓
	humps	⇕
	junction	⇑
	speed	⇕
traffic characteristics	congestion	⇑
	control delays	⇑
	driving mode	⇕
	traffic control	⇓

of the vehicle's longitudinal dynamics. The vertical dynamics are concerned with the vibration behaviour of the vehicle, with both driving safety and drive comfort are sought. The transverse dynamics are understood to mean the movement transversely to the longitudinal axis of the vehicle, the focus being on the cornering behaviour, tracking and driving stability (Ersoy & Gies, 2017).

In this thesis, the emphasis is on the longitudinal dynamics, which is described by the driving resistances in the following chapter.

2.3.1 Driving resistances

On the basis of the driving resistances it is possible to define the power requirement of a vehicle and thus fuel consumption (Ersoy & Gies, 2017). The driving resistance occurs in the vehicle movement as opposing force. This is subdivided into the wheel resistance F_{WR}, air resistance F_{WL}, gradient re-

sistance F_{WS} and acceleration resistance F_{WB}. The driving resistances are indicated as force in Newton [N]. The following sections will take a closer look at the individual driving resistance components.

Wheel resistance

Due to the different causes, the wheel resistance is divided into rolling resistance, surge resistance, bearing resistance, to-in resistance, curve resistance and suspicion resistance (Haken, 2011).

Rolling resistance Rolling resistance is defined as the resistance force at which an air-tired wheel rolls on a flat and dry road surface counter to the running direction (Wllentowitz, 2005). If the tire is loaded by the wheel load, then this deforms in the area of the contact zone with the road and it creates a footprint. The tire is sprung in the front area of the contact area when rolling (tire inlet) and rebounded in the rear area (tire outlet). Due to the acting spring force and damping forces, an uneven surface pressure in the area of the footprint arises (see figure 2.16a). If these two forces are combined to form a resultant, the normal force F_{N}, which acts in the direction of travel in front of the wheel centre and corresponds to the wheel load, is created (see figure 2.16b).

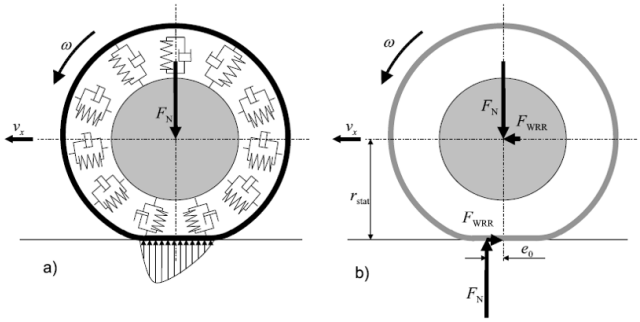

Figure 2.16: Model for illustrating the wheel resistance, (a) physical model without longitudinal forces, (b) forces due to the surface pressure (Haken, 2011, p.138)

The distance between the normal force and the centre of the wheel is marked with e_0. The wheel load is characterized by forces in the centre of the wheel. This results in a pair of forces acting as a moment against the wheel rotation. To conquer this moment the force F_{WRR} is necessary.

Therefore, the rolling resistance is as follows:

$$F_{WR} = \frac{e_0}{r_{stat}} \cdot F_N \tag{2.1}$$

Where,

e_0 = lever arm of rolling friction,
r_{stat} = distance between wheel axle and roadway.

If the parameters e_0 and r_{stat} are assumed to be constant, then the force F_{WRR} is directly proportional to the normal force F_{N} and therefore the rolling resistance coefficient can be calculated as follows:

$$f_R = \frac{e_0}{r_{stat}} \tag{2.2}$$

The rolling resistance coefficient is usually assumed to be constant. Accordingly, the following equation results:

$$F_{WRR} = f_R \cdot F_N \tag{2.3}$$

The sum of the wheel loads in the grade can also be expressed as $m \cdot g \cdot cos\alpha$, if no account is taken of aerodynamics up or down forces, where m is the vehicle mass, g is the gravitational acceleration ($9.81\,\text{m/s}^2$) and α the gradient angle (see figure 2.17). Therefore, the rolling resistance F_{WRR} is expressed as follows:

$$F_{WRR} = m \cdot g \cdot f_R \cdot cos\alpha \tag{2.4}$$

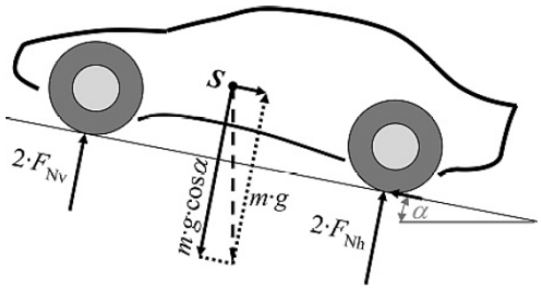

Figure 2.17: Determining factors of the rolling resistance in the gradient. S = center of gravity of the vehicle (Haken, 2011, p. 139)

Strictly speaking, the rolling resistance coefficient is not a constant, but depends on several factors, such as tire pressure, tire temperature, wheel

load, road and above all on the driving speed (Haken, 2011). Therefore, the rolling resistance coefficient can be expressed by the following equation:

$$f_R = f_{R0} + f_{R1} \cdot v + f_{R4} \cdot v^4 \tag{2.5}$$

Where,

f_{R0}, f_{R1}, f_{R4} = rolling resistance coefficients [-],[s/m],[s^4/m^4],
v = velocity [m/s] (Hausberger, 2009).

The rolling resistance accounts for more than 80 % of the total wheel resistance when the road surface is dry and firm, the track is set correctly, and the wheel bearings are undamaged. Therefore, the entire wheel resistance F_{WR} can be simplified expressed as:

$$F_{WR} \approx F_{WRR} \tag{2.6}$$

For this reason, this thesis did not deal with the further resistances that emboss the wheel resistance (Haken, 2011).

Air resistance

Air resistance refers to the force that develops due to the flow around and through the vehicle in the opposite direction of travel. The pressure resistance and the frictional resistance, which are dependent on the vehicle shape and the surface structure, together form the air resistance. The air resistance F_{WL} in calm weather can be determined from the Bernoulli equation:

$$F_{WL} = c_W \cdot A \cdot \frac{\rho}{2} \cdot v_x^2 \tag{2.7}$$

The resistance consists of the product of the aerodynamic drag coefficient c_W, the frontal area A of the vehicle, the air density ρ and the square of the driving speed (Fontaras et al., 2017). The coefficient is constant and basically expresses how the air circulates around the vehicle (Haken, 2011; Transition énergétique Québec, n.d.), as it depends on the body design (Haken, 2011). The frontal area is the surface area of the vehicle, which is directly visible when standing in front of it. Basically, it is the viewing of the vehicle profile on a vertical flat (Michelin, 2003). The design of the vehicle also determines the drag coefficient. The product of factors c_W and A is referred to as aerodynamic drag (Fontaras et al., 2017). In addition, it should be noted that the air resistance is proportional to the square of the driving speed (Transition énergétique Québec, n.d.).

Gradient resistance

In the vehicle's center of gravity, the weight can be divided into two parts. On the one hand, the wheel load (see chapter 2.3.1) is vertical to the road surface and, on the other hand, the gradient resistance is parallel to the roadway. The gradient resistance F_{WS} is therefore expressed by the following equation (see figure 2.18a):

$$F_{WS} = m \cdot g \cdot sin\alpha \tag{2.8}$$

Usually the road gradient is given as a percentage and not as an angle. The evaluation of the slope in degrees is based on the tangent and is shown in figure 2.18b. The calculation is based on the following:

$$tan\alpha = \frac{q}{100}$$

or

$$\alpha = arctan\left(\frac{q}{100}\right) \tag{2.9}$$

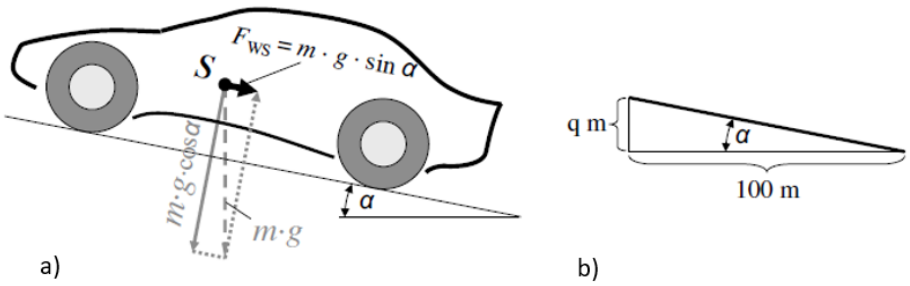

Figure 2.18: (a) Influencing variables for the gradient resistance. S = center of gravity of the vehicle. (b) Calculation of the slope in degree, where q is the slope in % (Haken, 2011, p. 155)

Acceleration resistance

Based on Newton's axiom, a force must be applied while accelerating (Haken, 2011). In order to set a vehicle in motion or to increase the speed, the acceleration resistance must be conquered. The vehicle mass m is driven by the translational acceleration a_x and the rotatable parts, such as wheels, gears and motor by means of rotatory acceleration (Ersoy & Gies, 2017).

The rotational component is expressed by the reduced moment of inertia of the drive train and the wheels. To simplify this, the rotational inertia factor ϵ is used. Thus, the following equation results for the acceleration resistance F_{WB}:

$$F_{WB} = m \cdot (1 + \epsilon) \cdot a_x \tag{2.10}$$

Total resistance

The individual proportions mentioned can now be summed up to a total driving resistance F_{W} (Haken, 2011):

$$F_W = m \cdot g \cdot \left[f_R \cdot cos\alpha + sin\alpha + (1 + \epsilon) \cdot \frac{a_x}{g} \right] + \frac{\rho}{2} \cdot c_x \cdot A \cdot v_r^2 + F_{WZ} \tag{2.11}$$

The total driving resistance is defined as demand force, as this energy must be provided to the driven wheels to move the vehicle to the desired condition (Ersoy & Gies, 2017). It can be seen from the equation 2.11 that all shares are proportional to the vehicle mass, with the exception of the air resistance, which increases with the square of the vehicle speed. If the vehicle moves in the plane at a constant speed, the normal driving resistance F_{W0} is calculated (= rolling resistance and air resistance) (Haken, 2011). Depending on the type of road, the individual resistances have different proportions of the total resistance. Figure 2.19 shows the different influences of individual resistances on "city", "rural road" and "highway" (Ersoy & Gies, 2017). Regarding the graphic, it should be noted that this is in German, since the source is also in this language.

Tractive-resistance losses

The power of translational movements is composed of the product of force and speed. If this is used for the total resistance, the following tractive-resistance losses P_{W} [W] results:

$$P_W = F_W \cdot v_x \tag{2.12}$$

For the individual driving resistances, the power is therefore composed as follows (Haken, 2011):

$$P_{WR} = F_{WR} \cdot v_x \quad P_{WS} = F_{WS} \cdot v_x \quad P_{WB} = F_{WB} \cdot v_x \quad P_{WL} = F_{WL} \cdot v_x \tag{2.13}$$

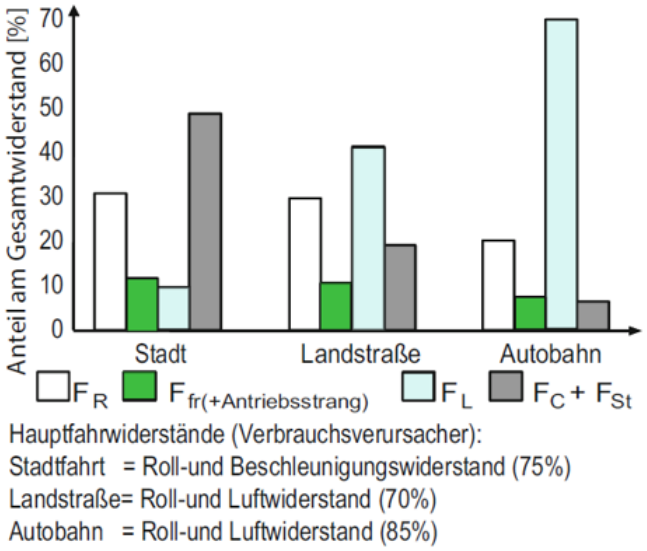

Figure 2.19: Shares of the individual driving resistance subdivided by road type (Ersoy & Gies, 2017, p.69)

2.3.2 Fuel consumption

In order for the driving resistances F_W of a vehicle to be mastered or the tractive-resistances losses P_W to be covered, the energy from an energy source is necessary. The fact that the energy density of diesel fuels and petrol fuels is very high, these are used as an energy source priority. The energy density serves as the basis for calculating the fuel consumption. In the strict sense, a specific fuel consumption, which relates to the driving distance is identified. This calculation serves as an essential basis for the determination of the cost of edges (see chapter 3.2.2). The consumption of fuel by additional equipment such as air conditioning, various assistance systems, light, etc. was not considered.

Driving performance

To overcome the driving resistance, the driving force is needed. When the available driving force is transmitted to the road, the driving resistance and the driving force balance each other. Thus, a demand map is equated to an offer map. These can also be specified in terms of performance (see figure 2.20).

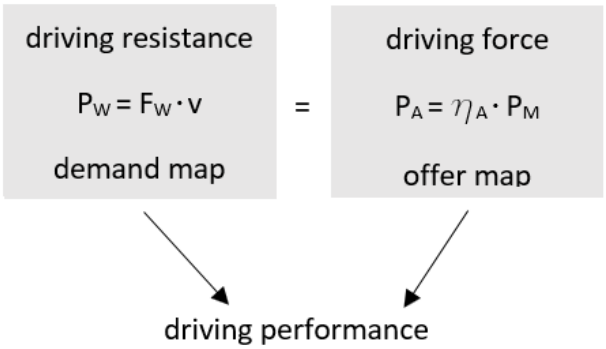

Figure 2.20: Development of the driving performance, modified after Haken (2011, p.191)

The drive power is composed of the engine power P_{M} and the efficiency of the power train η_A. Due to the fact that losses occur in the power train, these are described by their efficiency, which will be dealt with in more detail in the following chapter. From the driving condition, the actual engine power can be derived:

$$P_M = \frac{P_W}{(1 - \lambda_A) \cdot \eta_A} \tag{2.14}$$

In addition, the traction on which occurs during the power transmission of the wheels with the road still arises. However, this has no great influence on the determination of the driving performance and was mentioned only for the sake of completeness (Haken, 2011).

Track consumption

Based on the specific driving resistance F_{W} or the tractive-resistance losses P_{W}, the energy E_{Bed} [J] can be calculated for the distance travelled s_{x} [m] or the time travelled t_{x} [s]:

$$E_{Bed} = \int_0^{s_x} F_{Bed}(s) \cdot ds = \int_0^{t_x} P_{Bed}(t) \cdot dt \tag{2.15}$$

A connection between the expended energy E_{Bed} [J] and the distance consumption B_e [kg/m] can be established via the mass-specific calorific value H_u [kJ/kg] (Ersoy & Gies, 2017). The calorific value corresponds to the energy content of the fuel and therefore indicates the amount of energy in the fuel. More specifically, the lower calorific value is used. The calorific value for diesel and gasoline fuel can be found in table 2.6. Using the density of

Table 2.6: Mass specific calorific value and density according to fuel type (Ersoy & Gies, 2017, p.75)

Fuel	**Calorific Value H_u[kJ/kg]**	**Density ρ_K[kg/l]**
Gasoline	43500	0.755
Diesel	42000	0.845

the fuel, the calorific value can be expressed in energy per litre:

$$H_u\left[\frac{kJ}{l}\right] = H_u\left[\frac{kJ}{kg}\right] \cdot \rho_{\mathrm{K}}\left[\frac{kg}{l}\right] \tag{2.16}$$

The values for the density can be taken from the table 2.6, where it can be seen that diesel is considerably heavier than gasoline (Haken, 2011).

The conversion of the chemical energy in the fuel into the mechanical drive energy to the wheels causes losses. In the internal combustion engine of the vehicle due to friction, processes and cooling develop various losses. In addition, losses occur in the power train in the areas of bearings and gears. An overview of the losses in the power train is given in figure 2.21. This graphic is shown in German as the source was also written in this language. These losses are included in the calculation of fuel consumption B [kg] by the mean engine efficiency $\eta_{med,M}$ and the average power train efficiency $\eta_{med,A}$ (Ersoy & Gies, 2017). The efficiency of the engine is composed of the work done and the energy consumed and expresses the efficiency of an engine (Haken, 2011). The product of the two average efficiencies yields around 10 to 15 %. This means that only between 10 to 15 % of the energy can be used to conquer the driving resistances (Ersoy & Gies, 2017).

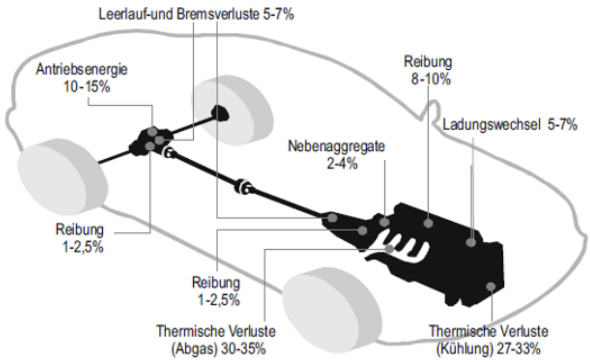

Figure 2.21: Overview of the most significant losses in the power train (Ersoy & Gies, 2017, p.76)

The efficiency of the combustion engine is strongly influenced by the operating condition, which differs depending on the revolution speed and

torques. In this case, the consumed fuel mass and the set-out work is determined in an operating condition, whereby the specific consumption is obtained. The specific consumption is often reflected in a shell diagram that compares torque and revolution speed of the motor (Haken, 2011). Accurate determination of specific consumption is determined by the engine map, which is very often implemented in emission models (see chapter 2.5).

The energy E_{Bed} that must be made available to the drive wheels in order to overcome the driving resistance F_{W} on the road s_{x} can be calculated from the fuel mass B and the calorific value H_{u}.

$$E_{Bed} = \eta_{med,M} \cdot \eta_{med,A} \cdot B \cdot H_u \tag{2.17}$$

Thus, the track specific consumption B_{e} results as follows (Ersoy & Gies, 2017):

$$B_e = \frac{B}{s_x} = \frac{1}{\eta_{med,M} \cdot \eta_{med,A} \cdot H_u \cdot s_x} \cdot E_{Bed} \tag{2.18}$$

At constant speed, the distance corresponds to the product of speed and time. In addition, it can be assumed that the efficiencies do not change. For these reasons, the distance consumption at a constant speed can be simplified (Lohse & Schnabel, 2011):

$$B_e = \frac{F_W}{\eta_{med,M} \cdot \eta_{med,A} \cdot H_u} \tag{2.19}$$

The equation 2.19 shows that with high efficiency and low driving resistance, fuel consumption is low. In order to achieve a lower fuel consumption and, in connection with this, lower CO_2 emissions from a vehicle-technical point of view, the following factors must be taken into account:

- the efficiency of the engine and the power train must be large,
- the rolling resistance coefficient must be small,
- the weight of the vehicle must be low,
- the aerodynamic drag, which consists of the product of the drag coefficient c_w and frontal area A of the vehicle must be small (Mitschke & Wallentowitz, 2014).

2.3.3 Coasting mode

To relieve the service brake, the engine braking effect can be exercised when driving downhill or when decelerating. This state of the internal combustion

engine is referred to as a coasting mode. This results in a braking torque that increases almost linearly with the speed, whereby the starting point being the torque zero. Depending on the engine speed, the fuel cutoff in the overrun enables fuel consumption to become zero when driving in the coasting mode. However, if the road grade or deceleration is so minimal that the wheel- or air resistance can compensate the deceleration, the coasting mode will not occur. In this context, the lowest consumption results when the engine is decoupled to idle, which is called sailing. Accordingly, the following track consumption [l/100km] results:

$$b_{100} = \frac{100}{v_x} \cdot b_{leer} \tag{2.20}$$

Where,

b_{leer} = idling fuel consumption [l/h]
v_x = driving speed [km/h] (Haken, 2011).

2.4 Air Quality

A poor air quality in cities not only endangers human health, it also interferes their activity planning. For these reasons, measures have been taken by countries, regions or cities to improve air quality. One measure is the development of an air quality indices to determine air quality. Based on sensor infrastructure, the air quality is measured and evaluated using the indices. This makes it possible to determine the degree of pollution in real time at any location (Ramos, Trilles, Muñoz, & Huerta, 2018). The development of Smart cities and the Internet of Things (IOT) will promote access to data for the population (Ramos et al., 2018; Zanella, Bui, Castellani, Vangelista, & Zorzi, 2014). The air pollution control has appeared a positive effect on public health in recent years (Correia et al., 2013).

In most countries air pollution monitoring is carried out with fixed stations (Marjovi, Arfire, & Martinoli, 2015). Another way to access air quality data is through sensors in vehicles, that constantly change their location. Such sensors are referred to as air quality sensors and are part of the air conditioning system (Seat, n.d.). More information about these sensors is given in chapter 2.4.3.

According to be able to use this data reasonably, some systems and interfaces have to be explained. In vehicles, there exist nowadays a variety of control systems, on the one hand to improve the safety and comfort for the driver on the other hand to reduce the fuel consumption and emissions (see chapter 2.2.3). In order that these control systems do not have point-to-point wiring, serial bus systems are used. This allows the systems to communicate

with each other and all the data can be read out at one interface (Dubitzky & Karacay, 2013). In order to use this data for geospatial applications, the interfaces of the OGC are of great importance. As part of the Sensor Web Enablement (SWE) initiative, some services and interfaces for the request, access or use of information of heterogeneous sensors have been created. The service SOS is responsible for the provision of sensor data (OGC, n.d.b). Thus, the air quality data of the sensors in the vehicles are made available to the user via CAN-Bus and SOS.

The important facts about CAN-Bus, the SWE initiative and the SOS standard are explained in the following section. Moreover, an overview about air quality indices is given, in particular, the index CAQI is mentioned.

2.4.1 CAN-Bus

Nowadays, most new vehicles have more than 100 ECUs (electronic control units) and up to eight kilometres of wires (Brünglinghaus, 2014). Due to the fact that the increased use of ECUs leads to enormous wiring harnesses in vehicles and many of these systems should communicate with each other, so-called bus systems have come into focus. Bus systems are line systems which serve for the data transmission of different systems. In the automotive sector, the CAN-Bus system has become established as a standard system (Verein Freier Ersatzteilemarkt e.V., n.d.).

Bus systems and interfaces are applied to network various ECUs in a vehicle. The CAN-Bus was developed by Robert Bosch GmbH in the 80ers, which is a differential fieldbus system. Basically CAN uses a two-wire cable (twisted pair) as the transmission medium (Alt, 2009). The application of the bus system not only reduces the wiring harness but also decreases the weight of the vehicle. The data transmission takes place after the broadcast network, where all ECUs receive messages. In addition, all nodes on the bus have equal rights, which is also referred to as a multi-master-system (Rathgeber, 2007). Each ECU consists of a host processor, a CAN-controller and a CAN-transceiver, which are responsible for the data transmissions (Rezha, Saputra, & Shin, 2015). In principle, the host processor sends messages with a unique identifier, without a specific destination. The host processor of all other controllers on the bus receives this message and decides on the basis of the identifier whether the message is relevant or can be ignored (Rezha et al., 2015; Zimmermann & Schmidgall, 2014). The transceiver converts the bits received from the controller into a signal and forwards it to the bus. It is also responsible for the reverse process. The CAN-controller serves as a buffer for the input and output notifications (Rezha et al., 2015). This system offers the advantage that measured variables which

are needed by other control units do not need to be recorded by their own sensors but are transmitted via the CAN network from another control unit (ME-Meßsysteme GmbH, n.d.).

As a result of CAN is low cost, non-sensitive and real-time capable, it is also used in many other sectors such as in medical technology, industrial automation or elevator control. The interference immunity is ensured primarily by the fact that the signal of the second line is transmitted redundantly inverted (= differential signal) to the first line. Basically, CAN is able to transmit bit rates up to 1 Mbit/s, with all nodes having to process the notification at the same time. Therefore, the cable length depends on the bit rate. For a bit rate of 1 Mbit/s, a cable length of about 25 m is necessary (ME-Meßsysteme GmbH, n.d.).

In the following figure 2.22, the concept of the CAN-Bus is shown schematically. The current loop is represented by the two twisted wires, CAN-High and CAN-Low, with a reversible voltage resistor at the end of the bus (Bates, 2014).

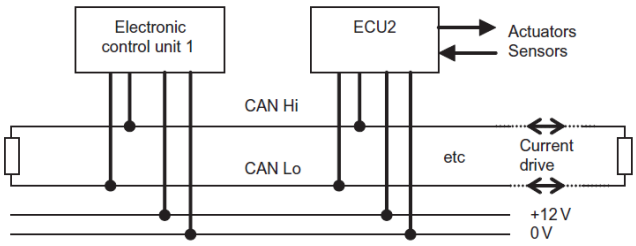

Figure 2.22: Schematic diagram of the CAN-Bus system (Bates, 2014, p.285)

2.4.2 Sensor Web Enablement

Sensors are able to monitor conditions such as temperature, vibration, sound, movement, pressure or pollutants at various positions. Several sensors are combined to form a sensor network that can be accessed through computer-aided networks (Reed et al., 2013). Since most sensors are built in a monolithic system and the data could not be used across system and domain boundaries, OGC developed the SWE-standard (Resch, 2010). This Geo-Sensor Web approach pursues a high degree of interoperability, scalability, intelligence and enables the integration of measurement data into spatial data infrastructures (Reed et al., 2013; Resch, 2010; Wupperverband, n.d.). Across the Web or other networks, it is possible to locate, access or use sensors by means of standard protocols or application program interfaces

(APIs) (Botts, Percivall, Reed, & Davidson, 2007; OGC, n.d.b; Reed et al., 2013). One of the most important components is the location, which plays an important role for every sensor (OGC, n.d.b).

Interoperable interfaces as well as metadata encodings enable heterogeneous sensors to be integrated into information infrastructures in real time. Moreover, the sensors can be incorporated into a wide variety of devices that have a Web connection. Examples include air pollution monitors, flood gauges, stress gauges on bridges, Webcams, or airborne earth imaging devices (Botts & Liang, n.d.). In order to implement the SWE initiative, a number of standard interfaces for web services are required (Reed et al., 2013). Among the most important OGC standards for the SWE belong (OGC, n.d.b):

- **Oberservations & Measurements (O&M)** - Standard that archives observations or measurements from a sensor in the form of XML and standard models, or makes them available in real time (Botts & Liang, n.d.).
- **PUCK Protocol Standard** - Protocol that enables automated installation, configuration and operation of the sensor. In addition, driver codes and other information (metadata) about the device are stored (OGC, n.d.a, n.d.b).
- **Sensor Model Language (SensorML)** – Standard, used to describe the sensor systems and processes transmitted as standard models or XML (OGC, n.d.b).
- **Sensor Oberservation Service (SOS)** - A web service to receive observations of sensors and sensor information (OGC, n.d.b).
- **Sensor Planning Service (SPS)** - A web service that can be used to query user-controlled observations and acquisitions, serving as an mediator between the client and a management system (Botts & Liang, n.d.).
- **SWE Common Data Model** - A model that identify the communication of sensor data between the nodes within the SWE architecture (OGC, n.d.b).
- **SWE Service Model** - A model that determines the data types for using the SWE services (OGC, n.d.b).

In addition, there are two important services that are not standards but are an integral part of the SWE.

- **Sensor Alert Service (SAS)** - A web service interface for issuing and subscribing to sensor alerts (Reed et al., 2013).
- **Web Notification Services (WNS)** - A web service interface, which is responsible for the asynchronous transmission of notifications and warnings generated by SAS and SPS (Reed et al., 2013).

Sensor Observation Service

SOS is a standardized interface that makes it possible to access observations from heterogeneous sensor systems and to manage and request metadata (Bröring, Stasch, & Echterhoff, 2012). The service supports both fixed and mobile sensors, which record the data in-situ or remotely. The interface communicates between a client and a data archive or a real-time sensor system. Sensor data are returned as observations to the client (Bröring et al., 2011). The sensor- and observation data can be retrieved or managed by using APIs. The data obtained from the sensor systems make up most of the geodata utilized in geospatial systems. Therefore, SOS is an important part of the SWE framework, which allows the access and integration of observation data from sensor systems (Reed et al., 2013). SOS employs the O&M - standard to model requests of the observations and the SensorML - standard to describe the sensors and sensor systems (Simonis, 2008).

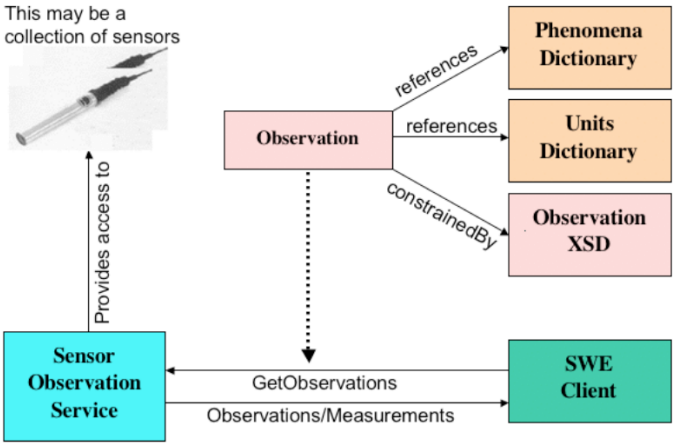

Figure 2.23: Sensor Observation Service Concept (Reed et al., 2013, p.11)

The SOS concept is described in figure 2.23, where an SWE client uses the SOS to receive observations from a collection of sensors. The requirements of the client can also be regulated by the SOS. Client affects the registries, which deliver metadata for the different sensor types and are able

to provide useful data (Reed et al., 2013).

Generally, the service and the client, which is the consumer, exchange standard messages via HTTP protocols. The requests to the service are made either through the HTTP POST or the HTTP GET method, indicating parameters and request type. The answers of the service are XML compliant with the corresponding components (istSOS - Instituto Scienza della Terra, n.d.).

The structure of the standard is divided into a core and extensions due to its operations and functionalities, whereby the core profiles are mandatory in an SOS service (istSOS - Instituto Scienza della Terra, n.d.; Simonis, 2008). The core includes the three operations *GetCapabilites*, *GetObersvation* and *DescribeSensore*. *GetCapabilities* delivers metadata and information about the operations being performed, *DescribeSensor* provides sensor descriptor queries, and *GetObservation* delivers direct access to observations based on spatial, temporal, and thematic filtering. In addition to the core extensions can be determined to add further operations. *Transactional Extension* (RegisterSensor, InsertOberservation) provides operations for inserting and deleting sensor descriptions and sensor observations, *Enhanced Extension* supplies additional functions for querying, for example, certain observed features, and *Result Handling Extension* is used for direct insertion or retrieval of observation results (Bröring et al., 2012).

An overview of the mentioned SOS requests is given in figure 2.24 as UML (Unified Modeling Language). On the left side the data consumers' view and on the right side those of the data producers are displayed.

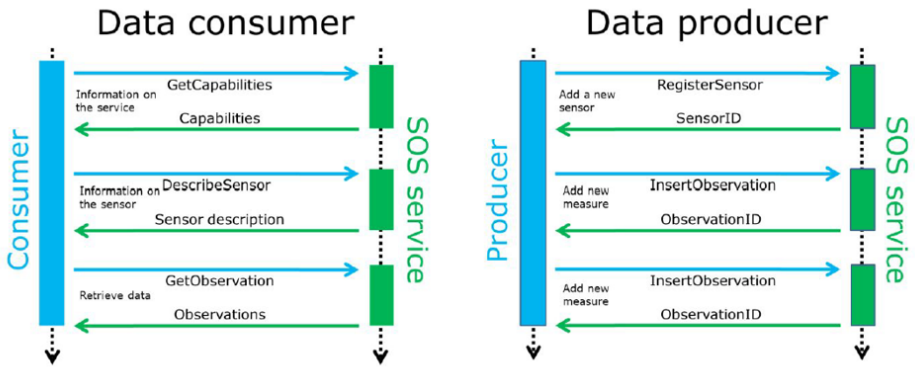

Figure 2.24: UML diagram from data consumer (left) and data producer (right) (istSOS - Instituto Scienza della Terra, n.d., p.8)

Basically, the SOS consists of the five objects, *Observations*, *Procedure*, *ObservedProperties*, *FeaturesOfInterest* and *Offering*. The heart of the stan-

dard are the *Observations* that describe measurements at specific times. These are presented according to the O&M data model. As a *Procedure*, the creator of the *Observations* is specified, which is usually a sensor. This is constituted in the form of the SensorML data model. The observed phenomena, such as air temperature or particulate matter, are referred to as *ObservedProperties*. These consist of a URI (uniform resource identifier), which conforms to the O&M standard. Accordingly, the individual *ObservedPropierties* are represented by om:observedProperty. The *FeatureOfInterest* refers to the *Observations*, where an in-place device is the sensor location and a remote device is the target location. These are appropriately described by O&M standard according to om:featureOfInterest. *Offerings* allow multiple sensors to be grouped together. These are represented as sos:OberservationOffering (istSOS - Instituto Scienza della Terra, n.d.).

istSOS An implementation of the SOS standard was carried out by the Institute of Earth Sciences (IST, Instituto Scienze della Terra), which is called istSOS. This has been operated since 2009, with the goal of making it easier to implement collected data into the SOS standard, ensuring better management, provisioning and integration of the data. The software is written in Python and uses PostgreSQL, Apache and GDAL. The software architecture of istSOS is comparable to a peach. The peel is represented by a Web Administration interface (wainterface). Using a graphical user interface (GUI), data can be managed better and faster. This interface is based on a RESTful service, the walib. This can be compared to the pulp of the peach. The core is described by the istsoslib. This originally served to support the implementation of the standard but has been enhanced by more advanced features. The three elements mentioned cooperate with each other and provide different interfaces for people, processes or clients. An overview about the software architecture of istSOS is given in figure 2.25.

The software structure is based on a factory approach with three modules. The first module consists of the filter, which represents an interface for converting the requests into python objects. The HTTP requests (GET or POST) contain the transmitted parameters and values. In the next step, the requests are accepted by the Responder module, which interacts with the istSOS database. The responder collects the necessary information. The third module is the renderer, which is accountable for the conversion of the information into the SOS response format. Generally, the SOS requests of istSOS are instantiated in the order factory_filter, then factory_responder and last factory_renderer. These call the responsible classes to acquire the right answer (istSOS - Instituto Scienza della Terra, n.d.).

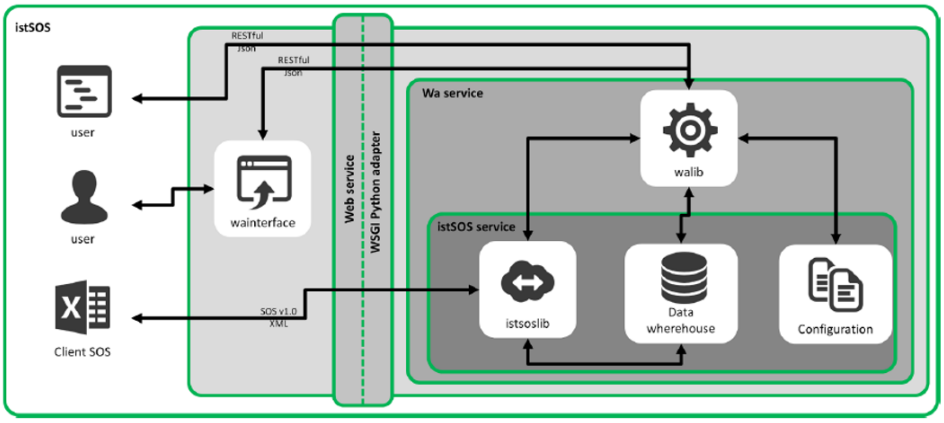

Figure 2.25: software architecture of istSOS (istSOS - Instituto Scienza della Terra, n.d., p.12)

2.4.3 Air quality sensor

The following paragraph introduces the air quality sensor built into the vehicles. Air quality sensors discover harmful gases in the outside air and prevent the entry of pollutants into the vehicle interior through ventilation systems (paragon AG, n.d.a). The sensor is located in the intake channel to directly measure the flow (HELLA KGaA Hueck & Co, n.d.). An integrated gas sensor responds to oxidizable (CO, C_6H_6, C_7H_{16}, C_6H_{14}) and reducible gases (NO_x, SO_2, H_2S, CS_2) and thus discovers the pollutants contained in the air (Gevatter & Grünhaupt, 2006; HELLA KGaA Hueck & Co, n.d.). This degradation is transferred via a signal to the climate control devise, whereby the fresh- recirculation control is automatically activated (HELLA KGaA Hueck & Co, n.d.). That means if the outdoor air quality is poor, the fresh air flaps are closed and the recirculating air is switched on to ensure good air quality inside the vehicle (Gevatter & Grünhaupt, 2006). In addition, the sensitivity of the sensor to parameters such as temperature, fan level, etc. is determined by a software (paragon AG, n.d.a).

Furthermore, there are also own particle sensors, which can be coupled with air quality sensors or CO_2 measurements. Such dust sensors can determine PM1, PM2.5, PM5 and PM10 values. In addition, these sensors can be equipped with a Bluetooth interface, which allows data to be transmitted in real time to a mobile device (paragon AG, n.d.b).

2.4.4 Air quality index

In many cities pollutant concentrations are continuously measured at several locations with monitoring stations (Plaia & Ruggieri, 2011). With such measurements predictions can be made or mathematical models can be reviewed. Many parameters such as the road structures, building structures or topography of a city influence the pollutant concentrations, which are not discussed in detail in this thesis (Bagieński, 2015). In order to provide pollutant concentrations to the population and to evaluate the health risk to humans, air quality indices are used (Bagieński, 2015; Plaia & Ruggieri, 2011). The benefit of using indexes is that they can sum up complex situations into one figure and therefore it is possible to make comparisons in time and space (Bruno & Cocchi, 2007). While creating an index is a broad generalization that involves information loss, it is indispensable for communication purposes. Because of these facts, there are many different indices (van den Elshout, 2012).

The literature describes several approaches for the calculation of indices which are similar in their basic concept but often differ in their practical implementation. The indices differ according to the number of classes, their descriptive terms and colour, update frequencies, pollutants used, class bounds and average times (Leeuw & Mol, 2005).

For the purpose of making the pollutant concentrations understandable for the population, the indices range mostly from good to poor (Plaia & Ruggieri, 2011). Shooter and Brimblecombe give a good definition about air quality index: *"Air quality indices aim at expressing the concentration of individual pollutants on a common scale where effects, usually health effects, occur at a value that is common to all pollutants"* (Shooter & Brimblecombe, 2009 quotes from Plaia & Ruggieri, 2011, p.166). This means that air quality indices are a simple and comprehensible method of measuring air quality, taking into account the impact on human health (Plaia & Ruggieri, 2011). Furthermore, Shooter and Brimblecombe refer two reasons to create an index. On the one hand, it serves to generate a link between air pollution and health effects in order to implement countermeasures or adjustments. On the other hand, an index provides a clear overview of complex information and can be used, for example, to develop guidelines or to review standards (Shooter & Brimblecombe, 2009 quotes from van den Elshout, Léger, & Heich, 2014). Van den Elshout, Léger, and Heich adds a third one to the two reasons. The index is also intended to help people understand air quality issues and to raise their awareness.

However, indices also bring their disadvantages. In particular, the relationship between air quality and health is not always clear and therefore

difficult to quantify. Furthermore, the index value usually only refers to an average time (daily, hourly, etc.), whereby the health effects can last both short term and long term (van den Elshout et al., 2014).

Ramos et al. describe a variety of methods for calculating the air quality index. The presented indices are clearly displayed in table A.2, which are listed by pollutants, number and ranges of categories, symbolization and health recommendations. The first eight indices originate from government agencies, and the remaining five indices were evolved by the research community (Ramos et al., 2018). Among the indices is the CAQI (Common Air Quality Index), which will be explained in more detail in the next section.

CAQI

The following paragraph introduces the index CAQI, which plays an important role in the European region. Due to the fact that ZAMG (Zentralanstalt für Meteorologie und Geodynamik) refers to the CAQI for the production of the air quality index in Austria, it will be considered in more detail (Umweltbundesamt, n.d.h).

In order to compare the air quality in European cities simply and comprehensibly, the CAQI was evolved as part of the CITEAIR project (an INTERREG IIIC project) (van den Elshout, 2012). Since 2006 exists a platform (www.airqualitynow.eu) on which the indices of over 100 cities are provided (CITEAIR, n.d.; van den Elshout, 2012).

The CAQI is divided into the following three indices depending on the time period. The hourly index represents today's air quality based on hourly values and is refreshed every hour. Another index is the daily index, which describes the average air quality from the previous day, based on daily values. This index is updated every day. In addition, the annual index characterises the air quality of a city for the whole year. The index is calculated on the basis of the annual mean values of pollutants and is updated annually.

Basically, the hourly and daily indices are calculated in a similar way (see table 2.7). These have a scale from '0' (very low) to '>100' (very high), which is divided into five levels. The air pollution is therefore expressed by relative values. To better assimilate the indices of the cities, the CAQI is subdivided in a background and a roadside index. The background index describes the common air quality in a city, using monitoring stations in the background. By contrast, the roadside index characterizes the air quality in streets based on monitoring station on the roadside. The indices consist of core pollutant, which are necessary to calculate the index value and other pollutant. The background index includes the three main pollutants NO_2,

PM10 and O_3 in the computation and if data are available the pollutants PM2.5, CO and SO_2. The main pollutants NO_2 and PM10 and as additional pollutants PM2.5 and CO are considered at the roadside index.

Generally, the determination of the index is based on the worst pollutant. First, the respective sub-index for all pollutants is decided by means of the grid. Subsequently, the total index is identified from the highest sub-index value. The grid thresholds were decided on the basis of EU air quality guidelines, values of similar indices, and pragmatic considerations (van den Elshout, 2012). To calculate a sub-index, the pollutant limits of the measured pollutant and the index range of the air quality index are used, which is explained in the following equation:

$$S_x = \frac{P_x - P_{lo}}{P_{up} - P_{lo}} \cdot (I_{up} - I_{lo}) + I_{lo} \tag{2.21}$$

Where,

S_x = sub-index,
P_x = measured pollutant concentration,
P_{lo} = lower limit value of pollutant concentration,
P_{up} = upper limit value of pollutant concentration,
I_{up} = upper index limit,
I_{lo} = lower index limit (Ramos et al., 2018).

Table 2.7: Pollutants and calculation grid for the CAQI hourly and daily grid (van den Elshout, 2012, p.3)

Index class	Grid	Traffic						City Background							
		core pollutants			pollutants			core pollutants				pollutants			
		NO2	PM10		PM2.5		CO	NO2	PM10		O3	PM2.5		CO	SO_2
			1-h.	24-h.	1-h.	24-h.			1-h.	24-h.		1-h.	24-h.		
Very low	0	0	0	0	*0*	*0*	0	0	0	0	0	*0*	*0*	0	0
	25	50	25	*15*	*15*	*10*	5000	50	25	*15*	60	*15*	*10*	5000	50
Low	25	50	25	*15*	*15*	*10*	5000	50	26	*15*	60	*15*	*10*	5000	50
	50	100	50	*30*	*30*	*20*	7500	100	50	*30*	120	*30*	*20*	7500	100
Medium	50	100	50	*30*	*30*	*20*	7500	100	50	*30*	120	*30*	*20*	7500	100
	75	200	90	50	*55*	*30*	10000	200	90	50	180	*55*	*30*	10000	*350*
High	75	200	90	50	*55*	*30*	10000	200	90	50	180	*55*	*30*	10000	*350*
	100	400	180	100	*110*	*60*	20000	400	180	100	240	*110*	*60*	20000	500
Very High*	> 100	> 400	>180	>100	*> 110*	*>60*	>20000	> 400	>180	>100	>240	*> 110*	*>60*	>20000	>500

NO_2, O_3, SO_2: hourly value / maximum hourly value in µg/m^3
CO: 8 hours moving average / maximum 8 hours moving average in µg/m^3
PM_{10}: hourly value / daily value in µg/m^3

* An index value above 100 is not calculated but reported as " > 100"

The background and traffic situation are also considered in the annual index, but this is calculated differently from the hourly and daily indices.

In general, the annual index gives the air quality in a city for one year compared to the European norms. In the strict sense, the distance to the objectives of the EU directives (annual air quality standards and objectives) is determined. The norms are based on suggestions and health care prepared by the World Health Organization. If the limit values for the pollutants are not met, the limit value is greater than one, otherwise it is lower. The limit values and the calculation of the annual index are shown in table 2.8 (van den Elshout, 2012).

Table 2.8: Calculation scheme for the year average index (van den Elshout, 2012, p.23)

Pollutant	Target value / limit value	Calculation
NO_2	Year average is 40 µg/m^3	Year average / 40
PM_{10}	Year average is 40 µg/m^3	Year average / 40
PM_{10} daily	Max. number of daily averages above 50 µg/m^3 is 35 days	Log(number of days+1) / Log(36)
Ozone	25 days with an 8-hour average value >= 120 µg/m^3	# days with 8-hour average >=120 / 25
$PM_{2.5}$	Year average is 20 µg/m^3	Year average / 20
SO_2	Year average is 20 µg/m^3	Year average / 20
Benzene	Year average is 5 µg/m^3	Year average / 5
CO	-	Not calculated

2.5 Eco-friendly Routing models

The basis for creating an eco-friendly routing system is the development of a vehicle emission model (Zeng et al., 2017). Such models are currently the most important applications for assessing the influence of developed transport technologies and transport projects. In general, there are many models that estimate fuel consumption and vehicle emissions. (Faris, Rakha, Kafafy, Idres, & Elmoselhy, 2011). Faris et al. subdivided them into the five classes, scale of the input variables-based modelling, formulation approach-based modelling, type of explanatory variable-based modelling, state variable value-based modelling and number of dimensions-based modelling. In this thesis, the models are presented according to the scaling, which are subdivided into macroscopic, mesoscopic or microscopic models, depending on the degree of accuracy of the desired model (Zeng et al., 2017). For the simulation of a dynamic behaviour of the traffic flow, it is often too imprecise to estimate emissions by means of traffic counts combined with statistical methods (Pandian et al., 2009). Therefore, it is important to use traffic flow models that allow accurate analyses of speed and acceleration in specific situations (Schmidt & Schäfer, 1998).

Macroscopic models calculate emission rates due to aggregated parameters or the average fuel consumption is estimated (Zeng et al., 2017). These are suitable for estimating emissions for larger areas but not for dynamic assessments (Barth et al., 2001). However, microscopic models take into account parameters such as the instantaneous speed, instantaneous engine condition, driving behaviour or interactions with the surrounding vehicles. Thus, the behaviour of the vehicles is constantly monitored (Pandian et al., 2009; Zeng et al., 2017). However, such models are not optimally suited for real-time eco-routing in large networks (Bandeira et al., 2014). Another disadvantage of microscopic models is that information such as split-second velocity profiles are not always available and therefore such models may not be ideally suited for routing applications. To avoid these constraint, mesoscopic models are recommended (Zeng et al., 2017). Mesoscopic models are between macroscopic and microscopic models, dealing with fuel consumption or vehicle emissions on a link (Pandian et al., 2009; Zeng et al., 2017). Therefore, it is not necessary to have instantaneous data about the vehicle (Zeng et al., 2017). Such models aggregate the behaviour of vehicle groups by considering simulations in small steps (Pandian et al., 2009).

In the following chapters a closer look at microscopic, macroscopic and mesoscopic models is given. The most important emission models for each scaling are presented. A brief overview of the structure of the individual models as well as their input parameters and outputs are given.

2.5.1 Microscopic models

Based on instantaneous speed and acceleration data, microscopic models evaluate fuel consumption and emission rates, which are aggregated for the entire network. Basically, the actual fuel consumption is determined from the fuel consumption rate and the vehicle performance. In order to do this, information about road conditions and vehicle characteristics are needed in a matter of seconds. Microscopic models are mostly used to estimate individual transportation projects because the information about fuel consumption is not suitable for aggregation. For microscopic traffic simulations in which the fuel consumption of individual vehicles is evaluated, these models can be exerted (Yue, 2008). The following paragraph presents the most important microscopic models, which refer to Faris et al., Elbassuoni and Abdel-sRahim and Yue.

CMEM

The Comprehensive Modal Emissions Model (CMEM) is a modal emission model suitable for light-duty vehicles and trucks, which was developed by An et al.. On the basis of a simple parametric physical concept, second-by-second emissions can be forecasted under different driving conditions. The model was developed on more than 300 real vehicles with their own dynamometer tests. Overall, the model includes six modules which are engine power, engine speed, air / fuel ratio, fuel use, engine-out emissions, and catalyst pass fraction. As input factors operating variables and model parameters are required. The operating variables include the three variables second-by-second speed, grade and accessory use. The model parameters are divided into three groups according to availability. The first group includes parameters from the public domain, which are for instance the mass or the air drag coefficient. Generic parameters such as rolling resistance belong to the second group. The third group includes parameters that must be calibrated based on measurements, such as engine friction factor. The result of the model are both the fuel consumption and the exhaust emissions (An et al., 1997). The traffic microsimulation software PARAMICS has taken over CMEM (Faris et al., 2011). The modular structure of this model is shown in figure 2.26.

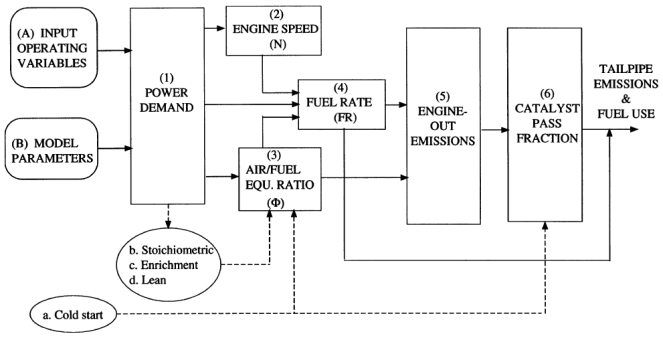

Figure 2.26: Modular structure of the CMEM (An, Barth, Norbeck, & Ross, 1997, p.26)

VT-microscopic model

Another microscopic model that estimates fuel consumption and emissions of vehicles is the Virginia Tech Microscopic energy and emission model (VT-Micro). Based on this model, the emissions of CO, HC, NO_x and CO_2 and the fuel consumption for individual vehicles can be predicted (Ahn, 2002).

The input parameters used are the instantaneous vehicle speed and acceleration profiles originally collected by the Oak Ridge National Laboratory on eight light duty vehicles. The calculation of the model is based on a multiple regression model consisting of linear, quadratic and cubic velocity and acceleration factors. To assure that fuel consumption or emission rates do not generate negative values, the natural logarithm is used (Ahn, 1998). The structure of the model is summarized as follows:

$$MOE_e \begin{cases} \sum_{i=0}^{3} \sum_{i=0}^{3} exp(k_{i,j}^{e} \cdot v^i \cdot a^j) \text{ for a} \geq 0 \\ \sum_{i=0}^{3} \sum_{j=0}^{3} exp(l_{i,j}^{e} \cdot v^i \cdot a^j) \text{ for a} < 0 \end{cases} \tag{2.22}$$

Where,

MOE_{e} = Instantaneous fuel consumption or emission rate [l/s or mg/s],
a = Instantaneous acceleration of vehicle [km/h/s],
v = Instantaneous speed of vehicle [km/h],
$k^{\mathrm{e}}{}_{\mathrm{i,j}}$ = Vehicle-specific acceleration regression coefficients for MOE_e,
$l^{\mathrm{e}}{}_{\mathrm{i,j}}$ = Vehicle-specific deceleration regression coefficients for MOE_e (Yue, 2008).

As the equation shows, the model considers the driving modes of acceleration, idling, cruising and deceleration. This takes into account the differences in emission rates between acceleration and deceleration modes (Yue, 2008). The accuracy of the model is less than 2.5 % deviation from the actual measured fuel consumption (Ahn, 1998). Because the structure of the model is not very complex, it can be used in any other microscopic traffic simulation model (Rakha & Ahn, 2004). VT-Micro has been integrated into the microscopic traffic simulation model INTEGRATION (Yue, 2008).

VeTESS

VeTESS (vehicle transient emissions simulation software) is a rather stationary modelling approach, which involves the dynamic behaviour of the engine. As a result, the engine power and the emission components NO_x, CO_x, HC and PM are estimated. The driving pattern, road grade and vehicle specifications are the three input parameters for the model. Basically, the total force that is done by the engine to move a vehicle is calculated (see equation 2.23).

$$F_{total} = F_{accel} + F_{grad} + F_{roll} + F_{aero} \tag{2.23}$$

Based on the applied force, the engine speed and the engine torque are derived. Subsequently, emission rates are evaluated using emission maps. The accuracy of the model for the estimation of fuel consumption and emissions is between 10 and 20 % (Faris et al., 2011). It should be noted that VeTESS only calculates emissions for a single vehicle during a driving cycle. The fuel consumption and emissions estimations are used in the CORSIM (corridor simulation) software, a microscopic simulation program (Elbassuoni & Abdel-sRahim, 2013).

VERSIT+

Another microscopic model is VERSIT+, which simulates emission factors and energy use factors for several vehicle fleets that can be used in different countries (Environmental Studies and Testing, n.d.). The model was developed from TNO (Netherlands Organisation for Applied Scientific Research) in the Netherlands and is able to calculate the emissions HC, CO, NO_x, NO_2, PM10 and CO_2 (Ligterink & De Lange, 2009). Depending on the traffic situation and type of vehicle, the emissions are distinguished considering real driving conditions. The special feature of VERSIT+ is that the model can be used at national, regional and local level. The model can be applied both for the development of national greenhouse gas decrease approaches and locally for enhancing air quality. In addition, environmental monitoring and environmental impact evaluations of transport arrangements can be carried out (Environmental Studies and Testing, n.d.). The model uses a database of over 20.000 measurements to predict emissions per vehicle for different driving behaviours (Ligterink & De Lange, 2009). The prediction is based on statistical modelling techniques that produce emission factor equations for each driving pattern, derived from velocity-time profiles (Environmental Studies and Testing, n.d.; TNO, n.d.). The forecasts serve as a support for decision-makers who can thereby create inducement for sustainable vehicle technologies. Furthermore, the model can be connected to traffic simulation models, thereby direct assessment of effect of transport measures such as green wave on air quality are enable (Environmental Studies and Testing, n.d.). However, the model has the disadvantage that the emission calculation is linearly dependent on the speed of the vehicle and thus the influence of the speed on the emission estimate is limited. One efficient traffic simulation software is the Advanced Interactive Microscopic Simulator for Urban and Non-urban Networks (AIMSUN), which is based on VERSIT+ (Faris et al., 2011).

PHEM

PHEM (passenger car and heavy duty vehicle emission model) is a microscopic model from the TU-Graz that simulates the energy consumption and the emissions CO, HC, NO_x, CO_2 and PM of vehicles and heavy duty vehicles (Rexeis, 2005; Zallinger, 2010). The model calculates the engine output, which varies with speed and road grade, for a given drive cycle from the driving resistances and driveline losses. The engine speed is computed from the driver's gearshift model, tire diameter and gear ratios. A performance map is used to interpolate the emissions for the current engine power and engine speed. The model structure of PHEM including the mentioned parameters is shown in figure 2.27. To improve the accuracy of the model, the method of dynamic correction as well as a cold start module was developed (Rexeis, 2005). The model has been integrated into the VISSIM software, which is a microscopic simulator for integrated networks (Faris et al., 2011).

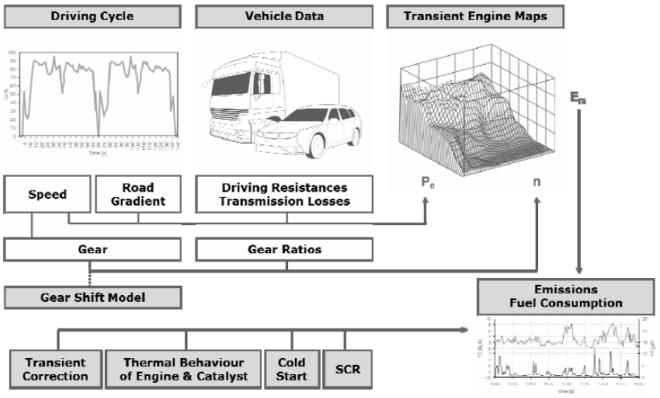

Figure 2.27: Overview of the model structure of PHEM (Haberl, Fellendorf, Luz & Hausberger, 2014, p.2)

EMIT

Another model which simulates instantaneous emissions and fuel consumption of vehicles is EMIT (emissions from traffic). EMIT considers the emissions of CO_2, CO, HC and NO_x, which was originally developed for gasoline vehicles, but can also be applied to diesel vehicles and other pollutants. The most essential components of the model are the engine-out emissions module and the tailpipe emissions module. The structure of the model is shown in figure 2.28. EMIT enables both to forecast exhaust emissions and emissions from the precursor engines. These model parts can better simulate, for instance, advancements in engine technologies or effectivity of mainte-

nance programs. The input parameter for the first module are the vehicle category and the instantaneous speed and acceleration, the output being the instantaneous fuel consumption and the engine-out emissions. Vehicle characteristics include, for instance, engine parameters, vehicle mass or catalytic converter. In addition, the road grade can be used as input, but this was given as zero in the development of the model. Instantaneous speed, acceleration and vehicle category are used as input to the second module, which calculates the instantaneous tailpipe emission rates (Cappiello, 2002).

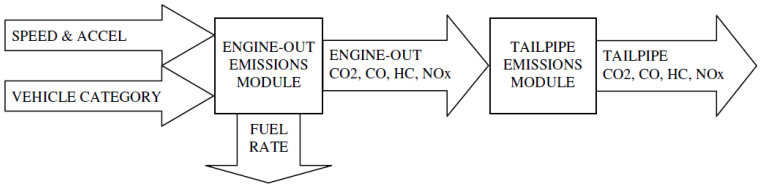

Figure 2.28: Structure of the model EMIT (Cappiello, 2002, p.55)

Vehicle dynamics models

Furthermore, there are also a vehicle kinematics model, constant or variable power vehicle dynamics model or a gearshift model for assessment the instantaneous acceleration of vehicles (Faris et al., 2011). Rakha, Lucic, Demarchi, Setti, and van Aerde has developed a suitable vehicle kinematics model in which vehicle acceleration is calculated from tractive effort, rolling resistance, aerodynamic drag, and grade resistance (Rakha et al., 2001). The vehicle dynamics model with constant power rates the acceleration exclusively with the vehicle's tractive effort. Because this method is simpler, it is not so accurate. In the variable power vehicle dynamics model, the constant vehicle dynamics model is expanded with a linearly increasing variable vehicle power. However, this only slightly improves the accuracy. A better modelling approach is vehicle dynamics or gear shifting, where parameters such as weather, tires or road surface conditions can be better integrated and adapted.

The traffic simulation software such as PARAMICS, AIMSUN, VISSIM and CORSIM correspond the kinematic approach to estimate the acceleration, whereas the software INTEGRATION is based on the vehicle dynamics model (Faris et al., 2011).

2.5.2 Macroscopic Models

Assessment of fuel consumption and emission rates are used in macroscopic models with aggregated network or link-based parameters (Yue, 2008). Such models typically use the average speed and are frequently deduced from the relationship between fuel economy and average vehicle performance (Elbassuoni & Abdel-sRahim, 2013). Macroscopic models use a flow-density relationship that characterize the average behaviour of a fleet over a given period of time (Pandian et al., 2009). Basically, the relationships of speed, density and flow of traffic streams are modelled (Alexiadis, Jeannotte, & Chandra, 2004). At intersections, the average speed is calculated by speed and traffic volume data (Pandian et al., 2009). Macroscopic models are particularly useful for estimating the regional environmental effects of transportation projects. In most cases, a traffic planning model is primarily utilized to identify the average speed and the total mileage throughout the network. Subsequently, average fuel consumption and emission rates are calculated using an emissions model (Yue, 2008). The following discussed models are based on those of Faris et al. and Yue.

MOBILE

For the sake of completeness, MOBILE will be briefly explained despite its replacement to the MOVES model (chapter 2.5.4)(U.S. Environmental Protection Agency, n.d.a). MOBILE is an emissions factor model developed by EPA (Environmental Protection Agency) in the USA that calculates HC, NO_x, CO, PM, SO_2, NH3 and CO_2 emissions and six air toxics for vehicles, motorcycles, and trucks (U.S. Environmental Protection Agency, n.d.a; U.S. Environmental Protection Agency, 2002). The model no longer takes vehicle and emission standards into account after 2004 and has been superseded by MOVES (U.S. Environmental Protection Agency, n.d.a). One of the main reasons why MOBILE was replaced by MOVES2010 in the USA is the lack of calculation of fuel consumption (Faris et al., 2011). The fuel consumption cannot be derived from CO_2 emissions, as CO_2 emissions depend only on the type of vehicle and not on speed, fuel type or temperature (Yue, 2008).

EMFAC

Another macroscopic emission model in the USA is the EMFAC (emission factor) developed by the California Air Resources Board (CARB), which is used only in the state of California (U.S. Environmental Protection Agency,

2015b). The model calculates HC, CO, NO_x, PM, CO_2 and SO_x emissions and fuel consumption for trucks, buses, vehicles, motorcycles and camper vans (California Environmental Protection Agency, 2014; U.S. Environmental Protection Agency, 2015b). In addition, it is possible to adjust over time, humidity, temperature, kilometres travelled etc.. The model can be used by decision-makers both at the state and local levels to support programs to improve air pollution (U.S. Environmental Protection Agency, 2015b). The most recent version is EMFAC2017, with the most recent approved version being EMFAC2014 (California Air Resources Board, n.d.).

Watson Model

The Watson model is a fuel consumption model developed by Watson, Milkins and Marshal which is based on average speeds (Yue, 2008). The model is also called a lumped coefficient model (Akcelik, 1983). The positive acceleration change of the kinetic energy is expressed as a forecast variable. The fuel consumption is calculated from the following formula (Yue, 2008):

$$F = K_1 + K_2/V_s + K_3 V_s + K_4 PKE \tag{2.24}$$

Where,

K_1 to K_4 are constants, which are yield from the regression analysis:

K_1 = rolling resistance, transmission losses, engine efficiency,

K_2 = idle consumption (no load, or base engine friction),

K_3 = aerodynamic drag, transmission losses, engine efficiency,

K_4 = vehicle mass, transmission losses, engine efficiency (Akcelik, 1983),

F = fuel consumed [l/km],

V_s = space mean speed [km/hr],

PKE (Positive kinetic energy) = sum of the positive kinetic energy changes during acceleration [m/s^2] and is expressed by:

$$PKE = \sum (V_f^2 - V_i^2)/(12.960 X_s) \tag{2.25}$$

Where,

V_f = final speed [km/hr] f,

V_i = initial speed [km/hr] i,

X_s = total section length [km] (Yue, 2008).

So, the input parameters are the average speed, final speed, initial speed and the total section length. Though the model can evaluate fuel consump-

tion well, microscopic models with instantaneous speed are more accurate (Faris et al., 2011).

COPERT

Another macroscopic model is COPERT, which is an EU standard vehicle emission calculator software for road transport within the EEA member countries. The model considers parameters such as vehicle population, speed, mileage, ambient temperature and estimates energy consumption and emissions for a desired region or country. In addition to the emissions, COPERT also calculates the non-exhaust emissions caused by fuel evaporation, tire or brake wear (EMISIA, n.d.). Depending on data availability, three different methods (tier 1, tier 2, tier 3) can be used (European Environment Agency, 2016a). In total, more than 450 different vehicle types are taken into account (EMISIA, n.d.). The basic equation for the estimation of emissions is composed of the activity data (AD) and the emission factors (EF), which is expressed as follows (European Environment Agency, 2016a):

$$Emission = AD * EF \tag{2.26}$$

COPERT is an essential tool for many European countries to calculate emissions at nation, regional or local scale. It contains all major pollutants from greenhouse gases to air pollutants up to toxic species. The advantage of using a software tool to estimate emissions is that transparency and standards are created, allowing for consistent, transnational comparisons (EMISIA, n.d.).

2.5.3 Mesoscopic Models

Mesoscopic models have both properties of microscopic models and of macroscopic models. The mesoscopic model, on the one hand, consider the individual vehicle as a unit, as does the microscopic model, and on the other hand, the movements of the vehicles are determined by means of average velocities on a link, as in the macroscopic model (Alexiadis et al., 2004). In general, the input parameters are more aggregated than microscopic models and disaggregated as macroscopic models (Yue, 2008). Although such models are less accurate than microscopic models, they are more suitable for planning analysis (Alexiadis et al., 2004). In the following, the two most important models MEASURE and Elemental model are discussed, which are based on the selection of Faris et al..

MEASURE

Mobile Emission Assessment System for Urban and Regional Evaluation (MEASURE) is a GIS-based modelling approach which was developed by researchers of the Georgia Institute of Technology (Bachman, 1998). The model considers various vehicle conditions for the modal operations start, idling, driving, acceleration and deceleration (Bachman, Sarasua, Hallmark, & Guensler, 2000). The calculation of emission rates is based on a refined tree-based regression analysis, with test data from the EPA and the California Air Resource Board. The start emission module and the on-road emission module are among the two main modules of the model. The start emission module is calculated from the start characteristics dispersion and the start emission rates. The on-road emission module evaluate emissions based on the operating modes (Yue, 2008).

As data input both vehicle technical attributes such as model year or engine size and operating requirements such as road gradient or road flow can be inserted. The emissions are presented as outputs depending on the type, grid cell, operating mode, facility type (Bachman et al., 2000). The emissions HC, CO and NO_x are taken into account (Bachman, 1998). Data for the following five categories are necessary to develop the MEASURE model: spatial character, temporal character, vehicle technology, modal activity and trip generation (Bachman et al., 2000).

Elemental model

The Elemental Model is a simple theoretical-based model suggested by Herman and his teammates. The model is based on average speed, which is determined considering urban conditions. The fuel consumption is calculated as a linear function from the reciprocal of the average speed (average travel time per unit distance). The model is expressed by the following equation:

$$\Phi = K_1 + K_2 T, V < 55 km/hr \tag{2.27}$$

Where,

Φ = fuel consumption per unit distance,
T = average travel time per unit distance,
V(=1/T) = average speed.

K_1 and K_2 present model parameters, whereat K_1 express the vehicle mass and K_2 is a function of the average speed (Yue, 2008). Fuel consumption in average speed models depends on the travel distance, travel time and average speed (Bowyer, Akcelik, & Biggs, 1985). Due to the fact that

this model does not appropriate consider the increase in aerodynamic drag at higher speeds, it should be exerted at average speeds of less than about 50 km/h (Biggs & Akcelik, 1985).

2.5.4 Mixed Models

Referring to the literature, the model MOVES has been identified as a microscopic model according to Faris et al. and as a macroscopic model according to Elbassuoni & Abdel-sRahim, therefore in this thesis it is assigned to the mixed models. This allocation also confirms the present description of the model, which aims at scaling on all levels.

MOVES

In the USA, the emission modelling system MOVES (Motor Vehicle Emission Simulator) was developed by the EPA for greenhouse gases, air pollutants and air toxics at national, county and project level (U.S. Environmental Protection Agency, n.d.b). The aim of MOVES is to provide a simple model that can simulate accurately pollutants and emission processes for all vehicles on the micro, meso and macro scales (Koupal, Cumberworth, Michaels, Beardsley, & Brzezinski, 2003). In order to be able to implement the model on all scales, the Vehicle Specific Power (VSP) approach is used for emission generation (U.S. Environmental Protection Agency, 2003). This approach is based on instantaneous speed values for each driving cycle and information about the vehicle type (U.S. Environmental Protection Agency, n.d.c). The model is also suitable for nonroad mobile sources and considering user specifies conditions. These conditions include vehicle type, geographic area, time period, vehicle operating characteristics, air pollutants and road type. By using a Graphical User Interface (GUI), the user is allowed to enter the desired data (U.S. Environmental Protection Agency, 2015a). The user has two options on the micro-scale for entering vehicle activity data. First, the instantaneous velocity profiles can be entered for each link. In the second option, the user announces the operating mode distribution in a table (Elbassuoni & Abdel-sRahim, 2013). In addition, there exist two options for calculating emissions. On the one hand, the emissions can be simulated within a region or time span, on the other hand, it is also possible to calculate emission rates per activity unit (U.S. Environmental Protection Agency, 2012). The MOVES2010 version has replaced the previously used model MOBILE6 in the USA (U.S. Environmental Protection Agency, 2011). The latest version is MOVES2014b (U.S. Environmental Protection Agency, n.d.b). Furthermore, the model is based on a default database that

contains emission-related information from the USA (U.S. Environmental Protection Agency, 2015a).

Chapter 3

Implemenation and Experiment

After the theoretical basics have been discussed in detail in the previous chapters, these will be put into practice in the following section. The aim of this part is to generate a model that calculates CO_2 and low-fuel routes in the city of Graz, whereby the PM pollution on these routes is low. The driving resistances from chapter 2.3.1 serve as the basis for the creation of the environmentally friendly route. Due to the fact that the presented eco-friendly routing models in chapter 2.5 are very often not freely available, are limited to special input data and cannot be changed for individual settings, they were not used for the routing approach. However, it is emerged from the chapter that the model created is based on the mesoscopic approach, since vehicles are viewed as individual elements and an average speed of the individual edges is assumed. Furthermore, the theoretical knowledge from chapter 2.2 about road, vehicle and traffic characteristics are linked to the routing model. So that the routes pass through areas with lower particulate matter pollution, the principles of chapter 2.4 are applied. The implementation of the practical part was done with Python as programming language either by means of QGIS or IDLE (Integrated Development and Learning Environment).

3.1 Data basis

The following chapter introduces the data sources used for the routing. In general, the most important foundation is a routable road graph, which should be consist of nodes and edges. Furthermore, intersections were included in the routing, which refer to another data source. Finally, an investigation area must be defined to, in which the routing is performed. The data basis for the PM values is described in the course of the integration of the pollution for the routing (chapter 3.5).

3.1.1 Road network

In order to be able to perform a routing at all, it is basically necessary to use a routable road graph. In this thesis, the road graph was used by the Graphenintegrations-Plattform (GIP), which is uniform and intermodal throughout Austria. This traffic reference system contains all required information necessary for the public transport infrastructure in Austria. The model can be used for the entire public transport network and can be employed for a wide variety of applications, such as accident data management or traffic information. In addition, hierarchical route calculations for traffic planning or in the area of traffic management can also be carried out. Due to the fact that the traffic infrastructure in Austria is operated by different institutions depending on the area of responsibility, the current and complete data must be transmitted by the operators to the GIP. The GIP finally merges the different data into a single uniform system.

Basically, the real traffic network is depicted as a linear model. All traffic areas are represented by lines and nodes, whereby the topological properties are included. As mentioned before, the graph must be routable. Such a graph basically consists of nodes and edges. One or more edges are used to move from a selected node to another desired node. In the network, there is always at least one path leading to the destination node. Using search algorithms, short paths in graphs can be found from any starting point to a desired destination point, taking into account the edge costs (Graphenintegrationsplattform [GIP], 2018).

The routable data are provided in the form of text files. Each text file consists of a four-line header that includes the start of the table, the column header, the format of each column, and the number of records. Each record is marked with the abbreviation *rec* at the beginning of the line. The content of each line is separated by a semicolon. At the end of the table the number of data sets is displayed again (see figure 3.1). Texts contain double quotes and unknown values are marked with value *-1*. The data use the geographic coordination system with the projection WGS-84 (EPSG 4326).

The relationships between the tables are shown in figure 3.2. For the routing in this thesis only the two tables *Node* and *TurnEdge* were used. The table *Node* includes all nodes from the graph with the attributes ID, X-coordinate, Y-coordinate and Z-coordinate. The coordinates are based on the WGS-84 projection, as mentioned before. The Z-coordinate, which is used in chapter 3.2.2 for the calculation of the slope, refers to the elevation model of data.gv.at / Geoland from the year 2015. All turns, that are allowed between links are included in the table *TurnEdge*. This means that for all links not found in the table, turning is prohibited. Accordingly, two

```
tbl;Node
atr;NODE_ID;LEVEL;VIRTUAL_TYPE;X;Y;VIRT_LINKID;VIRT_PERCENT;BIKE_DELAY;STATUS;NODE_OBJECTID;VIRT_LINK_OBJECTID
frm;decimal(10);decimal(3,1);decimal(1);decimal(9,7);decimal(9,7);decimal(10);decimal(7,4);decimal(3);string(1);decimal(20);decimal(20)
num;2
rec;10347591;0.0;0;16.3253032;48.2079073;-1;-1.0000;-1;"U";10347591;-1
rec;10347722;0.0;0;16.3286169;48.2087490;-1;-1.0000;-1;"U";10347722;-1
end;2
```

Figure 3.1: Description of the structure of the Table Nodes (Graphenintegrationsplattform [GIP], 2019, p.14)

values are entered in the table, provided the turn is allowed in both directions. Thus, the turning relations are treated directed. The table *TurnEdge* contain the ID of the turn, the ID of the From-Link, the ID of the To-Link, the ID of the Via-Node and the trafficability.

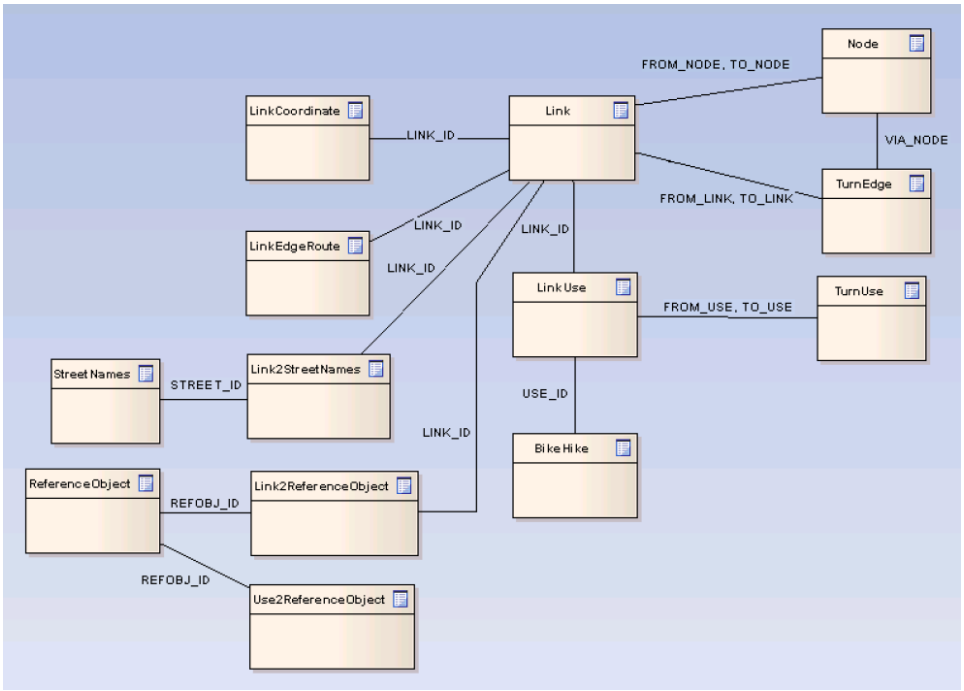

Figure 3.2: Overview about the relationship between the routing tables(Graphenintegrationsplattform [GIP], 2019, p.15)

In addition to the tables, there is still a geopackage, which contains the basis network of sections, nodes, links, usage strips and turning relations. Because the attributes are the same as in the *Link* table, the geopackage

was used in this thesis. The shapefile contains a multitude of attributes, which are listed in detail in the appendix (table A.1). For the routing, the columns ID of the link, ID of the from-node, ID of the to-node, average speed, maximum speed, drivability, length, structural form, construction status and one-way or driving ban are relevant (GIP, 2019).

3.1.2 Road junction

In addition to the road network, the locations of the intersections are needed. These can be downloaded for the city of Graz from the OpenStreetMap (OSM). Using the Overpass Turbo, an interactive query generator, independent queries about desired topics in the OSM can be made (Humanitarian OpenStreetMap Team, 2016). Afterwards the data can be exported into various data formats. For this thesis the traffic signals, stop signs and give way signs were exported as OSM raw data and saved as shapefile with the coordinate system WGS-84.

3.1.3 District boundaries

In order to determine the study area, the district boundaries of Styria, which are provided by data.gv.at were used. The data are available in the form of a shapefile in the coordinate system WGS-84 and includes the Styrian districts in 2015.

3.2 Data preparation

There are a few steps to take before the data can be used for routing. In the following section the preparation of the nodes and edges of the network graph are represented. In general, it should be mentioned that the GIP data are not completely correct, especially with regard to the permissible maximum speed of the roads and the turning relations, some incorrect informations are available. However, this is not relevant for the routing. Furthermore, the calculation of the edge costs, which is based on the driving resistances are explained. Finally, the traverse costs are described, which allow an integration of the turning behaviour for the routing.

3.2.1 Nodes and Edges

In order to prepare the road graph, first the area of investigation has to be defined. For this, the Graz city district was selected from the shapefile of the districts of Styria. The area of investigation determined based on the extend of the district of Graz. According to the study area, the road network was spatially selected, so that the data volume and thus the computing time are reduced. In the next step, the roads were again reduced by selecting only those roads that are in operation and are used and approved for vehicles only. The information for this was taken from the edges. Thus, the roads are prepared and can be used for the cost calculation (see chapter 3.2.2).

Next, the nodes were treated by selecting only those that are in the study area. The fact that the edges were selected again in the previous step, the nodes must also be reduced again, so that each edge has a beginning and an end node. Through these steps, a correct node-edge structure is given and the routing algorithm can be successfully performed. Thus, only those nodes were selected that are a start or end node of an edge. Finally, the road network is finished and can be used for further steps.

For the sake of completeness, it should be mentioned that basically no cycles are taken into account during routing. In order to realize this, it must be allowed to visit the node more often. Although this was implemented in the routing algorithm (see Chapter 3.4.2), the GIP data basis does not support cycles. Due to the fact that the cycles do not have much influence on the results of the routing, the data basis was not further processed.

3.2.2 Edge costs

In order to be able to carry out routing, costs have to be assigned to the edges. By looking for an environmentally friendly route in this case, the cost per edge is equivalent to fuel consumption in litres. Finally, the shortest path between two nodes is determined by the smallest sum of edge costs. The evaluation of the costs depends on the road, vehicle, and the traffic parameters mentioned in chapter 2.2. The basics for the calculation method of the costs are based on chapter 2.3.1. In addition to the fuel consumption, the time and length of the shortest paths are taken into account. Thereby, comparisons can be made between the shortest route after the fuel, after the time or after the path length.

As mentioned, one edge consists of a start and end node and there may be multiple polygon points in between. The edges contain several attributes, some of which were used for routing. The attributes trafficability and con-

Table 3.1: vehicle-relevant parameters for diesel cars (Hausberger, 2009, p.31)

	Mass [kg]	**Rated power [kW]**	**c_w-value [-]**	**A [m^2]**	**f_{R0} [-]**	**f_{R1} [s/m]**	**f_{R4} [s^4/m^4]**
Euro 6	1500	93	0.299	2.16	0.00872	0.000101	-1.38E-10

struction status were already utilized in the selection of the edges. One of the most important attributes used to calculate costs is the average speed. This includes plausible values for the travel time calculation (GIP, 2019). The speed is indicated both in and against the direction of travel and was assumed to be constant in the model. Another essential parameter which have to be evaluated before it could be used, is the slope. Therefore, the Z-coordinates from the nodes are used. On the basis of the Z-value from the start node, the Z-value from the end node and the length, the slope for each edge was calculated in percent. The length was already present in the dataset of the edges.

In order to calculate the driving resistances, vehicle-relevant parameters are still necessary. The parameters used in this thesis are from the model PHEM (chapter 2.5.1) and represent average vehicle data for diesel vehicles (see table 3.1). The values were assumed to be constant for the calculations. Another parameter that was adopted to be constant is the air density, which is necessary for the calculation of the air resistance. The standard value according to the International Standard Atmosphere (ISA) was used for this, which is 1.225 kg/m^3 at sea level and a temperature of 15 °C (Helmenstine, 2019).

On the basis of the driving speed, the slope and the vehicle-relevant parameters, the total driving resistances, which are composed of wheel, air, gradient and acceleration resistance, were calculated. Because the speed was assumed to be constant and intersections were implemented by traverse costs (see chapter 3.2.3), the acceleration was assigned the value zero. If the driving resistances are multiplied by the driving speed, the tractive-resistance losses results. Based on the calorific value and the efficiencies of the engine and power train, the fuel consumption in litres was identified. Thus, the consumption can be determined for any distance. By specifying the length of the edge, the cost was assigned to it. For those edges, where the fuel consumption is zero due to the road grade, the most economical track consumption, which arises when the engine is disengaged, was assigned (see chapter 2.3.3). Due to the fact that no engine speeds are known and therefore it is also unknown whether the engine is operating in coasting mode, this variant was selected. As parameter for the fuel consumption at idling, the value 0.6 l/h was used. This value is based on a study by Kumar, Singh,

Table 3.2: Overview of the factors that influence the emissions and fuel consumption of vehicles, that have been included or not in the routing

Category	**Factor**	**Routing**
road characteristics	grade	✓
	roughness	×
	texture	×
	road class	✓
	humps	×
	junctions	✓
	speed	✓
traffic characteristics	congestion	✓
	control delays	✓
	driving mode	×
	traffic control	×

Sharma, and Chalumuri that investigated the average fuel consumption of vehicles at idling (Kumar et al., 2015).

In addition, the calculation of fuel consumption is influenced by several factors, which were elaborated in chapter 2.2. Table 3.2 shows the main influencing factors of road and traffic characteristics, mentioned in the literature. The vehicle characteristics were only included by the mentioned constant parameters, a closer look at their influences for the routing would be too detailed. On the right side, the factors are marked with a checkmark if they are included in the routing and with a cross if not. The roughness and texture of the road are not taken into account because the roads in a city are mainly made of asphalt and therefore these two factors do not have much impact on fuel consumption. Due to the fact that there are only few humps and the locations of these in Graz are not known, these were also not included in the routing. The driving modes were not discussed in more detail, since the routing was carried out at constant speed. Furthermore, the traffic control was not included in the routing, but is briefly mentioned in the chapter 5.

Thus, road grade, road class, junctions, speed, congestion and control delays are included in the routing. The influence of the road slope was already considered at the slope resistance. The average speed was also embedded in the driving resistances. Control delays are inserted into the routing as part of the junctions. By performing the routing at constant speeds, no more in-depth quantifications are performed about control delays. For the integration of the factor congestion, a separate column was created at the edges. Thus, additional delays in seconds can be specified for each edge. The default value assigned to each edge is zero. As soon as the value is

Table 3.3: Influence of road classes on fuel consumption and CO_2

Max.speed [km/h]	**CO2 [g/km]**	**Fuel consumption [l/km]**	**Difference [l/km]**
> 60	1.4	0.000528302	0
<= 60	1.5	0.000566038	3.77358E-05
<= 50	1.8	0.000679245	0.000150943
<= 30	2.6	0.000981132	0.00045283

greater than zero, the factor is included in the routing. If the shortest route is calculated according to the time, the factor is adopted directly. However, if the route with the lowest fuel consumption is to be estimated, this factor is multiplied by 0.6 l per hour. As already mentioned at the driving resistances, this factor is based on the study by Kumar et al.. In addition to the congestion, intersections are still included in the routing. These are taken into account in the cost of traverses and thus presented in chapter 3.2.3.

The impact of different road classes on fuel consumption and emissions is based on chapter 2.2.1. Therefore, reference is made to the results of the study by Nesamani and Subrahmanian, where local roads cause the highest emissions. Local roads were adopted at up to 30 km/h, collector roads at up to 50 km/h, sub-arterial roads at up to 60 km/h and arterial roads at greater than 60 km/h. The allocation of the maximum speed to the road classes was based on The Indian Roads Congress. The CO_2 consumption was converted to fuel consumption by a factor of 2660, since 1 l of diesel burns CO_2 emissions of around 2.66 kilograms (Natural Resources Canada, 2014). The difference in fuel consumption between the classes of roads is added to each individual edge according to the maximum speed, taking the arterial roads as the starting point without additional fuel consumption (see table 3.3).

3.2.3 Traverse costs

In addition to the edges, traverses are also taken into account for the routing. Generally, traverses are complex edge to edge relationships, which usually employ as an orientated component. These form a connection from one node to another node via another node. Traverses are very commonly used to model turn behaviour (Hofmann-Wellenhof, Legat, & Wieser, 2003). However, this turning behaviour differs according to different possibilities at the individual intersections. On the one hand there is the possibility to turn in different directions and on the other hand there are different types of intersection, depending on traffic regulations. For the routing, traffic lights,

stop signs, give way signs and roundabouts were taken into account. The data for the traffic signs originates from the OSM, as already explained in chapter 3.1.2. In order to use the data for the network graph, it requires some processing steps.

First, the traffic signs were divided into two groups depending on the mapping. On the one hand, those traffic signs, which are located exactly at the intersection point of the streets, were selected (see figure 3.3(a)). These were assigned to the next node of the graph. Due to the different data bases (OSM and GIP), the edges have different topological structures. Accordingly, the traffic signs had to be partially reworked by hand. On the other hand, at more complex intersections, the traffic signs located on the incoming roads were processed (see figure3.3(b)). These were allocated to the nearest edges due to the street name and a minimum distance. All those edges for which one of these conditions were not applied had been manually revised. In addition, those traffic signs indicating the direction concerned were included. The flow direction of the OSM data was compared to that of the GIP dataset and changed accordingly. Thus, all traffic intersections were assigned either the next node or the next edge, depending on the mapping. For the roundabouts no processing steps had to be carried out, since these were already stored in the edges.

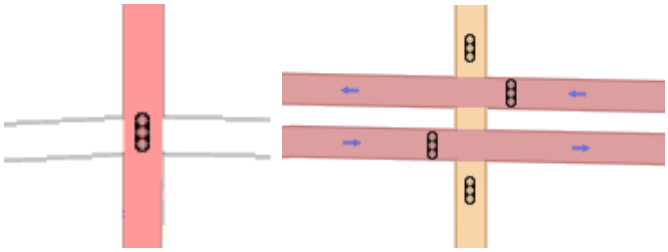

(a) Traffic signal at intersection point

(b) Traffic signal on each crossing

Figure 3.3: Intersection types depending on the mapping (OpenStreetMap Wiki, 2019)

All permitted turn behaviours are stored in the table *TurnEdge*. Based on the edges and nodes, the necessary turn behaviour for the graph was selected. The previously prepared traffic signs were finally assigned to the respective turning behaviour depending on the edge or node. Thus, the table *TurnEdge* with the traffic signs, which is necessary to overcome the edges, has been extended.

The weighting of the intersection for the additional fuel consumption was carried out according to the studies presented in chapter 2.2.1. Table 3.4 gives an overview of the additional fuel consumption of intersections compared to roads without junctions, which are found in the literature and have

Table 3.4: Overview of the influence of junctions on fuel consumption found in the literature

Junction	**Fuel consumption [%]**	**Literature**
traffic light	+ 45	+43 % (Dobre et al., 2012), +50 % (Wu et al., 2015)
stop intersection	+ 33	+16 % to roundabouts (Mandavilli et al., 2003)
roundabout	+ 17	-28 % to traffic lights (Várhelyi, 2002)
give way	+ 14	-3 % to roundabouts (Várhelyi, 2002)

been integrated into the routing. Dobre et al. and Wu et al. found that fuel consumption at intersections with traffic lights can increase by up to 50 %. The results of the study by Várhelyi showed that roundabouts cut fuel consumption by 28 % compared to traffic lights. In addition, Várhelyi found that give way signs decrease consumption for roundabouts by 3 %. By contrast, stop signs increase fuel consumption by 33 % over roundabouts, according to a study by Mandavilli et al.. The results of these studies were included in the calculation of costs. According to this, the costs were increased at traffic lights at 45 %, at stop signs at 33 %, at roundabouts at 17 % and at give way signs at 14 %. The additional costs were incorporated directly in the routing algorithm.

To model the turning direction, the approach of turn penalties was followed at intersections, which is visualized in figure 3.4. In this case, a typical intersection with two roads crossing at the intersection point A is shown. To cross the intersection, the following three turns are available from each direction: straight ahead, turn right or turn left. This results in a total of twelve options, each option being assigned to a penalty, which is represented in the table. When driving straight ahead there are no additional delays and therefore the combinations 1-3, 3-1, 2-4 and 4-2 have the penalty value zero. However, delays resulting in a penalty of one occur when turning to the right (2-1, 1-4, 3-2 and 4-3). For example, this value can represent the number of seconds. When turning left even longer delays appear, which have a penalty of two (1-2, 4-1 and 2-3). The combination 3-4 has a negative value (-1), since it is forbidden to turn in this direction (Rodrigue et al., 2017).

The modelling of the turning options was applied directly in the routing algorithm. For this purpose, in the first step, intersections were defined on the basis of the nodes, which touch more than two edges. In the next step, the angle defined by the two edges at the crossing point was determined in

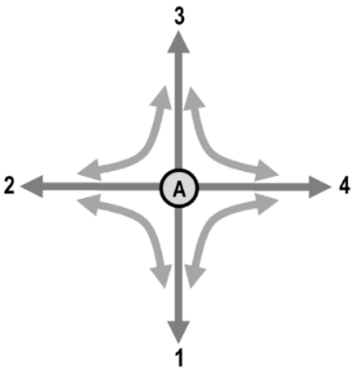

Turn Penalty Table – Node A		
From	To	Penalty
1	2	2
2	1	1
1	3	0
3	1	0
1	4	1
4	1	2
2	3	2
3	2	1
2	4	0
4	2	0
3	4	-1
4	3	1

Figure 3.4: Example of an intersection with turn penalties (Rodrigue et al., 2017)

order to be able to identify the direction of the turning behaviour. Thus, for the right turn and left turn additional costs were included in the routing. Since no cost factors were found in the literature for this approach, the method described by Rodrigue et al. was followed for the cost factor time. Therefore, one second is added as a cost factor when turning to the right and two seconds when turning left. The cost factor fuel consumption was determined on the basis of several test trials, with straight driving being sought. So, if the fuel consumption for the route should be minimal, the fuel consumption is increased by 20x0.6 l per hour at right turn and at left turn 20x1.2 l per hour. These factors are set so high thereby the route has as few turns as possible. The cost factor for fuel depends on Kumar et al., which was already used during the traffic congestion. In general, investigating the impact of turn penalties on time or fuel consumption in routing could be worked out in another research paper.

3.3 Data storage

After the road data had a routable node-edge structure, these were stored as adjacency lists. These could then be used for the routing algorithm. Storing the data in lists is the preferred option for navigation applications in networks. Basically, the edges are saved with the respective start node and end node as well as the costs in a list (Hofmann-Wellenhof et al., 2003). In this task, the list includes the cost values of distance, time, fuel consumption in flow direction and against flow direction. In addition, the attributes, direction, structural expression (FormOfWay), congestion in flow direction and congestion against flow direction were added to the edge list. On the basis of the unique identification of the nodes, the start nodes and end nodes

could be linked to those from the node list. This list stores the coordinates of the individual nodes. The list of traverses was also added to these two lists. This list includes the from link, the to link and the via node that connects these two edges. In addition, all intersections were listed according to the type, which are located on the traverse. Due to the unique designation of the from link, to link and the via node, they could be linked to the edge list or the node list. Because of this structure, all lists were linked together. An overview about the three lists is given in the figure 3.5.

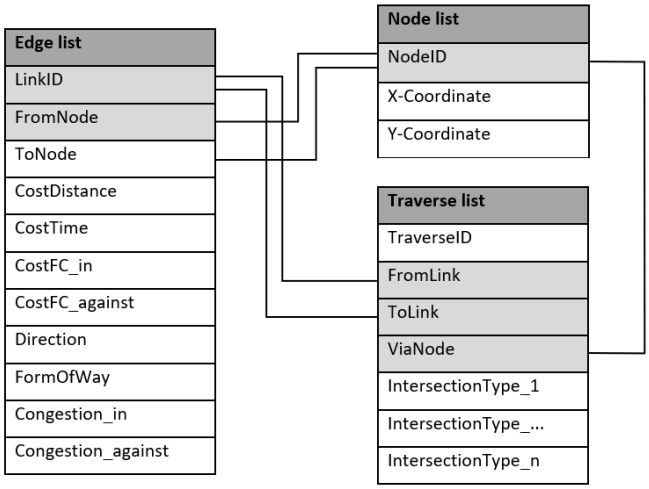

Figure 3.5: Data storage in three adjacency lists (edge list, node list, traverse list)

3.4 Shortest path algorithm

In order to find the shortest path from a given start node to a desired destination node, shortest path algorithm are used. One of the most popular path planning algorithms used in such topological applications is the A-star algorithm (Duchoň et al., 2014). The following chapter explains in more detail the basic principles, advantages and disadvantages of the A-star. In addition, the application of the algorithm for the routing is presented.

3.4.1 A - star algorithm

This algorithm uses not only the shortest path search but also the heuristic search (Duchoň et al., 2014). The heuristic approach pursues the goal of limiting the search space so that it comprehends the optimal route with

the highest probability (Hofmann-Wellenhof et al., 2003). Therefore the algorithm is also determined as best-first algorithm, which improves the time complexity because the set of visited nodes is decreased (Duchoň et al., 2014; Hofmann-Wellenhof et al., 2003). The negative point of this approach is that the solution can be a suboptimal path. The assessment is formed by the following function:

$$F(j) = G(j) + h(j) \tag{3.1}$$

This is compound of the actual distance between the starting node and the destination node $G(j)$ and the heuristic amendment $h(j)$, which is based on human path knowledge. The heuristic factor may be considered as a line-of-sight connection by the geometric line of sight distance being the distance between output node to destination node. If the distance is the cost factor and has to be minimal during routing, the geometric line of sight distance is selected as $h(j)$. If the cost factor of time is considered, then $h(j)$ is composed of the division of the geometric line of sight distance and a characteristically vehicle speed that arises in the network. In the cases mentioned, the rating number $F(j)$ enables a depth - first search in the direction of the destination node. The efficiency of the algorithm is determined by a good heuristic rating number $h(j)$. On the one hand, a low correlation between the distance of the output node and the destination with the heuristic value $h(j)$ does not improve the temporal complexity. On the other hand, a too strong correlation affects the solution, in which it may be that a non-optimal way is found. Another small negative aspect of the algorithm is that already visited nodes that have been assigned a fixed cost value can be corrected. This is due to the fact that through the best-first search, the nodes have been assigned incongruous costs. In summary it can be said that due to the cost correction the algorithm is flexible, and the integration of the heuristic improves the time complexity. These aspects are reflected in the heuristic search space, which takes on an elliptical form (figure 3.6) (Hofmann-Wellenhof et al., 2003).

3.4.2 Application of algorithm

This section explains the applied A-Star algorithm implemented for the routing. The algorithm is described using a pseudocode that is based on Hofmann-Wellenhof et al. and Rosetta Code (algorithm 3.1). In addition, the explanations of the symbols can be taken from the table 3.5. Each node of the graph, which is treated in the course of the routing, receives a label l. This are the cost from the starting node to another node in the graph, with the cost added to each node. During the search process, the nodes are

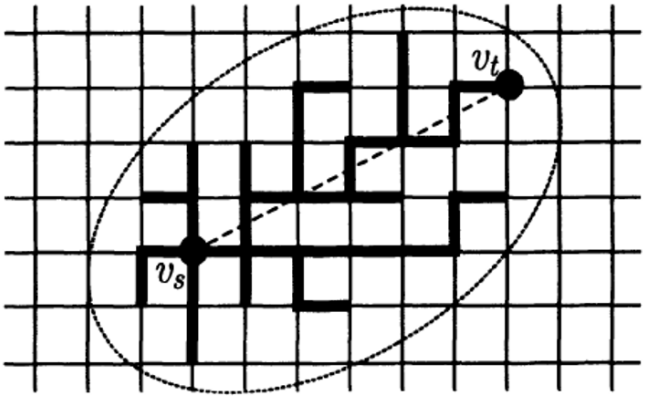

Figure 3.6: heuristic search space (Hofmann-Wellenhof et al., 2003, p.317)

assigned to either a temporary label T or a permanent label P. The nodes are first assigned to the temporary label and only when the shortest path has been determined, they are added to the permanent label. At the end of the algorithm, the costs of the shortest path are stored in the end node. In order to be able to determine the node sequence of the shortest path, the predecessor node is stored in the list $cameFrom$ for each node.

In the first step, the start values are initialized. To do this, an empty set G containing the actual costs from the start node to every other node and an empty set F including the estimated costs from the start node to the end node via the actual node are previously applied. The starting node $v(s)$ gets the label in the set G (G label) with zero, since the distance to itself is zero. In the set F, the heuristic approach $h(s)$ is taken. In the case of the geometric line of sight distance the distance between the start node $v(s)$ and the end $v(e)$ node is evaluated. All other nodes are assigned the value in sets G and F infinity. In addition, the start node $v(s)$ is assigned to the set of T and the sets P and $cameFrom$ are initialized as empty (line 1 – 11). As next is following a while-loop, which is the heart part of the algorithm (line 12). From this point on, the entire algorithm is executed until the set of T is empty. Within this loop, the node $v(j)$ with the lowest F label $f(j)$ is first searched for in the set of T. This node is $v(i)$ and is set as the current node and will be further processed (line 13). The node $v(i)$ is removed from the set of T and is added to the set of P (line 14, 15). In the next step, the neighbours $v(j)$ of the node $v(i)$ are determined in a for-loop (line 16). There are three options for the neighbouring accounts. The first possibility is that the neighbouring node $v(j)$ has not yet been visited, as is the case with the start node s (line 17). Therefore, the G label $G(j)$ is calculated from the label of the node $v(i)$ and the cost of the edge $c(ij)$. The F label $F(j)$ is evaluated from the G label $G(j)$ and the heuristic factor

Table 3.5: Pseudocode symbols, based on Hofmann-Wellenhof et al. (2003, p.303)

Symbol	**Explanation**
:=	Assignment to a label or node
{ }	Empty set
!=	Is not
&&	Logical and

$h(j)$. Furthermore, the node $v(j)$ is added to the set of T and the current node $v(i)$ is added to the predecessor list (line 18 – 21). If the node $v(j)$ is already visited and is in the set of the T, the second possibility occurs. In this case, care is taken to see whether the G label $G(j)$ is worse or better than the previous score (line 23). If the G label $G(j)$ is worse, the node $v(j)$ is ignored. However, if the G label $G(j)$ is better, it is taken over and the current node $v(j)$ is added to the list of predecessors. Furthermore, a F label $F(j)$ is calculated from the current G label $G(j)$ and the heuristic distance $h(j)$ (line 24 – 26). Thirdly, it may be that the neighbouring node $v(j)$ has already been visited and is already in the set of P (line 28). If the G label $G(j)$ is worse than previously found, then the node $v(j)$ is ignored. However, if the G label $G(j)$ is better than the previous one, it is fixed, and the current node $v(j)$ is added to the predecessor list. As in the cases before, a F label $F(j)$ is calculated from the new G label $G(j)$ and the heuristic factor $h(j)$. The node $v(j)$ is removed from the set of P and is added in the set of T (line 29 – 33). When the algorithm has found the destination node, the set of T is empty and all visited nodes are in the set of P. By means of the predecessor list $cameFrom$, the shortest route to the starting node $v(s)$ can be reconstructed.

3.5 PM integration

Basically, it was the idea that the particulate matter values are measured by means of air quality sensors in the vehicles and are readout using the CAN-Bus system. Based on the OGC standard SOS this data would be transmitted. Due to the fact that it was not possible to get such data, other data bases were used. The data preparation, the use of the SOS standard as well as the implementation of the particulate matter values for the routing are described in more detail in the following chapter.

Algorithm 3.1 A-Star algorithm pseudocode, based on Hofmann-Wellenhof et al. (2003, p.316) and Rosetta Code (2019)

V ... set of all nodes
T ... set of nodes with a temporary label
P... set of nodes with a permanent label
N ... set of adjacent nodes
$v(s)$ ... start node
$F(j)$ ... total rating number of a node v(j)
$G(j)$ ... label of a node v(j)
$h(j)$ ... heuristic rating number of a node v(j)
$cameFrom(j)$ ... predecessor of a node v(j)
$c(ij)$ ... cost of an edge

1: $G := \{\ \}$
2: $F := \{\ \}$
3: **for** each $v(j)$ in V **do**
4: $\quad G(j) := \infty$
5: $\quad F(j) := \infty$
6: **end for**
7: $G(s) := 0$
8: $F(s) := h(s)$
9: $P := \{\ \}$
10: $T := v(s)$
11: $cameFrom := \{\ \}$
12: **while** $T\ != \{\ \}$ **do**
13: $\quad v(i) := v(j)$ from T with min $F(j)$
14: $\quad T$ remove $v(i)$
15: $\quad P$ add $v(i)$
16: $\quad$ **for** each $v(j)$ in $N[v(i)]$ **do**
17: $\quad\quad$ **if** ($v(j)$ not in T) && ($v(j)$ not in P) **then**
18: $\quad\quad\quad G(j) := G(i) + c(ij)$
19: $\quad\quad\quad cameFrom(j) := v(i)$
20: $\quad\quad\quad F(j) := G(j) + h(j)$
21: $\quad\quad\quad T$ add $v(j)$
22: $\quad\quad$ **end if**
23: $\quad\quad$ **if** ($v(j)$ in T) && ($G(i) + c(ij) < G(j)$) **then**
24: $\quad\quad\quad G(j) := G(i) + c(ij)$
25: $\quad\quad\quad cameFrom(j) := v(i)$
26: $\quad\quad\quad F(j) := G(j) + h(j)$
27: $\quad\quad$ **end if**

Algorithm 3.1 A-Star algorithm pseudocode, based on Hofmann-Wellenhof et al. (2003, p.316) and Rosetta Code (2019) (continued)

```
28:         if (v(j) in P) && (G(i) + c(ij) < G(j)) then
29:             G(j) := G(i) + c(ij)
30:             cameFrom(j) := v(i)
31:             F(j) := G(j) + h(j)
32:             T add v(j)
33:             P remove v(j)
34:         end if
35:     end for
36: end while
```

3.5.1 Data preparation

Comprehensive data are necessary to be able to link individual edges with particulate matter data. The province of Styria is carrying out modelling of PM in the course of compilation of an immission register. On the basis of the estimated emissions of the known emission source, a dispersion calculation for one year is computed. Due to the fact that road dust resuspension from traffic and domestic fuel emissions are often unknown and difficult to quantify, these data cannot be metrologically validated and are not very reliable. In addition, the particulate matter varies depending on the weather, time of day and season. These factors are or cannot be taken into account in the modelling, which is based on annual mean values. Among other things, the most recent PM values date from 2010, as various input data are often available very late (S. A. Land Steiermark, personal communication, August 29, 2019). Due to the above reasons, these data were out of the question for this issue. As an alternative, air quality data for individual measuring stations in Styria can be requested online (for more information see `http://www.umwelt.steiermark.at/cms/beitrag/11710598/2060750/`). These data can be downloaded for specific emissions depending on the time interval and time period as an Excel spreadsheet. Therefore, measuring stations, which were located in the study area were selected and the PM values for the time window of the experiment were filtered out. All in all, the eight measuring stations, Graz Don-Bosco, Graz-Lustbühel, Graz-Mitte Gries, Graz-Nord, Graz-Ost (Petersgasse), Graz-Süd (Tiergartenweg), Graz-West, Judendorf-Süd were chosen (see figure 3.7). Since the routing is to be performed in near real time, the half-hour average was selected. The PM values are generally determined using a gravimetric and continuous measurement method. Since the gravimetric data obtained for the EU reference method are only available as daily averages, the data from the continuous measurement method were used (S. A. Land Steiermark, personal commu-

nication, August 29, 2019). Based on this data, a layer was interpolated for each half-hour average. IDW (Inverse Distance Weighted) was chosen as the interpolation method with a grid size of 10x10 m. Due to the fact that the PM is not only dependent on the traffic but also on the domestic fuel, a not too large grid size was chosen. In addition, random points were created on the road network representing vehicles for each layer. The distance of the points was set to 10 m, as this fits together with the cell size of the interpolated grid. In total, 10,000 random points were generated for each layer. The number of points was due to several routing attempts designed so that there are no major changes in the route guidance. These points (vehicles) query the corresponding half-hour average layer at the position in question. This approach is not quite optimal, but in view of the data basis and for the intended use, namely the testing of the algorithm, in order. In addition to the mobile measured values of the vehicles the measurements of the eight measuring stations were prepared in order to be included into the routing. For this purpose, only the data structure was changed.

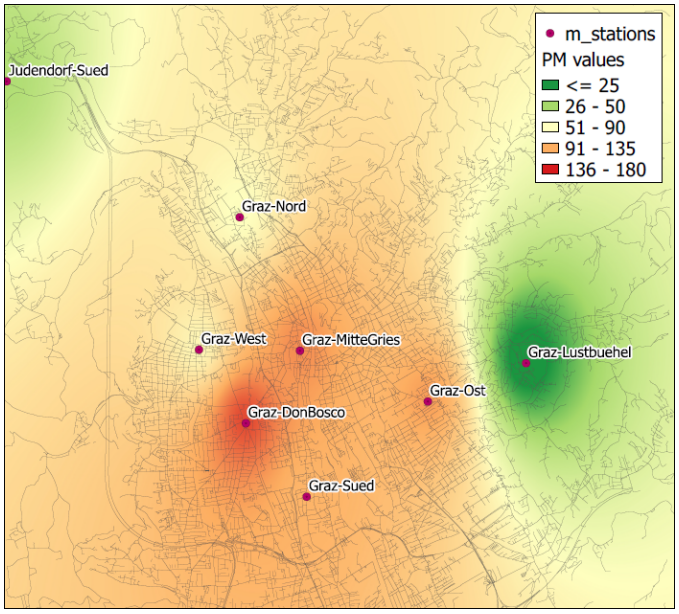

Figure 3.7: result of interpolation including measuring stations

3.5.2 Implementation of SOS

In the next step, the vehicles report the corresponding PM values to a server. This step was done through the implementation of the SOS standard. The data include the position of the vehicle, date, time and the particulate matter value. The data transmission is based on the SOS standards and the

web service was set up based on istSOS (see chapter 2.4.2). Due to the fact that istSOS is mostly used in Linux environment and the computer used is based on Windows, the istSOS service was set up by means of a virtual machine. Furthermore, a database and a service instance were created. Within this instance, a separate *Procedure* was established for each vehicle, which represents a mobile measuring station, and for each measuring station, which means a fixed station. As $FeatureOfInterest$ the location of Graz was indicated for the *Observations* of the vehicles. At the measuring stations, the coordinates of the respective location were specified as $FeatureOfInterest$. Finally, all measurements were inserted to these *Procedures*. The requests for the service were transmitted using the HTTP POST method. As *ObservedProperties* the particulate matter was selected, which had to be created before. In addition, the data can be validated based on a quality index. For this an interval between 0 and 500 has been set for the data. In order to differentiate the mobile and fixed measurements, the mobile ones has been assigned to the standard $Offeringtemporary$ and the fixed ones to the $Offeringstations$.

In order to be able to query the data for the routing, the SOS standard request was used. Using the GET method, the data can be output according to the desired time, sensor, data format or measured value. In addition, it was checked whether the quality index is fulfilled, whereby the validation only works for in-situ fixed points. The PM data were stored as a CSV (Comma-separated values) file for the desired period of investigation and then linked to the edges of the road network. Due to the fact, that the fixed measuring stations are not located directly on the edges of the road network, but a few meters away, within 25 m all edges were assigned the measured values of the station. Thus, except for the station Graz-Nord, which is located next to a non-public road, values of at least one edge could be assigned. Since the stations are also located next to intersections, the measured value was not assigned to the next edge.

Finally, the PM values can be taken into account in the routing algorithm. On closer inspection, it happens frequently that edges have been assigned multiple PM values on the one hand and no PM values on the other hand. For the one case, if an edge has more PM values, the maximum value, which is the worst one, was taken. In the other case, if no PM value is available, the last PM values are used, which may not be older than two hours. If there is still no value, then the value of the nearest vehicle is used.

In order to use the values adequately in the routing, the CAQI was applied as described in chapter 2.4.4. Therefore, the PM values can be weighted differently depending on the optimization parameters. Because there were no values above $180\,\mu g/m^3$ in Graz during the investigation period and a large proportion of the values were in the range between 90 and $180\,\mu g/m^3$

Table 3.6: Classification of PM values into different classes, according to the CAQI

Index class	**PM-value** [$\mu g/m^3$]
very low	0 - 25
low	26 - 50
medium	51 - 90
high	91 - 135
very high	136 - 180

on the PM day, this interval was divided in the middle. This makes the PM hotspots more visible. The breakdown of the different classes is shown in table 3.6.

However, the weighting of the particulate matter values plays an important role in determining the optimal route. On the one hand, a too low weighting leads to the fact that the routes still lead through PM areas. On the other hand, a too high weighting causes PM zones to be avoided, but the bypass is much too long, meaning that the routes are pointless. For this reason, many tests have been carried out in order to obtain an optimal evaluation of the PM values.

Chapter 4

Results

On the basis of the prepared network graph and the created routing algorithm it is possible to select different cost factors as parameters for finding the shortest path. Generally, the shortest path between a start node and a destination node was determined. Furthermore, the turn restrictions were taken into account in all calculations. For the pathfinding after the time and fuel consumption, the edges and traverses evaluations, as explained in chapter 3, were included. In addition, the selection can be made at each path finding, that areas with high particulate matter content, are avoided. Accordingly, the following route options arise:

- Shortest route
- Shortest route with consideration of PM
- Fastest route
- Fastest route with consideration of PM
- Fuel consumption route
- Fuel consumption route with consideration of PM

As result, the sum of all perambulated edges is displayed from the start node to the destination node. In addition to the optimization parameter, all other costs are also saved. Thus, the results of the individual routes of all parameters can be compared. To demonstrate the impact of each route on the environment, the pollutant CO_2 was included. This was derived directly from the fuel consumption (see chapter 3.2.2). The following section introduces use cases that were developed with the created algorithm.

4.1 Use cases

In order to test the algorithm, some use cases were tried out in the study area. A different starting and destination node were chosen for each scenario.

For the purpose of evaluating the effects of the PM pollution, a day with high particulate matter values and a day with lower values were selected for each scenario. The website of the Federal Environment Agency shows the exceeded PM days of the individual measuring stations in Austria. As a limit for not exceeding, the daily mean value of 50 µg/m³ is employed. As PM day the 16.01.2019 was selected, since on that day most of the measuring stations in Graz had exceeded pollutions. In total, particulate matter values above 50 µg/m³ were measured on five of the eight measuring stations in the study area. As day with less PM pollution the 23.10.2019 was picked, because on this day the Plabutschtunnel, which serves as bypass for the city of Graz, was closed in the morning. Whether this lock has an effect on the choice of routes should show the scenarios. For this day, PM values were measured at all eight measuring stations. For both of these days a routing in the morning, at 06:00 and at 06:30, and one in the evening, at 18:00 and at 18:30, was carried out. Since the particulate matter values are available as half-hourly mean values, routes were developed for every half hour in the mentioned investigation period. Generally, a traffic jam in front of the Plabutschtunnel was simulated on all routes, so that all vehicles have to drive through the city. The reason for this is that no PM values are presented in the tunnel.

For all scenarios, the six optimization options mentioned in the previous section were performed. First, there is always a plot of the shortest path by distances, time and fuel consumption, without considering the particulate matter values. Subsequently, the routes are displayed depending on the investigation period and on the PM pollution. In the background, the results of the interpolation with the PM values at the respective times are displayed. For all visualisations, the routes are shown in blue according to the distance, in red according to the time and in green according to the fuel consumption. Finally, the results of all routes including their parameters are clearly represented in a table. Thus, the differences between the individual routes for each scenario can be seen according to the optimization parameters, which are used to answer the first research question. The values are greyed out for all those PM-routes which have the same route without PM values and the parameter with the best result, which corresponds to the smallest value, is highlighted. According to this it has to be mentioned that due to the A-star algorithm is used, the best value does not always match the routing optimization parameter. However, the differences are so marginal that these do not mean any significant changes to the results.

4.1.1 Scenario 1

This scenario searches for an optimal path from the north of Graz (district Andritz) to the south-east (community Raaba). Because the route leads from one location to another location of a company, this route is referred to as the worker route. On the whole, the routes have a similar course according to the optimization parameters, but the routes differ depending on the period under investigation and on the PM values. The routes with the optimization parameters distance, time and fuel consumption pass in the east the city without taking into account the PM values (figure 4.1).

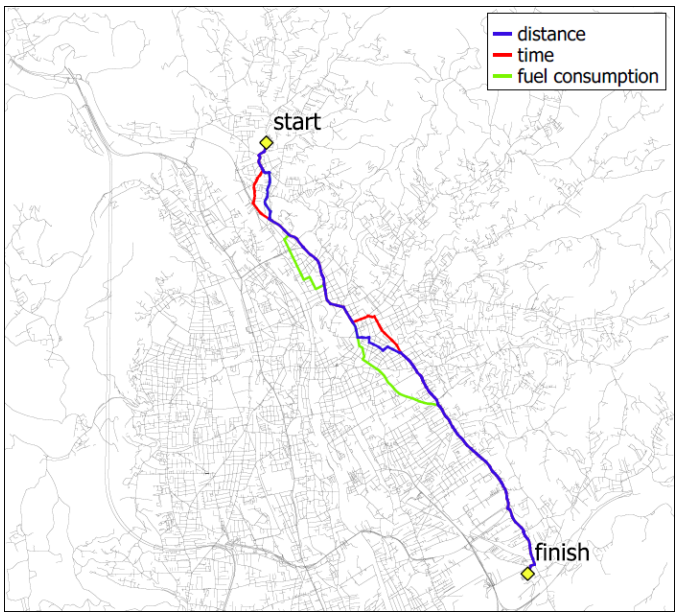

Figure 4.1: Scenario 1 - Presentation of the calculated routes without consideration of PM values

Considering the PM values of the 16.01.2019, the routes in the morning show no differences to the routes without including PM values, because there are no increased PM values in the morning (figure 4.2(a) & 4.2(b)). However, in the evening different courses of the routes occur. Due to the fact that there is higher particulate matter pollution in the south area of Graz, the routes lead around the hotspot in the south-east. The routes between 18:00 (figure 4.2(c)) and 18:30 (figure 4.2(d)) show the same courses, with the exception of the route by distance. This differs only marginally in the north of Graz, as there is a significantly lower pollution in this area at 18:30. The improvement in air quality in this area had no effect on the other routes.

In addition, the routes are represented according to the distance optimization parameter for each time interval in the figure 4.3. In the back-

ground, the results of the interpolation of the PM values of 18:30 can bee seen. It is shown again, that the routes at 06:00 and 06:30 have a similar course, however the routes at 18:00 and 18:30 bypass the hotspot of the PM values to the west.

The parameters distance, time, fuel consumption and CO_2 can be taken from the table 4.1 for each individual route. Overall, the routes do not differ significantly according to the parameters. By choosing the most fuel-efficient route, consumption can be reduced between 0.03 and 0.05 l, whereby the routes are up to 290 m longer and the journey time is extended by up to 3 minutes.

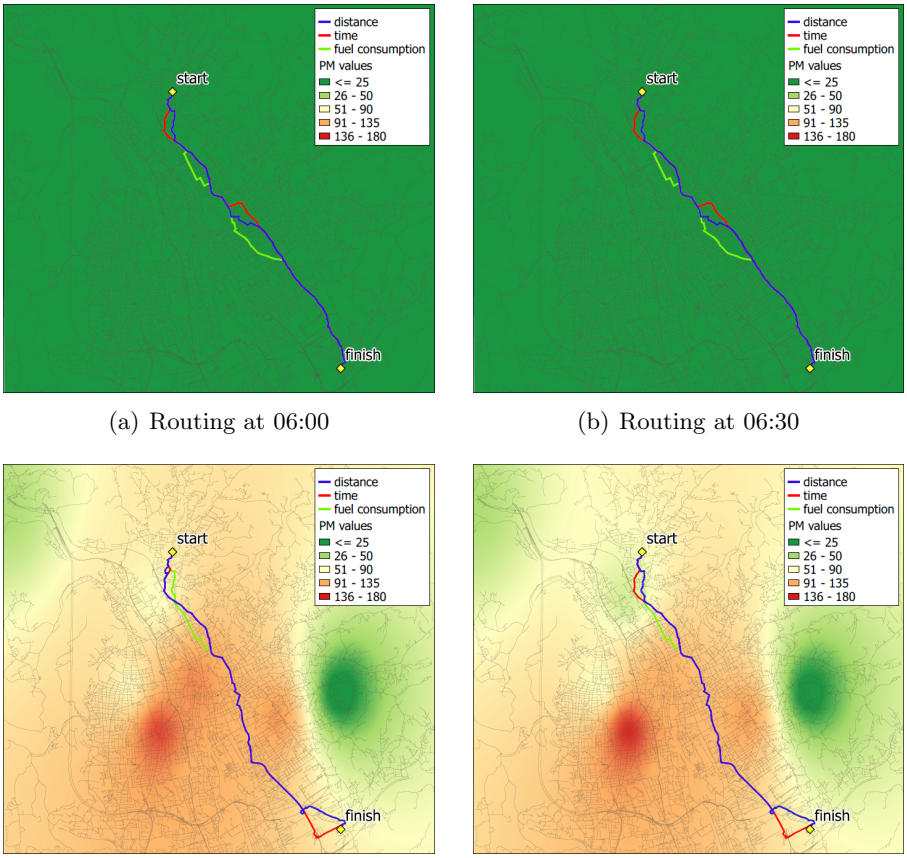

(a) Routing at 06:00

(b) Routing at 06:30

(c) Routing at 18:00

(d) Routing at 18:30

Figure 4.2: Scenario 1 - Presentation of the calculated routes with consideration of the high PM day (16.01.2019) at different times

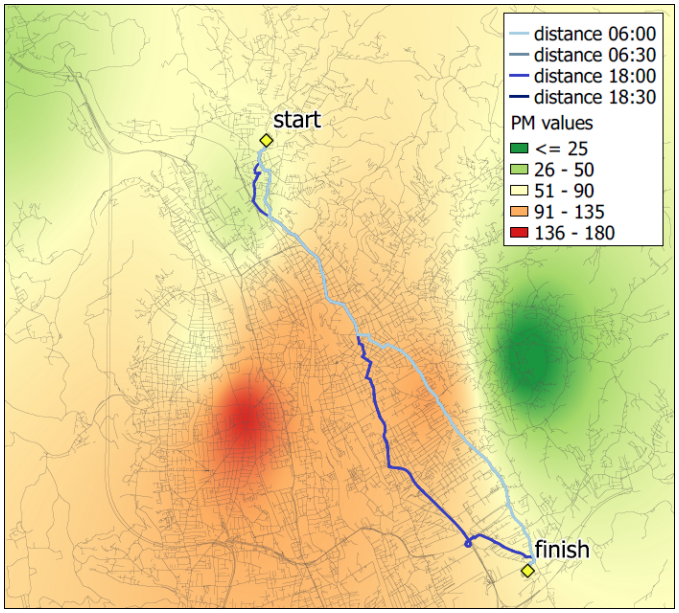

Figure 4.3: Scenario 1 - Comparison of routes by distance depending on the investigation period (background: PM values of 18:30)

Table 4.1: Scenario 1 - Overview of the results of the individual routes (high PM-day)

Route	**Distance [km]**	**Time [min]**	**Fuel consumption [l]**	**CO2 [g]**
Dis - min	**11.95**	24.26	0.66	1745.80
Time - min	11.98	**23.36**	0.66	1753.47
Fuel - min	12.24	25.88	**0.63**	**1682.25**
DisPM 06:00 - min	**11.95**	24.26	0.66	1745.80
TimePM 06:00 - min	11.98	**23.36**	0.66	1753.47
FuelPM 06:00 - min	12.24	25.88	**0.63**	**1682.25**
DisPM 06:30 - min	**11.95**	24.26	0.66	1745.80
TimePM 06:30 - min	11.98	**23.36**	0.66	1753.47
FuelPM 06:30 - min	12.24	25.88	**0.63**	**1682.25**
DisPM 18:00 - min	12.91	25.44	0.79	2113.51
TimePM 18:00 - min	**12.81**	**24.09**	0.78	2080.14
FuelPM 18:00 - min	12.96	27.08	**0.74**	**1965.34**
DisPM 18:30 - min	**12.78**	25.82	0.76	2024.69
TimePM 18:30 - min	12.81	**24.09**	0.78	2080.14
FuelPM 18:30 - min	12.96	27.08	**0.74**	**1965.34**

The results on a PM poor day are very similar to those on the PM day, since there are also low PM values in the morning and in the evening increased pollution in the south-east of Graz. Although the Plabutschtunnel was closed, it was not possible to achieve high particulate matter values in the morning and the routes therefore show identical courses with the routes without PM observations (figure 4.6(a) & 4.6(b)). In the evening, especially in the south-east of Graz, a higher particulate matter pollution arises, and

therefore the routes lead around this hotspot. Compared to the PM day, the course of the routes guides further west from the hotspot, since there is less pollution in this area. The environmentally friendly route in particular evades this area enormously and even crosses the river Mur. The routes according to time and fuel consumption show different courses at 18:00 and 18:30, however, the route according to the distance at both times is the same (figure 4.6(c) & 4.6(d)). The exact values can be found in table 4.2.

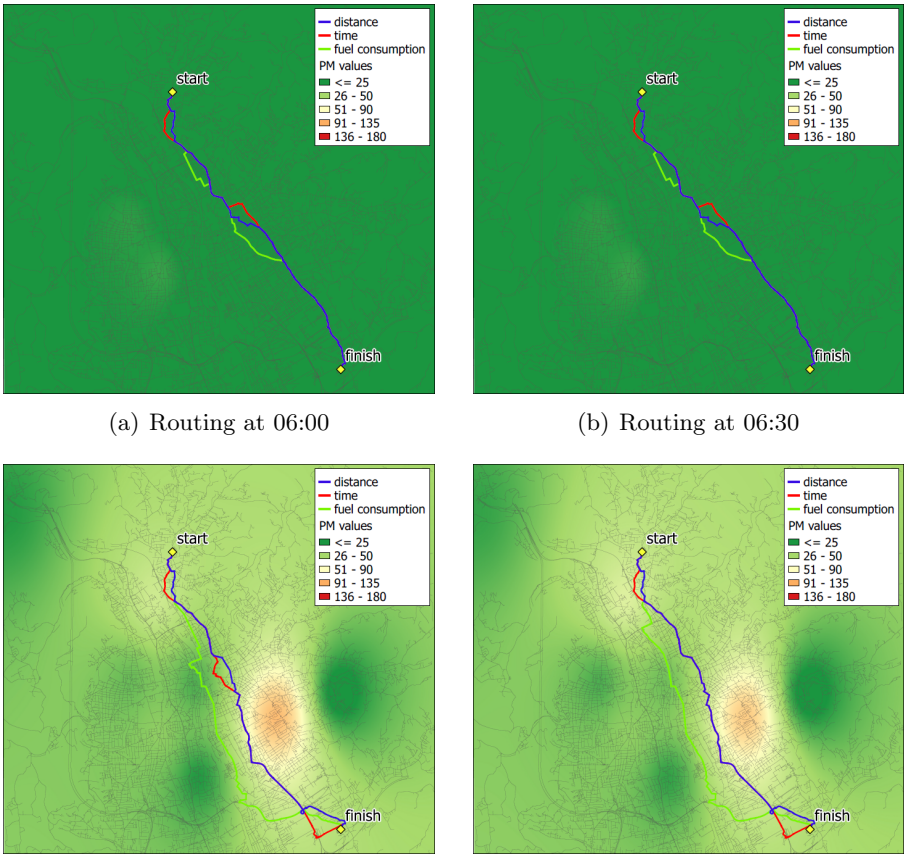

(a) Routing at 06:00

(b) Routing at 06:30

(c) Routing at 18:00

(d) Routing at 18:30

Figure 4.4: Scenario 1 - Presentation of the calculated routes with consideration of the less PM day (23.10.2019) at different times

Table 4.2: Scenario 1 - Overview of the results of the individual routes (less PM-day)

Route	Distance [km]	Time [min]	Fuel consumption [l]	CO2 [g]
Dis - min	**11.95**	24.26	0.66	1745.80
Time - min	11.98	**23.36**	0.66	1753.47
Fuel - min	12.24	25.88	**0.63**	**1682.25**
DisPM 06:00 - min	**11.95**	24.26	0.66	1745.80
TimePM 06:00 - min	11.98	**23.36**	0.66	1753.47
FuelPM 06:00 - min	12.24	25.88	**0.63**	**1682.25**
DisPM 06:30 - min	**11.95**	24.26	0.66	1745.80
TimePM 06:30 - min	11.98	**23.36**	0.66	1753.47
FuelPM 06:30 - min	12.24	25.88	**0.63**	**1682.25**
DisPM 18:00 - min	**12.78**	25.82	0.76	2024.69
TimePM 18:00 - min	12.94	**23.98**	0.80	2134.81
FuelPM 18:00 - min	14.22	33.18	**0.70**	**1863.94**
DisPM 18:30 - min	**12.78**	25.82	0.76	2024.69
TimePM 18:30 - min	12.81	**24.09**	0.78	2080.14
FuelPM 18:30 - min	13.97	31.54	**0.66**	**1760.97**

4.1.2 Scenario 2

The second scenario starts in the south-west of Graz at the rescure center and leads to the east to the state hospital, which is the destination. Since this route is often used for ambulances due to the start and destination nodes, it is referred to as the Red Cross route.

If the routes are considered by distance, time and fuel consumption without taking the particulate matter values into account (figure 4.5), it is noticeable that all three routes have different courses, but these are only minimally reflected in the result of the individual parameters (table 4.3). Since, as already shown in scenario 1, the PM values in the morning are very low, the routes at 06:00 and 06:30 also have the same course in this scenario as those without considering PM observations (figure 4.6(a) & 4.6(b)). Due to the increased particulate matter pollution in the south and in the center of Graz in the evening, the routes at 18:00 and 18:30 no longer lead through the city. The routes bypass the hotspot and thus the city center in the north,whereby the routes are completely identical for both times. In addition, the routes in terms of distance and time have the same course. Rerouteing the areas with high PM pollution means that a distance of 1 km, a time of around 2.5 minutes and a fuel consumption of 0.06 l are more expended. More informations about the results of the individual parameters can be taken from table 4.3.

In order to have a better comparison of the different results depending on the investigation period, the routes according to the optimization parameter time are shown in the figure 4.7. It is made clear once again that in the morning the routes lead through the city and in the evening, due to the

Table 4.3: Scenario 2 - Overview of the results of the individual routes (high PM-day)

Route	Distance [km]	Time [min]	Fuel consumption [l]	CO2 [g]
Dis - min	**8.63**	22.32	0.69	1825.90
Time - min	8.73	**20.03**	0.65	1719.69
Fuel - min	9.60	22.69	**0.61**	**1611.44**
DisPM 06:00 - min	**8.63**	22.32	0.69	1825.90
TimePM 06:00 - min	8.73	**20.03**	0.65	1719.69
FuelPM 06:00 - min	9.60	22.69	**0.61**	**1611.44**
DisPM 06:30 - min	**8.63**	22.32	0.69	1825.90
TimePM 06:30 - min	8.73	**20.03**	0.65	1719.69
FuelPM 06:30 - min	9.60	22.69	**0.61**	**1611.44**
DisPM 18:00 - min	**9.63**	**22.61**	0.71	1876.11
TimePM 18:00 - min	**9.63**	**22.61**	0.71	1876.11
FuelPM 18:00 - min	9.81	23.26	**0.67**	**1792.92**
DisPM 18:30 - min	**9.63**	**22.61**	0.71	1876.11
TimePM 18:30 - min	**9.63**	**22.61**	0.71	1876.11
FuelPM 18:30 - min	9.81	23.26	**0.67**	**1792.92**

pollution, these pass the city center in the north. In the background, the interpolation results of the PM values are shown at 18:00.

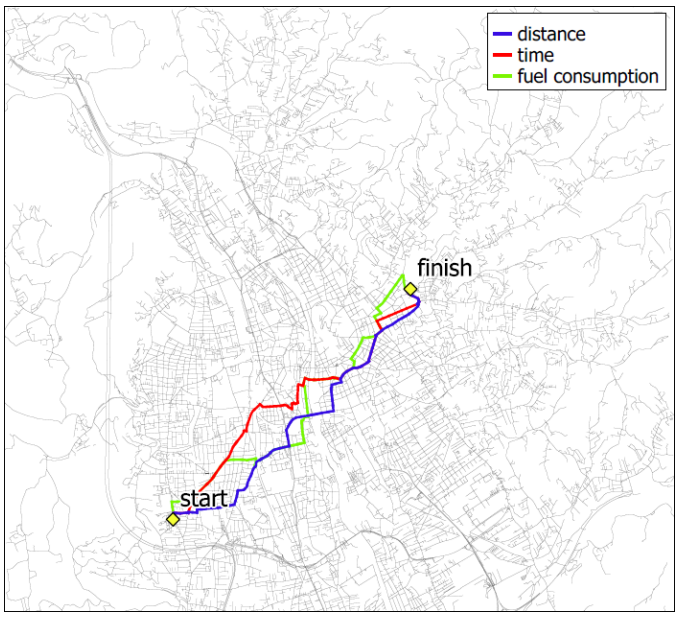

Figure 4.5: Scenario 2 - Presentation of the calculated routes without consideration of PM values

On the whole, the results on the low PM-day for scenario 2 indicate similar results for all times, but the courses differ slightly (table 4.4). This is due to the fact that there is hardly any pollution in the early morning and in the evening the PM-hotspot does not lead along the routes. The greatest

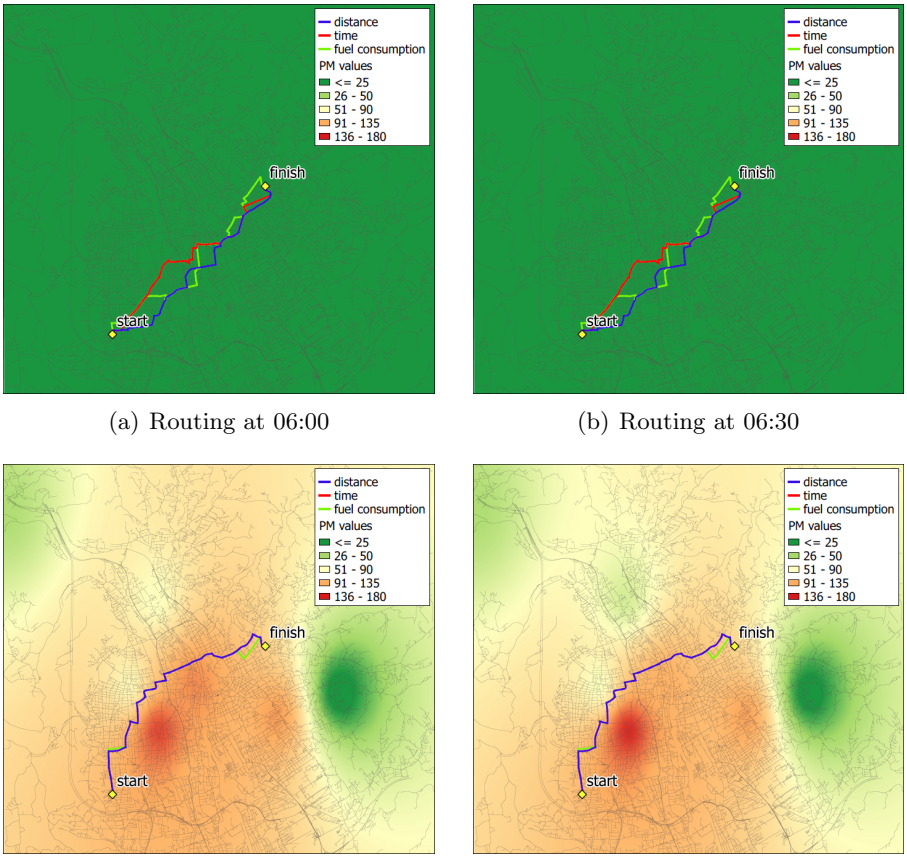

(a) Routing at 06:00

(b) Routing at 06:30

(c) Routing at 18:00

(d) Routing at 18:30

Figure 4.6: Scenario 2 - Presentation of the calculated routes with consideration of the high PM day (16.01.2019) at different times

differences in the course are shown by the route according to the distance at which the area with the low PM values, which is a little more north, is aimed for in the evening. However, the route with the lowest fuel consumption in the evening has only minor changes compared to the one in the morning. The route according to the time is at all times completely identical (figure 4.8).

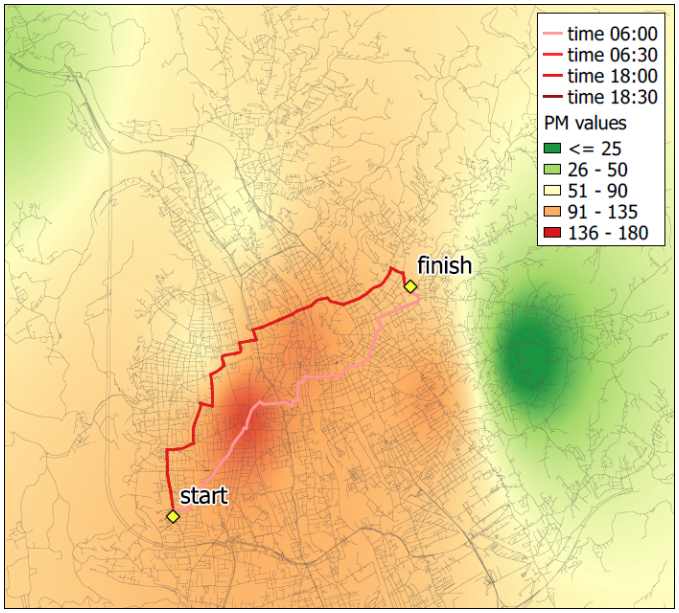

Figure 4.7: Scenario 2 - Comparison of routes by time depending on the investigation period (background: PM values of 18:00)

Table 4.4: Scenario 2 - Overview of the results of the individual routes (less PM-day)

Route	**Distance [km]**	**Time [min]**	**Fuel consumption [l]**	**CO2 [g]**
Dis - min	**8.63**	22.32	0.69	1825.90
Time - min	8.73	**20.03**	0.65	1719.69
Fuel - min	9.60	22.69	**0.61**	**1611.44**
DisPM 06:00 - min	**8.53**	21.85	0.67	1785.50
TimePM 06:00 - min	8.73	**20.03**	0.65	1719.69
FuelPM 06:00 - min	9.36	22.21	**0.60**	**1588.63**
DisPM 06:30 - min	**8.53**	21.85	0.67	1785.50
TimePM 06:30 - min	8.73	**20.03**	0.65	1719.69
FuelPM 06:30 - min	9.36	22.21	**0.60**	**1588.63**
DisPM 18:00 - min	**8.51**	20.13	0.66	1742.98
TimePM 18:00 - min	8.73	**20.03**	0.65	1719.69
FuelPM 18:00 - min	9.10	21.28	**0.60**	**1607.15**
DisPM 18:30 - min	**8.51**	20.13	0.66	1742.98
TimePM 18:30 - min	8.73	**20.03**	0.65	1719.69
FuelPM 18:30 - min	9.10	21.28	**0.60**	**1607.15**

4.1.3 Scenario 3

The third scenario leads from the Graz University of Technology, which is located slightly in the south-east of the center of Graz, to a traditional Austrian wine tavern in the south west (district Wetzelsdorf). Because of the choice of start and destination, this route is called student route. Considering the routes without PM values, the routes in terms of distance, time and

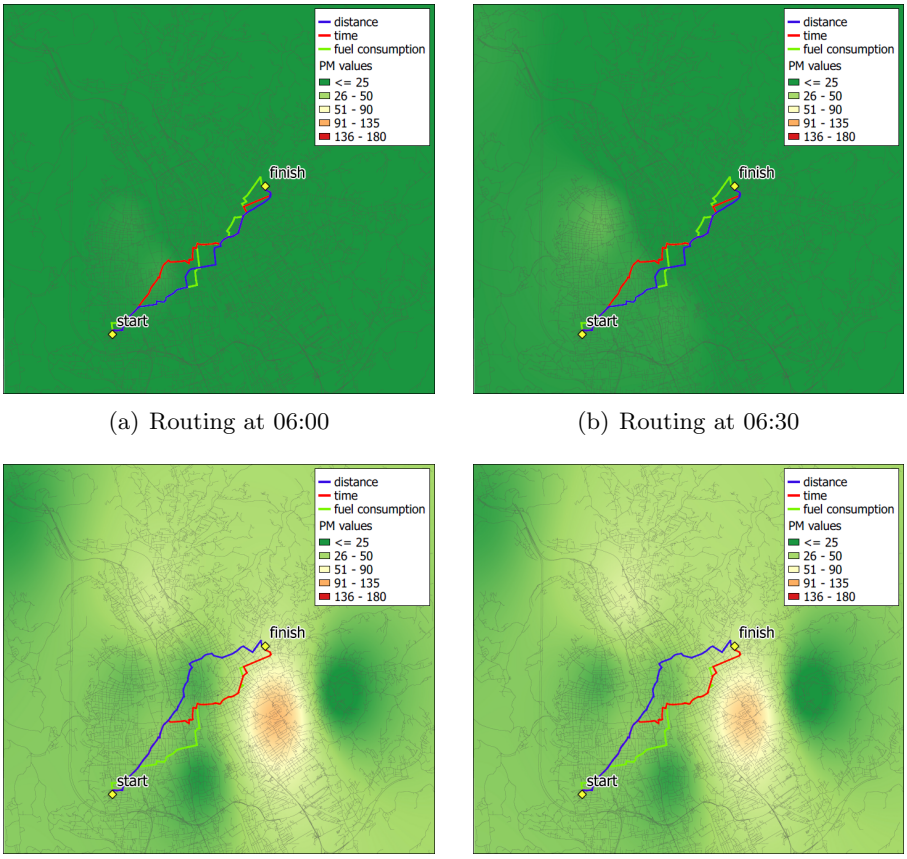

(a) Routing at 06:00

(b) Routing at 06:30

(c) Routing at 18:00

(d) Routing at 18:30

Figure 4.8: Scenario 2 - Presentation of the calculated routes with consideration of the less PM day (23.10.2019) at different times

fuel consumption lead from east to west, across the city and have similar courses (figure 4.9).

As with the other two scenarios before, the routes in the morning are identical to those for which no PM values have been taken into account (figure 4.10(a) & 4.10(b)). Due to the high PM values in the south and in the center of Graz in the evening, the routes at 18:00 and 18:30 show significantly different results. These two hotspots will be bypassed at 18:00 in the north of the route according to distance and in the south according to the routes of time and fuel consumption (figure 4.10(c)). Because the PM pollution in the city is lower at 18:30 than half an hour earlier, the routes initially lead across the city center and only bypass the hotspot, which is located in the south-west, to the north (figure 4.10(d)). The enormous bypassing of the high polluted areas at 18:00 causes a longer distance of around 3.5 km, a longer

travel time of over 8 minutes and a fuel consumption of 0.19 l compared to the route without considering PM values. Further values of the parameters can be found in table 4.5.

The different routes depending on the time for the lowest fuel consumption are shown in the figure 4.11. The effects of the PM values on the routing are clarified again, whereby in the morning the route leads across the city, at 18:00 southerly and at 18:30 northerly.

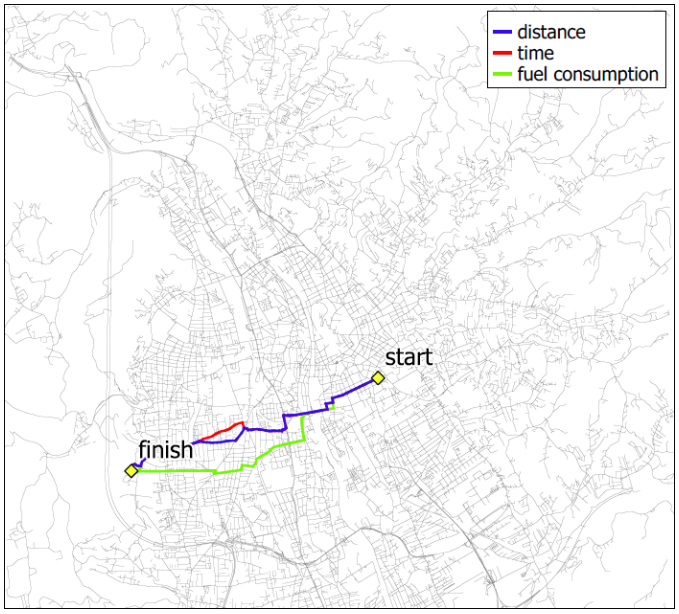

Figure 4.9: Scenario 3 - Presentation of the calculated routes without consideration of PM values

Due to the fact that the routes are located in areas with low PM values for all times of the PM lower day, hardly any different results can be realized. The routes according to the distance and time are completely identical for all times, only the shortest route after the fuel consumption changes minimally with the times (figure 4.12). The exact results can be found in the table 4.6.

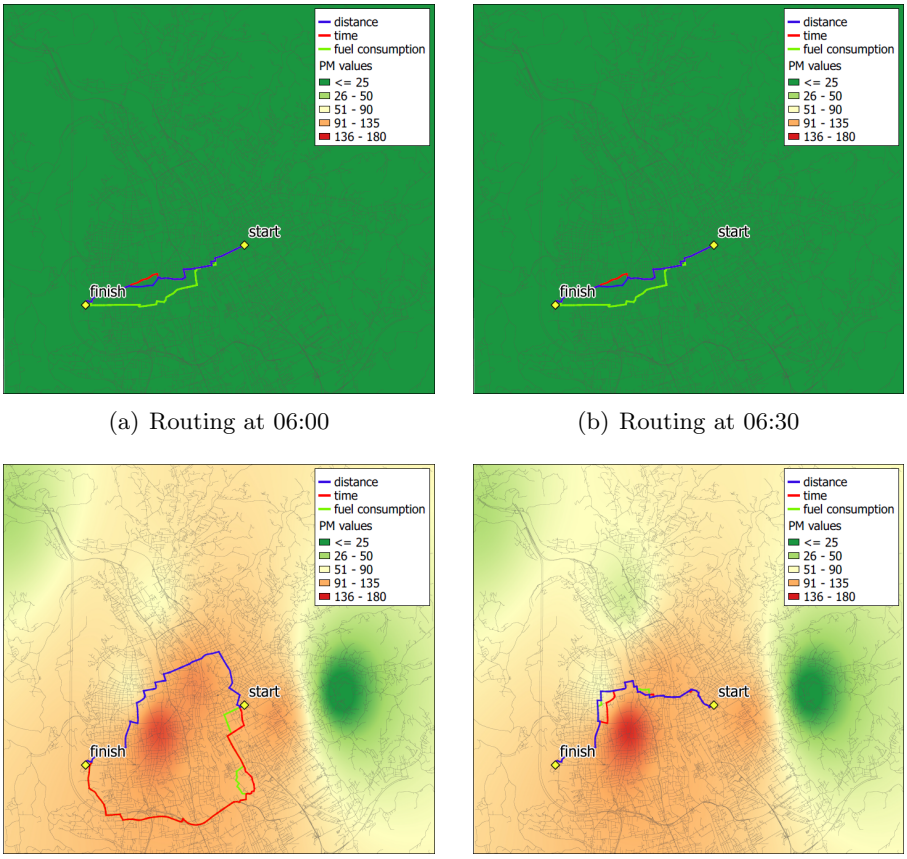

(a) Routing at 06:00

(b) Routing at 06:30

(c) Routing at 18:00

(d) Routing at 18:30

Figure 4.10: Presentation of the calculated routes with consideration of the high PM day (16.01.2019) at different times

4.2 Influence on weighting

In the following short subsection the importance of weighting the particulate matter values is discussed in more detail. If the values of the polluted areas are weighted too high, the algorithm searches for areas with low pollution and therefore the routes often become too long and uneconomical. Although these routes increasingly lead through clean areas, the longer travel time and distance has a negative impact due to additional consumption. In contrast, if the weighting of the PM values is too low, routes have shorter journey time and distance, but lead across the polluted areas, which should be avoided. This means that the parameters for the weighting have to be taken well, in order to obviate polluted areas on the one hand and to prevent rerouteing that are too long on the other. According to the figure 4.13 the impacts of

Table 4.5: Scenario 3 - Overview of the results of the individual routes (high PM-day)

Route	Distance [km]	Time [min]	Fuel consumption [l]	CO2 [g]
Dis - min	**6.40**	16.47	0.47	1262.65
Time - min	6.44	**16.35**	0.48	1266.01
Fuel - min	6.80	16.49	**0.46**	**1227.90**
DisPM 06:00 - min	**6.40**	16.47	0.47	1262.65
TimePM 06:00 - min	6.44	**16.35**	0.48	1266.01
FuelPM 06:00 - min	6.80	16.49	**0.46**	**1227.90**
DisPM 06:30 - min	**6.40**	16.47	0.47	1262.65
TimePM 06:30 - min	6.44	**16.35**	0.48	1266.01
FuelPM 06:30 - min	6.80	16.49	**0.46**	**1227.90**
DisPM 18:00 - min	**9.46**	**23.73**	0.71	1899.44
TimePM 18:00 - min	11.32	24.61	0.66	1756.89
FuelPM 18:00 - min	11.49	25.33	**0.65**	**1723.73**
DisPM 18:30 - min	8.44	21.13	0.58	1553.78
TimePM 18:30 - min	**8.34**	**20.20**	0.59	1581.77
FuelPM 18:30 - min	8.48	20.94	**0.57**	**1513.78**

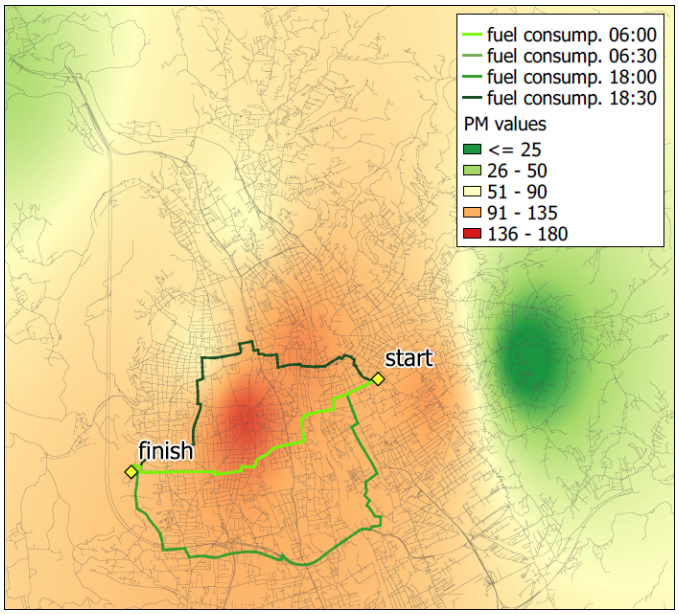

Figure 4.11: Scenario 3 - Comparison of routes by fuel consumption depending on the investigation period (background: PM values of 18:00)

an overweighting (route violet) and an underweighting (route red) on the routes are shown.

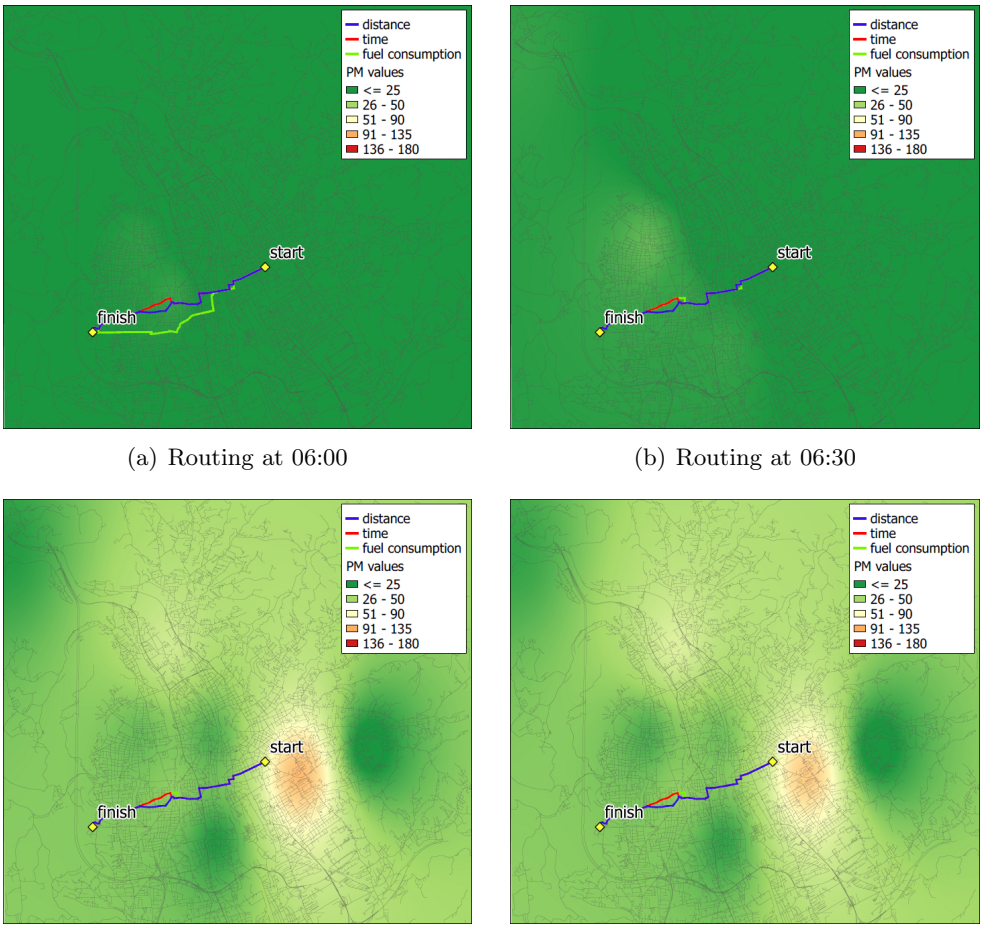

(a) Routing at 06:00

(b) Routing at 06:30

(c) Routing at 18:00

(d) Routing at 18:30

Figure 4.12: Scenario 3 - Presentation of the calculated routes with consideration of the less PM day (23.10.2019) at different times

4.3 Hotspot analysis

In order to establish a better connection between the routes and the polluted areas on the one hand, and on the other hand the results not only appear visually but are also substantiate by numbers, some hotspot analyses are developed. Because no applicable analyses for this topic were found in the literature, attempts were made to obtain meaningful results using a combination of two hotspot analyses. As original data the times 18:00 and 18:30 on the PM day were chosen, because at these times there was the highest pollution of PM in the study period. Based on this data, the local centroid was defined, with only those were selected that fall within the last interval

Table 4.6: Scenario 3 - Overview of the results of the individual routes (less PM-day)

Route	Distance [km]	Time [min]	Fuel consumption [l]	CO2 [g]
Dis - min	**6.40**	16.47	0.47	1262.65
Time - min	6.44	**16.35**	0.48	1266.01
Fuel - min	6.80	16.49	**0.46**	**1227.90**
DisPM 06:00 - min	**6.40**	16.47	0.47	1262.65
TimePM 06:00 - min	6.44	**16.35**	0.48	1266.01
FuelPM 06:00 - min	6.80	16.43	**0.46**	**1219.70**
DisPM 06:30 - min	**6.40**	16.47	0.47	1262.65
TimePM 06:30 - min	6.44	**16.35**	0.48	1266.01
FuelPM 06:30 - min	6.46	16.26	**0.45**	**1203.65**
DisPM 18:00 - min	**6.40**	16.47	0.47	1262.65
TimePM 18:00 - min	6.44	**16.35**	0.48	1266.01
FuelPM 18:00 - min	6.48	16.33	**0.46**	**1217.53**
DisPM 18:30 - min	**6.40**	16.47	0.47	1262.65
TimePM 18:30 - min	6.44	**16.35**	0.48	1266.01
FuelPM 18:30 - min	6.48	16.33	**0.46**	**1217.53**

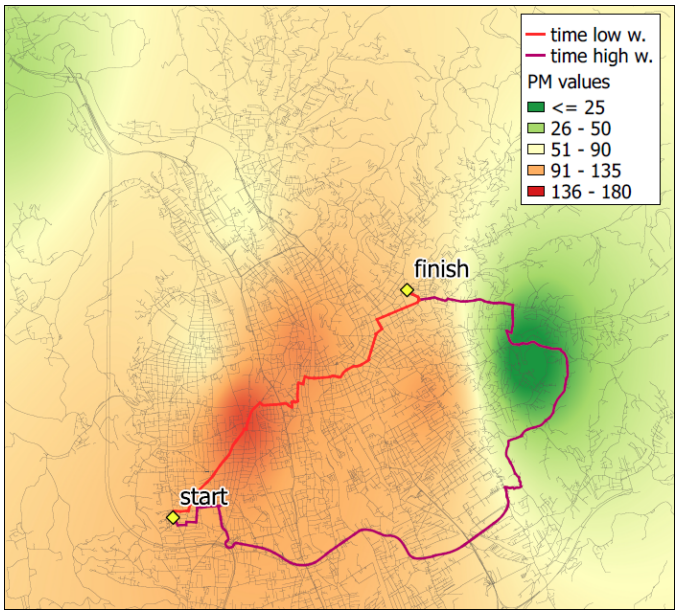

Figure 4.13: Effects of the different weightings of the PM values on the route selection (background: PM values of 18:00)

of the quality index. For the PM values at 18:00 in total three centroids were calculated, at 18:30 there were only two centroids, as the pollution in the city improved. The location of the centroids can be seen in figure 4.14, on the left side the PM values at 18:00 and on the right side the PM values at 18:30.

The first analysis deals with the minimum distance between each indi-

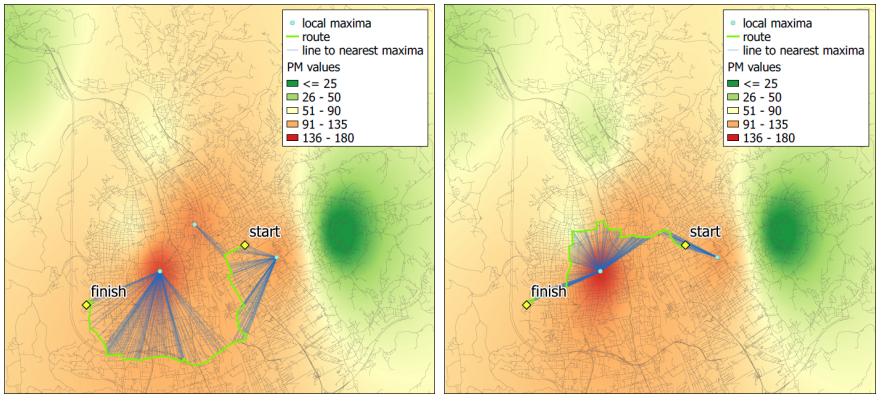

(a) PM values at 18:00 (b) PM values at 18:30

Figure 4.14: Visualisation of the PM hotspots and the average distance between the centroid hotspots and the line segments of the routes

Table 4.7: Minimum distance between PM centroids and routes at 18:00

Routes at 18:00	**dis [m]**	**disPM [m]**	**time [m]**	**timePM [m]**	**fuel [m]**	**fuelPM [m]**
Scenario 1	135.31	1065.57	135.31	1065.57	81.55	1065.57
Scenario 2	829.44	674.24	52.30	674.24	625.66	674.24
Scenario 3	199.79	674.24	112.33	1081.97	829.44	1109.44
Total	**1164.53**	**2414.05**	**299.94**	**2821.78**	**1536.65**	**2849.25**

vidual route and the respective centroids of the polluted areas. The results of the scenarios depending on the optimisation parameters of the routes are shown for the time 18:00 in table 4.7 and for the time 18:30 in table 4.8. The routes with taking into account PM values are compared with the routes without taking into account PM values. In general, the minimum distance of the centroid to the routes with PM values is significantly further away than those routes without particulate matter values. Only scenario 2 shows exceptions, whereby the routes without PM values are already far away from the centroid. If the results of all scenarios are added up, the routes without considering PM values are on average around 340 m away from the hotspot centroid, and the routes with considering PM values are on average around 900 m away. This means that the minimum distance between the centroid and the routes including PM values is more than twice as far, more precisely by a factor of around 2.6 compared to routes without considering PM values.

In the second hotspot analysis, the entire route was considered by calculating the average distance of each line segment to the PM centroids. These distances are shown in the figure 4.14 as blue lines. On the basis of these results, the average value of the line segments was formed for each route and the routes with PM values and without PM values were compared at 18:00 (table 4.9) and at 18:30 (table 4.10) again. For almost all scenarios,

Table 4.8: Minimum distance between PM centroids and routes at 18:30

Routes at 18:30	**dis [m]**	**disPM [m]**	**time [m]**	**timePM [m]**	**fuel [m]**	**fuelPM [m]**
Scenario 1	135.31	1065.57	135.31	1065.57	81.55	1065.57
Scenario 2	829.44	751.40	52.30	751.40	803.05	751.40
Scenario 3	199.79	977.83	112.33	751.40	829.44	977.83
Total	**1164.53**	**2794.81**	**299.94**	**2568.38**	**1714.04**	**2794.81**

Table 4.9: Average distance between PM centroids and line segments of the routes at 18:00

Routes at 18:00	**dis [m]**	**disPM [m]**	**time [m]**	**timePM [m]**	**fuel [m]**	**fuelPM [m]**
Scenario 1	1947.95	2274.01	1968.14	2431.10	2043.67	2297.95
Scenario 2	1537.07	1489.63	1295.74	1489.63	1388.60	1477.64
Scenario 3	1145.68	1218.51	1099.12	2552.57	1399.94	2588.44
Total	**4630.70**	**4982.14**	**4363.01**	**6473.29**	**4832.21**	**6364.04**

the average distance of the line segments and the routes considering the PM values is greater than those routes without considering PM values. Only in Scenario 2 at 18:00 the average distance is smaller by a minimum at the route after the distance without PM values, whereby both routes are significantly away from the PM centroids. If all results are summed up, the average distance between the centroids and the routes without considering PM values is around 1660 m and for the routes with considering PM values around 2100 m, which makes a difference of 440 m.

The combination of the two results of the analyses shows that the minimum distance of the routes with PM values compared to routes without PM values is clearly away from the PM centroids, but the average distance of the entire routes is not that far away. This means that the routes with PM values avoid the PM hotspots, but overall these routes are not further away from the routes without PM values.

Table 4.10: Average distance between PM centroids and line segments of the routes at 18:00

Routes at 18:30	**dis [m]**	**disPM [m]**	**time [m]**	**timePM [m]**	**fuel [m]**	**fuelPM [m]**
Scenario 1	2467.49	3085.93	2480.56	3185.09	2634.30	3084.24
Scenario 2	1660.60	1970.00	1471.77	1970.00	1621.86	1946.75
Scenario 3	1191.65	1594.17	1143.07	1547.63	1441.52	1590.71
Total	**5319.74**	**6650.10**	**5095.40**	**6702.72**	**5697.68**	**6621.70**

An essential part after the experiment is the evaluation, which is not trivial due to the special topic for this thesis. Basically there are various online route planners, but these usually only show the fastest route. The choice of the shortest route or the most environmentally friendly is hardly possible in this regard. In addition, there is no facility of carrying out a valuation for the routes that take pollutants into account. One of the world's most famous route planners is Google Maps, which shows the fastest route and other alternative routes, but one of the alternative routes is not always the shortest one after the distance. In addition, no information about fuel consumption is available. For the reasons mentioned, an alternative was sought that offers all three optimization options for the routing. The route planner OpenRouteService (ORS), which was developed by the HeiGIT (Heidelberg Institute for Geoinformation Technology), offers solutions for two optimisation options for the routing and was therefore used for the evaluation. By means of ORS it is possible to calculate the fastest route according to the time and the shortest route according to the distance for a certain start and destination location. A route according to the lowest fuel consumption is also not available for this route planner, but it is possible to display the fuel consumption for each route carried out, which is determined experimentally. In addition, various parameters such as driving speed, auto brand, vehicle class, fuel type, etc. can be specified. For the evaluation of the scenarios a driving speed of 50 km/h, the fuel type diesel and the vehicle class medium cars were selected. The differences between the independently calculated routes and the routes according to ORS are represented in the following subsections both visually using graphics and with numerical values using tables. In the tables, the distinctions between the routes are given only with positive numbers. With regard to CO_2 emissions, it should be mentioned that these differ for all routes, since this value is calculated based on fuel consumption and ORS uses a factor of 2621, whereas a factor of 2660 was used for the self-calculated routes. For this reason, only the parameters distance, time and fuel consumption are dealt with in more detail in the following scenarios.

4.4.1 Scenario 1

For scenario 1, the route according to the distance is first compared with the calculated route and the route according to the ORS. It can be seen that the courses are largely identical to each other, only in the city center there is a short, different course (figure 4.15(a)). The route according to the time also indicates the same course in the north of Graz, from the city center the

(a) routing after distance (b) routing after time

Figure 4.15: Scenario 1 - Comparison of the calculated routes with the routes from ORS

Table 4.11: Scenario 1 - Overview and comparison between the results of the calculated routes and the ORS-routes

Scenario 1	**Distance [km]**	**Time [min]**	**Fuel consumption [l]**	**CO2 [g]**
Dis - min	11.95	24.26	0.66	1745.80
Dis - min ORS	11.90	31.00	0.51	1331.83
Difference Dis	**0.05**	**6.74**	**0.15**	**413.98**
Time - min	11.98	23.36	0.66	1753.47
Time - min ORS	13.00	25.00	0.55	1451.80
Difference Time	**1.02**	**1.64**	**0.11**	**301.67**

two routes separate and run parallel to each other to the destination (figure 4.15(b)). The results of the individual parameters reflect the leading routes mentioned, for which there are only minimal differences. The only outlier is the route according to the minimum distance at which the calculated route is more than 6 minutes faster than the route from ORS. This is difficult to explain, since in principle no current traffic volume is taken into account in both routings. The result was therefore tried to be evaluated using Google Maps route planner, whereby 24 minutes are required for the route in light traffic, which corresponds to the self-calculated approach.

4.4.2 Scenario 2

Both the route according to the distance and the route according to the time have different courses between the calculated route and the ORS route (figure 4.16). The two routes after the distance lead almost parallel to each other, whereby the ORS route runs more north than the independently

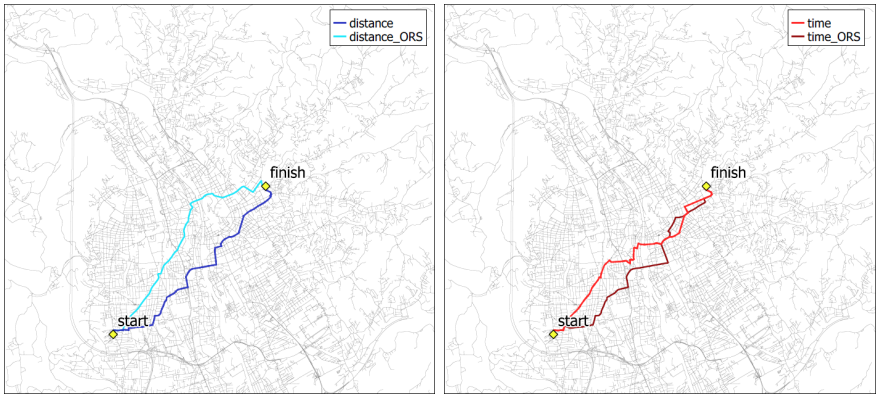

(a) routing after distance (b) routing after time

Figure 4.16: Scenario 2 - Comparison of the calculated routes with the routes from ORS

Table 4.12: Scenario 2 - Overview and comparison between the results of the calculated routes and the ORS-routes

Scenario 2	**Distance [km]**	**Time [min]**	**Fuel consumption [l]**	**CO2 [g]**
Dis - min	8.63	22.32	0.69	1825.90
Dis - min ORS	8.40	21.00	0.36	943.13
Difference Dis	**0.23**	**1.32**	**0.33**	**882.78**
Time - min	8.73	20.03	0.65	1719.69
Time - min ORS	8.90	21.00	0.38	992.58
Difference Time	**0.17**	**0.97**	**0.27**	**727.11**

calculated one. The fastest routes after the time lead next to each other, cross each other twice near the city center before these reach the destination. If the routes are compared corresponding to the parameters, the routes after the minimum distance differ of just 230 m and the routes after time by less than a minute. However, there are greater differences in fuel consumption, which is almost twice as high for the independently calculated routes. The reason for this will be explained in more detail in the next chapter (4.4.4). Further values can be taken from table 4.12.

4.4.3 Scenario 3

In the third scenario, the routes according to the distance show similar courses for the self-calculated route as well as for the route from ORS, with only minor deviations (figure 4.17(a)). However, the routes differ corresponding to the time, whereby the routes often cross and then continue in exactly the contrary direction (figure 4.17(b)). Though, when comparing

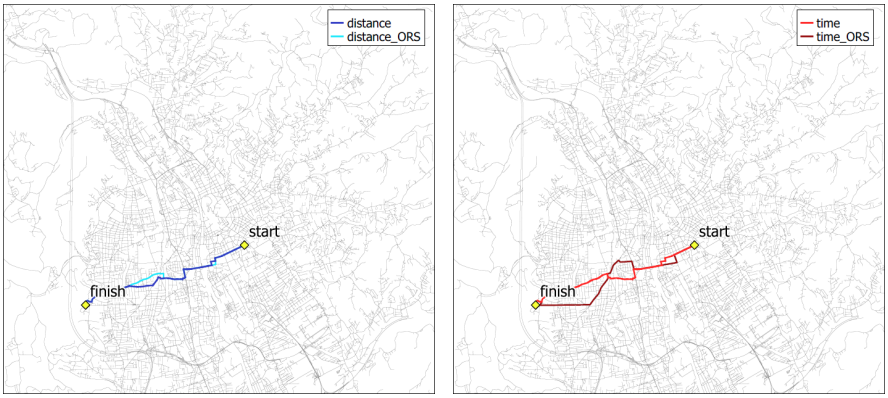

(a) routing after distance (b) routing after time

Figure 4.17: Scenario 3 - Comparison of the calculated routes with the routes from ORS

Table 4.13: Scenario 3 - Overview and comparison between the results of the calculated routes and the ORS-routes

Scenario 3	**Distance [km]**	**Time [min]**	**Fuel consumption [l]**	**CO2 [g]**
Dis - min	6.40	16.47	0.47	1262.65
Dis - min ORS	6.50	18.00	0.28	725.25
Difference Dis	**0.10**	**1.53**	**0.19**	**537.41**
Time - min	6.44	16.35	0.48	1266.01
Time - min ORS	7.10	16.00	0.30	790.09
Difference Time	**0.66**	**0.35**	**0.18**	**475.92**

the parameters, it is noticeable that the difference between the two routes over time is just 21 seconds. Also for the routing according to the shortest route, the two routes have only a difference of 100 m (see table 4.13). Larger distinctions of less than 0.2 l occur in fuel consumption, which can be considered large due to the short distance. An attempt to explain the significantly different fuel consumption is given in the following section.

4.4.4 Verification of the differences in fuel consumption

The attempt was made to determine why there were significant differences in fuel consumption between the self-calculated routes and the ORS routes in two of three scenarios. Due to the fact that no information about the approach of the fuel consumption of ORS is available, changes were made to the scenarios in order to come closer to the difference in fuel consumption. When trying to swap the start and destination locations of the scenarios, the results were logically different with the self-calculated approach. However,

Table 4.14: Results of the routes when driving uphill and downhill

Route	**Distance [km]**	**Time [min]**	**Fuel consumption [l]**	**CO2 [g]**
Route uphill	1.92	4.70	0.48	1269.89
Route-ORS uphill	1.90	5.00	0.08	215.24
Route downhill	1.92	4.72	0.09	243.48
Route-ORS downhill	1.90	5.00	0.08	215.24

the fuel consumption when routing using ORS was mostly identical and also approximated to the values of the self-calculated approach for the scenarios two and three.

Since the last two scenarios increase slightly compared to the first, it was concluded that the differences in height had to be examined more closely. Therefore, a short route with less than 2 km was chosen, which has a height difference of over 120 m (see figure 4.18 & 4.19). It was found that the ORS routes have a fuel consumption of 0.08 l when driving uphill and downhill. In contrast, the self-calculated route has a consumption of 0.48 l when driving up and 0.09 l when driving downhill (table 4.14). This means that the route difference from ORS takes little or no account of the difference in altitude. This is the reason why scenarios two and three are difficult to adjust as these lead slightly uphill. The scenario one, however, leads slightly downhill and therefore the results of the fuel consumption of the two approaches distinguish only minimal.

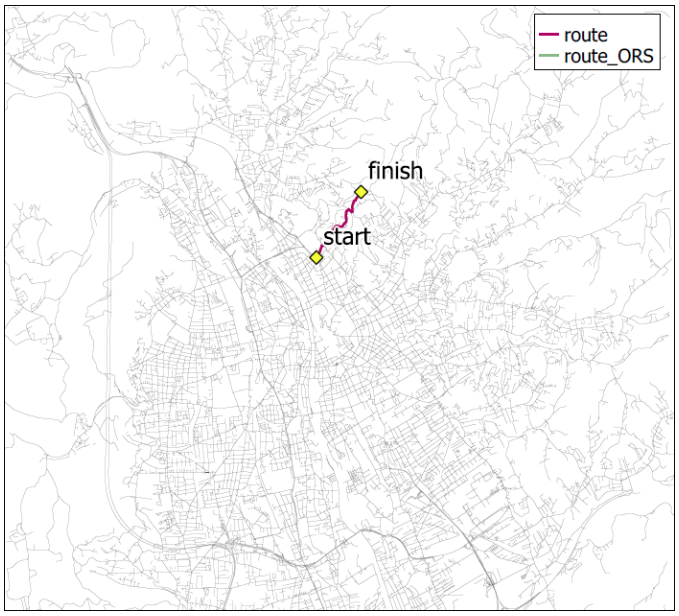

Figure 4.18: Presentation of a short test route with a clear difference in altitude

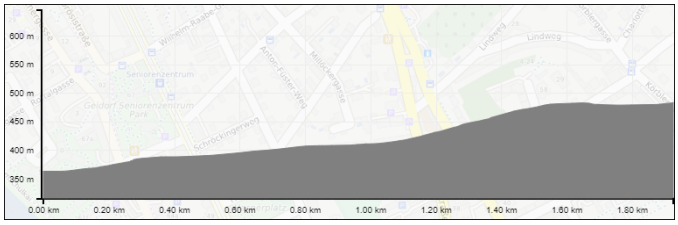

Figure 4.19: Elevation profile of the test route (OpenRouteService, n.d.)

Chapter 5

Conclusion and Discussion

In the course of this thesis it was demonstrated that it is possible to generate an environmentally friendly route using a wide range of parameters. This is mainly influenced by vehicle, road and traffic characteristics, of the latter two the most important ones have been implemented in the routing, but many other factors could be taken more into account. It was found that the effects of these factors on fuel consumption are not always present in the literature, such as when turning at intersections. The model for calculating the fuel consumption is based on the driving resistance, whereby the determination of the specific consumption was carried out in a simplified manner. Due to the lack of data, the specific consumption was not determined using the much more precise engine map. To answer the first research question, the exact results between the individual routes can be found in the tables of the scenarios in the chapter 4. Overall, it can be seen that the routes do not differ significantly when considering the optimization parameters distance, time, fuel consumption and CO_2 for the selected scenarios, since the course of the routes was often identical.

In addition to the environmentally friendly route, current particulate matter data are taken into account when generating a route. Basically, it was the idea that this data would be obtained directly on the roads through the air quality sensors used in the vehicles. Because there were no access to this data and the state of Styria did not have any current comprehensive data for the city of Graz, the data were received from the measuring stations. Finally, the data for the investigation area were calculated using an interpolation method. This approach is not the most correct, but it is sufficient for this purpose. It is a little bit disappointing that despite the enormous PM pollution in the city of Graz, no current area-wide data are available. By storing the data on a server, the data can be queried continuously and used for a wide variety of applications. The fact that this was developed based on the SOS standard from OGC ensures interoperability and standardization.

Many navigation systems already developed the most environmentally friendly route, but no real-time pollutant data are implemented. This approach has shown that areas with an extremely high pollution are avoided

and the routes are only led through areas with low pollution values, which answers the first part of the second research question. In order to respond the second part of the question, the results of the hotspot analysis are used. It can be seen that the "re-routing" means that the minimum distance of the routes with taking the PM values into account, is clearly a factor of 2.6 away from the centroid of pollution compared to the routes without particulate matter. However, considering the average distance to the centroid, the routes only differ by around 440 m. Overall, the "re-routing" makes the routes a little bit longer, but the distance to the centroid of the pollutant hotspot is fundamental further away. Of great importance is the weighting of the pollutant values, which was carried out using an air quality index. On the one hand, an insufficient assessment of the pollutant values means that the route still leads through areas with high pollution. On the other hand, too high weighting of the pollutant values causes that the routes consume enormously long and much more fuel and thus become uneconomical. In general, it would be very interesting to know from which additional consumption a route becomes uneconomical. The inclusion of PM values would mean that the route selection would vary more frequently, which could enable a better distribution of traffic. The use of traffic control could support this approach. In addition, the particulate matter values would be better distributed across the city and individual areas would no longer be affected by extremely high levels of pollutants.

A detailed evaluation of the achieved results could not be carried out because there are no comparable approaches in this field. Only the results of the routes according to the optimization parameters time and distance could be fully verified with the route planner from ORS. Although the most environmentally friendly route could not be evaluated, the fuel consumption was also specified for the route according to the time and distance and compared with the self-calculated model. The routes showed similar results in terms of time and distance, as well as the routes for fuel consumption in the plain and when driving downhill. There were only differences when driving uphill, as ORS either takes the height differences very little or not at all into account.

The PM values could also be used for other applications for which a pure air is very important. For example, an app could be developed that suggests a route for cyclists or runners through areas with less pollution. Since these user groups are directly in the air compared to the drivers and are often not tied to a specific destination, this would be a sensible alternative. In addition, different routes ensure a good diversification due to different pollutant data depending on the date and time.

This concept is an impetus to distribute pollutant emissions more evenly in cities and thus to reduce the formation of air pollution hotspots. The best

way to protect the environment is, of course, to not use the vehicle as often as possible. We only can save the world when everyone pull together.

Bibliography

Aavik, A., Kaal, T., & Jentson, M. (Eds.) (2013). Use of Pavement Surface Texture Characteristics Measurement Results in Estonia.

ADAC e.V. (n.d.). Sprit sparen: Wieviel Sprit kosten Klima, Strom und Zuladung usw. im Auto? Retrieved from `https://www.adac.de/infotestrat/tanken-kraftstoffe-und-antrieb/spritsparen/`

Ahn, K. (1998). Microscopic Fuel Consumption And Emission Modeling (Masterarbeit). Virginia Polytechnic Institute and State University, Blacksburg.

Ahn, K.(2002). Modeling Light Duty Vehicle Emissions Based on Instantaneous Speed and Acceleration Levels (Dissertation). Virginia Polytechnic Institute and State University, Blacksburg.

Akcelik, R. (1983). Progress in Fuel Consumption Modelling for Urban Traffic Management (No. 124). Vermont South, Australia.

Alexiadis, V., Jeannotte, K., & Chandra, A. (June 2004). Traffic Analysis Toolbox Volume I: Traffic Analysis Tools Primer (No. FHWA-HRT-04-038).

AllSecur Deutschland AG (n.d.). Alles zu Schadstoffklasse & Euronorm. Retrieved from `https://www.allsecur.de/kfz-versicherung/schadstoffklasse-ratgeber/#schadstoffklasse-bedeutung`

Alt, O. (2009). Car Multimedia Systeme Modell-basiert testen mit SysML (1st ed.). Wiesbaden: Vieweg+Teubner. https://doi.org/10.1007/978-3-8348-9567-7

An, F., Barth, M., Norbeck, J., & Ross, M. (1997). Development of Comprehensive Modal Emissions Model: Operating Under Hot-Stabilized Conditions. Transportation Research Record: Journal of the Transportation Research Board, 1587(1), 52–62. https://doi.org/10.3141/1587-07

Anderl, M., Burgstaller, J., Gugele, B., Gössl, M., Haider, S., Heller, C., . . . Zechmeister, A. (2018). Klimaschutzbericht 2018 (REP-0660). Wien.

Arthur D. Little (2006). Market and Technology Study Automotive Power Electronics 2015.

Auto Research Center (n.d.). The Effect of Aerodynamic Drag on Fuel Economy. Retrieved from `http://www.arcindy.com/effect-of-`

aerodynamic-drag-on-fuel-economy.html

Bachman, W., Sarasua, W., Hallmark, S., & Guensler, R. (2000). Modeling regional mobile source emissions in a geographic information system framework. Transportation Research Part C: Emerging Technologies, 8(1-6), 205–229. https://doi.org/10.1016/S0968-090X(00)00005-X

Bachman, W. H. (August 1998). A GIS-Based Modal Model of Automobile Exhaust Emissions: Final Report. Atlanta.

Bagieński, Z. (2015). Traffic air quality index. The Science of the Total Environment, 505, 606–614. https://doi.org/10.1016/j.scitotenv.2014.10.041

Bandeira, J. M., Fontes, T., Pereira, S. R., Fernandes, P., Khattak, A. J., & Coelho, M. C. (2014). Assessing the Importance of Vehicle Type for the Implementation of Eco-routing Systems. Transportation Research Procedia, 3, 800–809. https://doi.org/10.1016/j.trpro.2014.10.063

Bansal, R., & Sharma, R. B. (2014). Drag Reduction of Passenger Car Using Add-On Devices. Journal of Aerodynamics, 2014. https://doi.org/10.1155/2014/678518

Barth, M., & Boriboonsomsin, K. (2009). Traffic Congestion and Greenhouse Gases. Access, 35.

Barth, M., Malcolm, C., Younglove, T., & Hill, N. (2001). Recent Validation Efforts for a Comprehensive Modal Emissions Model. Transportation Research Record, 1750(1), 13–23. https://doi.org/10.3141/1750-02

Bates, M. (2014). Serial Communications. In Interfacing PIC Microcontrollers (pp. 263–297). Elsevier. https://doi.org/10.1016/B978-0-08-099363-8.00008-X

Beuving, E., Jonghe, T. de, Goos, D., Lindahl, T., & Stawiarski, A. (March 2004). Environmental Impacts and Fuel Efficiency of Road Pavements.

Beydoun, M., & Guldmann, J.-M. (2006). Vehicle characteristics and emissions: Logit and regression analyses of I/M data from Massachusetts, Maryland, and Illinois. Transportation Research Part D: Transport and Environment, 11(1), 59–76. https://doi.org/10.1016/j.trd.2005.09.003

Biggs, D. C., & Akcelik, R. (1985). An Interpretation of the Parameters in the Simple Average Travel Speed Model of Fuel Consumption. Australian Road Research Board, 15(1), 46–49.

Boriboonsomsin, K., & Barth, M. (2009). Impacts of Road Grade on Fuel Consumption and Carbon Dioxide Emissions Evidenced by Use of Advanced Navigation Systems. Transportation Research Record, 2139(1), 21–30. https://doi.org/10.3141/2139-03

Bosch Robert GmbH (n.d.). Für die Zukunft der Mobilität: sparsames

Fahren und saubere Stopps. Retrieved from https://de.bosch-automotive.com/de/parts_and_accessories/motor_and_sytems/start_stop_system/functionality_start_stop_system/functionality_start_stop_system

Botts, M., & Liang, S. (n.d.). Sensor Web Enablement DWG. Retrieved from http://www.opengeospatial.org/projects/groups/sensorwebdwg

Botts, M., Percivall, G., Reed, C., & Davidson, J. (2007). OGC Sensor Web Enablement: Overview And High Level Architecture. (OGC 07-165).

Bowyer, D. P., Akcelik, R. , & Biggs, D. C. (1985). Guide to Fuel Consumption Analysis for Urban Traffic Management (No. 32). Vermont South, Australia.

Bröring, A., Echterhoff, J., Jirka, S., Simonis, I., Everding, T., Stasch, C., . . . Lemmens, R. (2011). New generation Sensor Web Enablement. Sensors (Basel, Switzerland), 11(3), 2652–2699. https://doi.org/10.3390/s110302652

Bröring, A., Stasch, C., & Echterhoff, J. (2012). OGC Sensor Observation Service Interface Standard. (OGC 12-006).

Brünglinghaus, C. (2014). Elektronik und Software beherrschen Innovationen im Auto. Automobilelektronik & Software.

Bruno, F., & Cocchi, D. (2007). Recovering information from synthetic air quality indices. Environmetrics, 18(3), 345–359. https://doi.org/10.1002/env.834

Bundesministerium für Nachhaltigkeit und Tourismus (2019). Statusbericht zu den CO2-Emissionen neu zugelassener Pkw in Österreich: Abnehmender Trend der CO2- Emissionen gebrochen. Retrieved from https://www.bmnt.gv.at/umwelt/luft-laerm-verkehr/co2-monitoringPKW1.html

Bundesministerium für wirtschaftliche Zusammenarbeit und Entwicklung, Referat Wasser, Stadtentwicklung, Mobilität (August 2016). Urbane Mobilität: Strategien für lebenswerte Städte.

Buxbaum, I., Nagl, C., Spangl, W., Schieder, W., Anderl, M., Haider, S., & Pazdernik, K. (2018). Analyse der Feinstaub-Belastung: 2009-2017. Im Auftrag der Plattform Saubere Luft. Wien.

Caldow, J. (May 2008). Feeling the Pain: The Impact of Traffic Congestion on Commuters.

California Air Resources Board (n.d.). Mobile Source Emission Inventory — Categories. Retrieved from https://ww3.arb.ca.gov/msei/categories.htm

California Environmental Protection Agency (2014, April 30). EMFAC2014 Volum 1 - User's Guide: Mobile Source Analysis Branch.

Cappiello, A. (2002). Modeling Traffic Flow Emissions (master's thesis). Massachusetts Institute of Technology, Cambridge.

CITEAIR (n.d.). Participating cities. Retrieved from `http://www.airqualitynow.eu/about_participating_cities.php`

Commission for Integrated Transport (2007). Transport and Climate Change: Advice to Government from the Commission for Integrated Transport. London.

Consumer Reports (n.d.). Guide to Car Safety Features: These features can help make driving safer. Retrieved from `https://www.consumerreports.org/cro/2012/04/guide-to-safety-features/index.htm`

Correia, A. W., Pope, C. A., Dockery, D. W., Wang, Y., Ezzati, M., & Dominici, F. (2013). Effect of air pollution control on life expectancy in the United States: An analysis of 545 U.S. Counties for the period from 2000 to 2007. Epidemiology (Cambridge, Mass.), 24(1), 23–31. https://doi.org/10.1097/EDE.0b013e3182770237

Costagliola, M. A., Costabile, M., & Prati, M. V. (2018). Impact of road grade on real driving emissions from two Euro 5 diesel vehicles. Applied Energy, 231, 586–593. https://doi.org/10.1016/j.apenergy.2018.09.108

Crolla, D.A. (2009). Automative Engineering: Powertrain, Chassis System, and Vehicle Body: Butterworth-Heinemann is an imprint of Elsevier.

De Moura, M. B. B., & Tribess A. (2007). Climate control system improvements for better cabin environmental conditions and reduction of fuel consumption. SAE Technical Papers. (2007-01-2673).

Dobre, C., Pop, F., Cristea, V., & Xhafa, F. (2012). Intelligent Traffic Lights To Reduce Vehicle Emissions. Proceedings 26th European Conference on Modelling and Simulation, 504–511. https://doi.org/10.7148/2012-0504-0511

Dubitzky, W., & Karacay, T. (2013). CAN – From its early days to CAN FD. CAN Newsletter, 1, 8–11.

Duchoň, F., Babinec, A., Kajan, M., Beňo, P., Florek, M., Fico, T., & Jurišica, L. (2014). Path Planning with Modified a Star Algorithm for a Mobile Robot. Procedia Engineering, 96, 59–69. https://doi.org/10.1016/j.proeng.2014.12.098

Dudenhöffer, F., & John, E. M. (2009). EU-Normen für Verbrauchangaben von Autos: Mehr als ein Ärgernis für Autokäufer. ifo Schnelldienst,

62(13), 14–17.

Elbassuoni, S., & Abdel-sRahim, A. (2013). Modeling Fuel Consumption And Emissions At Signalized Intersection Approaches: A Synthesis Of Data Sources And Analysis Tools. 54th Annual Transportation Research Forum, Annapolis, Maryland, March 21-23, 2013. (206953).

Elgowainy, A., Rousseau, A., Wang, M., Ruth, M., Andress, D., Ward, J., . . . Das, S. (2013). Cost of ownership and well-to-wheels carbon emissions/oil use of alternative fuels and advanced light-duty vehicle technologies. Energy for Sustainable Development, 17(6), 626–641. https://doi.org/10.1016/j.esd.2013.09.001

EMISIA (n.d.). Copert: The industry standard emissions calculator. Retrieved from `https://www.emisia.com/utilities/copert/`

Environmental Studies and Testing (n.d.). VERSIT+: TNO state-of-the art road traffic emission model.

Errampalli, M., Senathipathi, V., & Thamban, D. (2015). Effect of Congestion and Fuel Cost and Travel Time Cost on Multi-Lane Highways in India. International Journal for Traffic and Transport Engineering, 5(4), 458–472. https://doi.org/10.7708/ijtte.2015.5(4).10

Ersoy, M., & Gies, S. (2017). Fahrwerkhandbuch: Grundlagen · Fahrdynamik · Fahrverhalten · Komponenten · Elektronische Systeme · Fahrerassistenz · Autonomes Fahren · Perspektiven (5. Auflage). Wiesbaden: Springer Fachmedien Wiesbaden. https://doi.org/10.1007/978-3-658-15468-4

European Commission (n.d.). A Consumer's Guide to Energy-Efficient Tyres.

European Commission (2006). Study SI2.408210 Tyre/Road Noise: Volume 1: Final Report.

Verordnung (EG) Nr. 443/2009 des Europäischen Parlaments und des Rates vom 23. April 2009 zur Festsetzung von Emissionsnormen für neue Personenkraftwagen im Rahmen des Gesamtkonzepts der Gemeinschaft zur Verringerung der CO2-Emissionen von Personenkraftwagen und leichten Nutzfahrzeugen (2009).

Verordnung Nr. 1222/2009 des Europäischen Parlaments und des Rates vom 25. November 2009 über die Kennzeichnung von Reifen in Bezug auf die Kraftstoffeffizienz und andere wesentliche Parameter (Text von Bedeutung für den EWR) (2009).

European Commission (February 2013). Technical Guidelines for the preparation of applications for the approval of innovative technologies pursuant to Technical Guidelines for the preparation of applications for

the approval of innovative technologies pursuant to Regulation (EC) No 443/2009 of the European Parliament and of the Council. Brussels, Belgium.

European Environment Agency (November 2009). Car occupancy rates: Car occupany rates between 2004 and 2008.

European Environment Agency (2016a). EMEP/EEA air pollutant emission inventory guidebook 2016: Technical guidance to prepare national emission inventories (No. 21). Luxembourg.

European Environment Agency (2016b). Monitoring of CO2 emissions from passenger cars – Regulation (EC) No 443/20092016.

European Environment Agency (2018). Emissions of air pollutants from transport. Copenhagen.

Faris, W. F., Rakha, H. A., Kafafy, R. I., Idres, M., & Elmoselhy, S. (2011). Vehicle Fuel Consumption and Emission Modelling: An In-Depth Literature Review. International Journal of Vehicle Systems Modelling and Testing, 6(3/4), 318–395.

Feuerecker, G., Schafer, B., & Strauss, T. (2005). Auxiliary Heating Systems of Conventional and Heat Pump Type: Technology, Performance and Efficiency. SAE Technical Papers. (2005-01-2055).

FIA (n.d.). Lightening Up: How Less Heavy Vehicles Can Help Cut CO2 Emissions. Retrieved from `https://www.fiaregion1.com/lightcarlowcarbon/`

Filip, G. M., & Brezoczki, V. M. (2017). Particulate matter urban air pollution from traffic car. IOP Conference Series: Materials Science and Engineering, 200(1), 12027. Retrieved from `http://stacks.iop.org/1757-899X/200/i=1/a=012027`

Fontaras, G., & Dilara, P. (2012). The evolution of European passenger car characteristics 2000–2010 and its effects on real-world CO2 emissions and CO2 reduction policy. Energy Policy, 49, 719–730. https://doi.org/10.1016/j.enpol.2012.07.021

Fontaras, G., & Samaras, Z. (2010). On the way to 130gCO2/km—Estimating the future characteristics of the average European passenger car. Energy Policy, 38(4), 1826–1833. https://doi.org/10.1016/j.enpol.2009.11.059

Fontaras, G., Zacharof, N.-G., & Ciuffo, B. (2017). Fuel consumption and CO2 emissions from passenger cars in Europe – Laboratory versus real-world emissions. Progress in Energy and Combustion Science, 60, 97–131. https://doi.org/10.1016/j.pecs.2016.12.004

Frey, H. C., Unal, A., Rouphail, N. M., & Colyar, J. D. (2003). On-Road Measurement of Vehicle Tailpipe Emissions Using a Portable Instrument. Journal of the Air & Waste Management Association, 53(8), 992–1002. https://doi.org/10.1080/10473289.2003.10466245

Gevatter, H.-J., & Grünhaupt, U. (2006). Handbuch der Mess- und Automatisierungstechnik im Automobil: Fahrzeugelektronik, Fahrzeugmechatronik (2., vollständig bearbeitete Auflage). VDI-Buch. Berlin, Heidelberg: Springer-Verlag Berlin Heidelberg. https://doi.org/10.1007/3-540-29980-7

Gilliéron, P., & Kourta, A. (2008). Automobile et environnement : contribution de la recherche aérodynamique à la réduction des gaz à effet de serre. Mécanique & Industries, 9(6), 519–531. https://doi.org/10.1051/meca/2009016

Graphenintegrationsplattform (2018). Intermodaler Verkehrsgraph Österreich: Standardbeschreibung der Graphenintegrationsplattform (GIP), 2.2. Graphenintegrationsplattform (2019). Dokumentation: Intermodales Verkehrsreferenzsystem Österreich.

Greene, S., Akbarian, M., Ulm, F.-J., & Gregory, J. (August 2013). Pavement Roughness and Fuel Consumption.

Greenwood, I. D., & Bennett, C. R. (1996). The effects of traffic congestion on fuel consumption. Road & Transport Research, 5(2), 18-32.

Guensler, R. (1993). Data Needs for Evolving Motor Vehicle Emission Modeling Approaches. University of California.

Haberl, M., Fellendorf, M., Luz, R., & Hausberger, S. (2014). Integrating an Emission Minimizing Extension in an adaptive Signal-Control Optimization Algorithm. International Transport and Air Pollution Conference (TAP).

Haken, K.-L. (2011). Grundlagen der Kraftfahrzeugtechnik: Mit 36 Tabellen sowie 20 Übungsaufgaben (2., aktualisierte und erw. Aufl.). Fahrzeugtechnik. München: Hanser. Retrieved from `http://www.hanser-elibrary.com/isbn/9783446426047`

Harrington, W. (1997). Fuel Economy and Motor Vehicle Emissions. Journal of Environmental Economics and Management, 33(3), 240–252. https://doi.org/10.1006/jeem.1997.0994

Hausberger, S. (2009). Emission Factors from the Model PHEM for the HBEFA Version 3 (No. I-20a/2009 Haus-Em 33a/08/679). Graz, Austria.

HELLA KGaA Hueck & Co (n.d.). Kurz-Info: Luftgütesensoren (Air Quality Sensor / AQS). Lippstadt.

Helmenstine, A. M. (2019). What Is the Density of Air at STP?: How the Density of Air Works. Retrieved from https://www.thoughtco.com/density-of-air-at-stp-607546

Hofmann-Wellenhof, B., Legat, K., & Wieser, M. (2003). Navigation: Principles of Positioning and Guidance. Vienna, s.l.: Springer Vienna. https://doi.org/10.1007/978-3-7091-6078-7

Höglund, P. G., & Niittymäki, J. (1999). Estimating Vehicle Emissions and Air Pollution related to Driving Patterns and Traffic Calming. Paper for the Conference Urban Transport Systems, Lund, 103–113.

Hucho, W.-H., & Sovran, G. (1993). Aerodynamics of Road Vehicles. General Motors Research and Environmental Staff. (48090-9055).

Huhn, W. (2008). Low Energy Automotive Lighting. SAE Technical Papers. (2008-21-0048).

Humanitarian OpenStreetMap Team (2016). OSM-Daten beschaffen: Overpass Turbo. Retrieved from `https://learnosm.org/de/osm-data/getting-data/`

The Indian Roads Congress. (2001). Geometric design standards for urban roads in plains. New Delhi.

International Energy Agency (2018). CO2 Emissions from Fuel Combustion 2018: Highlights.

International Organization of Motor Vehicle Manufacturers (n.d.). Vehicle Emissions. Retrieved from urlhttp://www.oica.net/category/auto-and-fuels/emissions/

IstSOS - Instituto Scienza della Terra (n.d.). Exploring the Sensor Observation Service Standard Enhanced by istSOS Special Features: Workshop. (2.3.0).

Kakooza, R., Luboobi, L. S., & Mugisha, J.Y.T. (2005). Modeling Traffic Flow and Management at Un-signalized, Signalized and Roundabout Road Intersections. Journal of Mathematics and Statistics, 1(3), 194–202. https://doi.org/10.3844/jmssp.2005.194.202

Kemle, A., Manski, R., Harald, R., & Weinbrenner, M. (2008). Reduction of Fuel Consumption in Air Conditioning Systems. SAE Technical Papers. (2008-28-0025).

Ko, K., Jeong, S., Yoo, I., Lee, S., Kim, J., & Tsunokawa, K. (2009). The change rate of fuel consumption for different IRI of paved roads. Future roads: safer, greener and smarter: proceedings 13th REAAA conference.

Koupal, J., Cumberworth, M., Michaels, H., Beardsley, M., & Brzezinski, D. (2003). Design and Implementation of MOVES: EPA's New Generation

Mobile Source Emission Model.

Kumar, P.V.P., Singh, A., Sharma, N., & Chalumuri, R. S. (2015). Evaluation of Idling Fuel Consumption of Vehicles Across Different Cities. Conference: Recent Advznces in Treffic Engg.

Leeuw, F. de, & Mol, W. (November 2005). Air Quality and Air Quality Indices: a world apart ?: ETC/ACC Technical Paper 2005/5.

Ligterink, N. E., & De Lange, R. (2009). Refined vehicle and driving-behaviour dependencies in the VERSIT+ emission model. Environment & Transport. (122), 1–8.

Local Government & Municipal Knowledge Base (n.d.). Road Roughness. Retrieved from http://lgam.wikidot.com/road-roughness

Lohse, D., & Schnabel, W. (2011). Grundlagen der Straßenverkehrstechnik und der Verkehrsplanung: Band 1 ; Straßenverkehrstechnik (3. Aufl.). Beuth Studium. s.l.: Beuth Verlag GmbH. Retrieved from http://gbv.eblib.com/patron/FullRecord.aspx?p=2032860

Lopez Arteaga, I. (2010). Influence of material damping on the prediction of road texture and tread pattern related rolling resistance. ISMA 2010 International Conference on Noise and Vibration Engineering, 1.

Mandavilli, S., Russell, E. R., & Rys, M. J. (Eds.) (2003). Impact of Modern Roundabouts on Vehicular Emissions.

Marjovi, A., Arfire, A., & Martinoli, A. (2015). High Resolution Air Pollution Maps in Urban Environments Using Mobile Sensor Networks. In 2015 International Conference on Distributed Computing in Sensor Systems (DCOSS): 10 - 12 June 2015, Fortaleza, Brazil : [including workshop papers] (pp. 11–20). Piscataway, NJ: IEEE. https://doi.org/10.1109/DCOSS.2015.32

Mathew, T.V. (2014). Transportation Systems Engineering.

ME-Meßsysteme GmbH (n.d.). CAN Bus Grundlagen. Retrieved from https://www.me-systeme.de/de/technik-zuerst/elektronik/can-bus-grundlagen

Michelin (2003). The tyre: Rolling Resistance and fuel savings.

Mickūnaitis, V., Pikūnas, A., & Mackoit, I. (2007). Reducing fuel consumption and CO2 emission in motor cars. Transport, 22(3), 160–163.

Mitschke, M., & Wallentowitz, H. (2014). Dynamik der Kraftfahrzeuge. Wiesbaden: Springer Fachmedien Wiesbaden. https://doi.org/10.1007/978-3-658-05068-9

Nasir, M. K., Md Noor, R., Kalam, M. A., & Masum, B. M. (2014).

Reduction of fuel consumption and exhaust pollutant using intelligent transport systems. The Scientific World Journal, 2014, 836375. https://doi.org/10.1155/2014/836375

Natural Resources Canada (2014). Learn the facts: Fuel consumption and C02. Retrieved from https://www.nrcan.gc.ca/sites/www.nrcan.gc.ca/files/oee/pdf/transportation/fuel-efficient-technologies/autosmart_factsheet_6_e.pdf

Natural Resources Canada (2018). Vehicle weight. Retrieved from https://www.nrcan.gc.ca/energy/efficiency/transportation/21024

Nesamani, K. S., & Subrahmanian, K. P. (2006). Impact of Real-World Driving Characteristics on Vehicular Emissions. JSME International Journal Series B, 49(1), 19–26. https://doi.org/10.1299/jsmeb.49.19

ÖAMTC (n.d.). Umstellung der Normverbrauchs-Messung von NEFZ auf WLTP: Änderungen bei Neufahrzeugen: Was ist zu beachten? Retrieved from https://www.oeamtc.at/thema/steuern-abgaben/umstellung-der-normverbrauchs-messung-von-nefz-auf-wltp-23987937

O'Driscoll, R., Stettler, M. E.J., Molden, N., Oxley, T., & ApSimon, H. M. (2018). Real world CO2 and NOx emissions from 149 Euro 5 and 6 diesel, gasoline and hybrid passenger cars. Science of The Total Environment, 621, 282–290. https://doi.org/10.1016/j.scitotenv.2017.11.271

OGC (n.d.a). OGC PUCK Protocol Standard. Retrieved from http://www.opengeospatial.org/standards/puck

OGC (n.d.b). Why is the OGC involved in Sensor Webs? Retrieved from http://www.opengeospatial.org/domain/swe

OpenRouteService (n.d.). Openrouteservice Maps. Retrieved from https://maps.openrouteservice.org/directions?n1=47.091207&n2=15.443666&n3=15&a=47.08705,15.436134,47.099154,15.448505&b=0&c=1&k1=en-US&k2=km

OpenStreetMap Wiki (2019). Tag:highway=traffic signals. Retrieved from https://wiki.openstreetmap.org/w/index.php?title=Tag:highway%3Dtraffic_signals&oldid=1894208

Othayoth, D., & Rao, K. K.V. (2018). Estimation of stopped delay to control delay conversion factor and development of delay model for non-lane based heterogeneous traffic. European Transport, 69(3).

Pandian, S., Gokhale, S., & Ghoshal, A. K. (2009). Evaluating effects of traffic and vehicle characteristics on vehicular emissions near traffic intersections. Transportation Research Part D: Transport and Environment, 14(3), 180–196. https://doi.org/10.1016/j.trd.2008.12.001

Paragon AG (n.d.a). Luftgütesensor AQS Mk X: Air Quality Sensor. Delbrück.

Paragon AG (n.d.b). PM2.5 Partikelsensor. Delbrück.

Park, S., & Rakha, H. (2006). Energy and Environmental Impacts of Roadway Grades. Transportation Research Record, 1987(1), 148–160. https://doi.org/10.1177/0361198106198700116

Pavement Interactive (n.d.). Roughness. Retrieved from https://www.pavementinteractive.org/reference-desk/pavement-management/pavement-evaluation/roughness/

Pavlovic, J., Marotta, A., Anagnostopoulos, K., Tsiakmakis, S., Ciuffo, B. [B.], Fontaras, G., & Zacharof, N. G. (2016). Review of in use factors affecting the fuel consumption and CO2 emissions of passenger cars. EUR, Scientific and technical research series: Vol. 27819. Luxembourg: Publications Office.

Pischinger, S., & Seiffert, U. (2016). Vieweg Handbuch Kraftfahrzeugtechnik (8. Auflage). Wiesbaden: Springer Fachmedien Wiesbaden. https://doi.org/10.1007/978-3-658-09528-4

Plaia, A., & Ruggieri, M. (2011). Air quality indices: a review. Reviews in Environmental Science and Bio/Technology, 10(2), 165–179. https://doi.org/10.1007/s11157-010-9227-2

Porsche Austria GmbH & Co OG (n.d.a). Volkswagen CC: Start-Stopp-System mit Bremsenergie-Rückgewinnung. Retrieved from https://www.volkswagen.at/service-zubehoer/vorgaengermodelle/volkswagen-cc/start-stopp-system

Porsche Austria GmbH & Co OG (n.d.b). WLTP: Neue Standards für Verbrauchswerte.: Näher am Realverbrauch: WLTP überholt die Verbrauchswerte. Retrieved from https://www.volkswagen.at/wltp

The Public Sector Digest, INC. (n.d.). An analysis of traffic congestion and policy solutions for canadian municipalities.

Rakha, H., & Ahn, K. (2004). Integration Modeling Framework for Estimating Mobile Source Emissions. Journal of Transportation Engineering, 130(2), 183–193. https://doi.org/10.1061/(ASCE)0733-947X(2004)130:2(183)

Rakha, H., Lucic, I., Demarchi, S. H., Setti, J. R., & van Aerde, M. (2001). Vehicle Dynamics Model for Predicting Maximum Truck Acceleration Levels. Journal of Transportation Engineering, 127(5), 418–425. https://doi.org/10.1061/(ASCE)0733-947X(2001)127:5(418)

Rakha, H., van Aerde, M., Ahn, K. , & Trani, A. (2000). Requirements

for Evaluating Traffic Signal Control Impacts on Energy and Emissions Based on Instantaneous Speed and Acceleration Measurements. Transportation Research Record: Journal of the Transportation Research Board, 1738(1), 56–67. https://doi.org/10.3141/1738-07

Ramos, F., Trilles, S., Muñoz, A., & Huerta, J. (2018). Promoting Pollution-Free Routes in Smart Cities Using Air Quality Sensor Networks. Sensors (Basel, Switzerland), 18(8). https://doi.org/10.3390/s18082507

Rathgeber, F. (May 2007). CAN - Controller Area Network. Erlangen.

Reed, C., Botts, M., Percivall, G., & Davidson, J. (2013). OGC Sensor Web Enablement: Overview And High Level Architecture. (OGC 07-165r1).

Resch, B. (2010). Geosensornetzwerke — Echtzeitmessungen für Monitoring- und Informationssysteme. HMD Praxis der Wirtschaftsinformatik, 47(6), 50–58. https://doi.org/10.1007/BF03340531

Rexeis, M. (August 2005). Berechnung der emissionsseitigen Auswirkungen der Einführung einer durchgehenden 100 km/h Beschränkung auf der A 12 zwischen Imst und Landeck/Zams. Graz.

Rezha, F. P., Saputra, O. D., & Shin, S. Y. (2015). Extending CAN bus with ISA100.11a wireless network. Computer Standards & Interfaces, 42, 32–41. https://doi.org/10.1016/j.csi.2015.04.002

Rodrigue, J.-P., Comtois, C., & Slack, B. (2017). The geography of transport systems (4th edition). London, New York: Routledge Taylor & Francis Group.

Rosetta Code (2019). A* search algorithm. Retrieved from `http://rosettacode.org/wiki/A*_search_algorithm#Python`

Rosqvist, S. L. (2007). Vehicular emissions and fuel consumption for street characteristics in residential areas. Lund, Sweden.

Roujol, S., & Joumard, R. (2009). Influence of passenger car auxiliaries on pollutant emission factors within the Artemis model. Atmospheric Environment, 43(5), 1008–1014. https://doi.org/10.1016/j.atmosenv.2008.01.016

Rouphail, N. M., Frey, H. C., Colyar, J. D., & Unal, A. (2001). Vehicle emissions and traffic measures: exploratory analysis of field observations at signalised arterials. Proceedings of the 80th Annual Meeting of the Transportation Research Board, Washington, DC.

Schäfer, F., & Basshuysen, R. (1995). Reduced Emissions and Fuel Consumption in Automobile Engines. Vienna, s.l.: Springer Vienna. Retrieved from `http://dx.doi.org/10.1007/978-3-7091-3806-9https://doi.org/10.1007/978-3-7091-3806-9`

Schmidt, H., & Johannsen R. (2011). Pilotprojekt zur Relevanzanalyse von Einflussfaktoren bei der Ermittlung der CO2-Emissionen und des Kraftstoffverbrauchs im Rahmen der Typgenehmigung von Pkw.

Schmidt, M., & Schäfer, R.-P. (1998). An integrated simulation system for traffic induced air pollution. Environmental Modelling & Software, 13(3-4), 295–303. https://doi.org/10.1016/S1364-8152(98)00030-9

Seat (n.d.). Air Quality Sensor. Retrieved from https://www.seat.com/car-terms/a/air-quality-sensor.html

Shooter, D., & Brimblecombe, P. (2009). Air quality indexing. International Journal of Environment and Pollution - INT J ENVIRON POLLUTION, 36. https://doi.org/10.1504/IJEP.2009.021834

Simonis, I. (2008). OGC Sensor Web Enablement Architecture. (06-021r4).

Sudin, M. N., Abdullah, M. A., Shamsuddin, S. A., Ramli, F. R., & Tahir, M.M. (2014). Review of research on vehicles areodynamic drag reduction methods. International Journal of Mechanical & Mechatronics Engineering IJMME-IJENS, 14(2), 35–47.

TNO (n.d.). EnViVer: model traffic flow and emissions. Retrieved from https://www.tno.nl/en/focus-areas/traffic-transport/roadmaps/sustainable-traffic-and-transport/sustainable-mobility-and-logistics/improving-air-quality-by-monitoring-real-world-emissions/enviver-model-traffic-flow-and-emissions/

Tong, H. Y., Hung, W. T., & Cheung, C. S. (2000). On-Road Motor Vehicle Emissions and Fuel Consumption in Urban Driving Conditions. Journal of the Air & Waste Management Association, 50(4), 543–554. https://doi.org/10.1080/10473289.2000.10464041

Transition énergétique Québec (n.d.). Aerodynamic force. Retrieved from https://ecomobile.gouv.qc.ca/en/bases/aerodynamic_force.php

Transport & Environment (n.d.). Road vehicles and air quality. Retrieved from https://www.transportenvironment.org/what-we-do/air-quality-and-transport/road-vehicles-and-air-quality

U.S. Department of Energy (n.d.). Many Factors Affect Fuel Economy: How You Drive. Retrieved from https://www.fueleconomy.gov/feg/factors.shtml

U.S. Environmental Protection Agency (n.d.a). Description and History of the MOBILE Highway Vehicle Emission Factor Model: What was MOBILE? Retrieved from https://www.epa.gov/moves/description-and-history-mobile-highway-vehicle-emission-factor-model

U.S. Environmental Protection Agency (n.d.b). Latest Version of

MOtor Vehicle Emission Simulator (MOVES). Retrieved from https://www.epa.gov/moves/latest-version-motor-vehicle-emission-simulator-moves

U.S. Environmental Protection Agency (n.d.c). What is Vehicle Specific Power (VSP)? Retrieved from https://www.epa.gov/moves/what-vehicle-specific-power-vsp

U.S. Environmental Protection Agency (2002). User's Guide to MOBILE6.1 and MOBILE6.2: Mobile Source Emission Model Factor-Final Version. (EPA420-R-02-028).

U.S. Environmental Protection Agency (2003). Proof of Concept Investigation for the Physical Emission Rate Estimator (PERE) to be Used in MOVES. (EPA420-R-03-005).

U.S. Environmental Protection Agency (2011). Development of Emission Rates for Light-Duty Vehicles in the Motor Vehicle Emissions Simulator (MOVES2010): Final Report. (EPA-420-R-11-011).

U.S. Environmental Protection Agency (2012). Motor Vehicle Emission Simulator (MOVES): User Guide Version, MOVES2010b. (EPA-420-B-12-001b).

U.S. Environmental Protection Agency (2015a). MOVES2014a User Guide. (EPA-420-B-15-095).

U.S. Environmental Protection Agency (2015b). Official Release of EMFAC2014 Motor Vehicle Emission Factor Model for Use in the State of California. (EPA-R09-OAR-2015-0779).

Umweltbundesamt (n.d.a). Autokauf: Sind Diesel- oder Benzinmotoren umweltfreundlicher? Retrieved from https://www.umweltbundesamt.de/service/uba-fragen/sind-diesel-benzinmotoren-umweltfreundlicher

Umweltbundesamt (n.d.b). Durchschnittlich besitzt jeder zweite Österreicher einen PKW. Retrieved from https://www.umweltbundesamt.at/umweltsituation/verkehr/fahrzeugtechnik/pkw/

Umweltbundesamt (n.d.c). Feinstaub (PM10). Retrieved from http://www.umweltbundesamt.at/umweltsituation/luft/luftschadstoffe/staub/pm10/

Umweltbundesamt (n.d.d). Feinstaub (PM2,5). Retrieved from http://www.umweltbundesamt.at/umweltsituation/luft/luftschadstoffe/staub/pm25/

Umweltbundesamt (n.d.e). Schadstoffe: Verkehr belastet die Umwelt. Retrieved from http://www.umweltbundesamt.at/umweltsituation/

verkehr/auswirkungen_verkehr/verk_schadstoffe/

Umweltbundesamt (n.d.f). Treibhausgase. Retrieved from http://www.umweltbundesamt.at/umweltsituation/luft/treibhausgase/

Umweltbundesamt (n.d.g). Verkehr beeinflusst das Klima: Hauptverursacher bei den klimarelevanten Gasen. Retrieved from http://www.umweltbundesamt.at/umweltsituation/verkehr/auswirkungen_verkehr/verk_treibhausgase/

Umweltbundesamt (n.d.h). Vorhersagen Luftschadstoffbelastung. Retrieved from http://www.umweltbundesamt.at/umweltsituation/luft/luftguete_aktuell/luftqualitaetsindex/

Van den Elshout, S. (2012). CAQI Air quality index: Comparing Urban Air Quality across Borders - 2012.

Van den Elshout, S., Léger, K., & Heich, H. (2014). Caqi Common Air Quality Index–update with PM(2.5) and sensitivity analysis. The Science of the Total Environment, 488-489, 461–468. https://doi.org/10.1016/j.scitotenv.2013.10.060

Van Mensch, P., Ligterink, N. E., & Cuelenaere, R. F. A. (2014). The effect on road load due to variations in valid coast down tests for passenger cars. https://doi.org/10.13140/2.1.2300.9283

Várhelyi, A. (2002). The effects of small roundabouts on emissions and fuel consumption: a case study. Transportation Research Part D: Transport and Environment, 7(1), 65–71. https://doi.org/10.1016/S1361-9209(01)00011-6

Verein Freier Ersatzteilemarkt e.V. (n.d.). CAN-Bus. Retrieved from https://www.mein-autolexikon.de/autolexikon/detail/can-bus.html

Vlieger, I. de, Keukeleere, D. de, & Kretzschmar, J.G. (2000). Environmental effects of driving behaviour and congestion related to passenger cars. Atmospheric Environment, 34(27), 4649–4655. https://doi.org/10.1016/S1352-2310(00)00217-X

Volkswagen AG (n.d.). WLTP: Zeitliche Implementierung. Retrieved from https://www.volkswagenag.com/de/group/fleet-customer/WLTP.html

Weilenmann, M. F., Alvarez, R., & Keller, M. (2010). Fuel consumption and CO2/pollutant emissions of mobile air conditioning at fleet level - new data and model comparison. Environmental Science & Technology, 44(13), 5277–5282. https://doi.org/10.1021/es903654t

Wenzel, T., Singer, B. C., & Slott, R. (2000). Some Issues in the Statistical

Analysis of Vehicle Emissions. Journal of Transportation and Statistics, 1–14.

Wenzel, T. P., & Ross, M. (Eds.) (1997). I/M failure rates by vehicle model.

Willis, R. J., Robbins, M. M., & Thompson, M. (June 2015). Effects on pavement properties on vehicular rolling resistance: a literature review. Auburn, Alabama.

Wllentowitz, H. (2005). Längsdynamik von Kraftfahrzeugen. Schriftreihe Automobiltechnik, 10. Auflage.

Wood, R. M. (2004). Impact of Advanced Aerodynamic Technology on Transportation Energy Consumption. SAE Technical Papers. Advance online publication. https://doi.org/10.4271/2004-01-1306

The World Bank Group (May 2014). Cairo traffic congestion study: executive note.

World Health Organization (n.d.a). Air pollution. Retrieved from `https://www.who.int/sustainable-development/transport/health-risks/air-pollution/en/`

World Health Organization (n.d.b). Ambient (outdoor) air quality and health. Retrieved from `https://www.who.int/news-room/fact-sheets/detail/ambient-(outdoor)-air-quality-and-health`

World Health Organization (n.d.c). Ambient air pollution: Health impacts. Retrieved from `https://www.who.int/airpollution/ambient/health-impacts/en/`

World Health Organization (2016). Ambient air pollution: A global assessment of exposure and burden of disease. Geneva.

Wu, L., Ci, Y., Chu, J., & Zhang, H. (2015). The Influence of Intersections on Fuel Consumption in Urban Arterial Road Traffic: A Single Vehicle Test in Harbin, China. PloS One, 10(9), e0137477. https://doi.org/10.1371/journal.pone.0137477

Wupperverband (n.d.). Was ist Sensor Web? Retrieved from `http://fluggs.wupperverband.de/v2p/web/fluggs/was-ist-sensor-web1`

Wyatt, D. W., Li, H., & Tate, J. E. (2014). The impact of road grade on carbon dioxide (CO2) emission of a passenger vehicle in real-world driving. Transportation Research Part D: Transport and Environment, 32, 160–170. https://doi.org/10.1016/j.trd.2014.07.015

Yue, H. (2008). Mesoscopic fuel consumption and emission modeling (Doctor thesis). Virginia Polytechnic Institute and State University, Blacksburg, USA. Retrieved from `http://www.researchgate.net/publication/`

228999987_Mesoscopic_fuel_consumption_and_emission_modeling

Zallinger, M. S. (2010). Mikroskopische Simulation der Emissionen von Personenkraftfahrzeugen (Dissertation). Technische Universität Graz, Graz.

Zanella, A., Bui, N., Castellani, A., Vangelista, L., & Zorzi, M. (2014). Internet of Things for Smart Cities. IEEE Internet of Things Journal, 1(1), 22–32. https://doi.org/10.1109/JIOT.2014.2306328

Zeng, W., Miwa, T., & Morikawa, T. (2017). Application of the support vector machine and heuristic k-shortest path algorithm to determine the most eco-friendly path with a travel time constraint. Transportation Research Part D: Transport and Environment, 57, 458–473. https://doi.org/10.1016/j.trd.2017.10.001

Zimmermann, W., & Schmidgall, R. (2014). Bussysteme in der Fahrzeugtechnik: Protokolle, Standards und Softwarearchitektur (5th ed.). Wiesbaden: Springer Fachmedien Wiesbaden. https://doi.org/10.1007/978-3-658-02419-2

Appendix

Table A.1: Description of the attributes with data types of the geopackage layer LINKNETZ (GIP, 2019, p.12)

Attribute	**Data type**	**Description**
LINK_ID	integer	Unique ID of the GIP link.
FROM_NODE	integer	Unique ID of the start node. This implicitly defines the direction of digitization of the link.
TO_NODE	integer	Unique ID of the end node.
NAME1	string	Main name of the link. Usually this is the name given by the municipality which is also relevant for routing.
NAME2	string	Possibly existing further name of the link.
SPEEDCAR_T	integer	Average speed for vehicles in the digitization direction in km / h.
SPEEDCAR_B	integer	Average speed for vehicles against digitalization direction in km / h.
VMAX_CAR_T	integer	Maximum speed for vehicles in the digitization direction in km / h.
VMAX_CAR_B	integer	Maximum speed for vehicles against digitalization direction in km / h.
ACCESS_TOW	integer	Accessibility according to the bit mask in the digitization direction on the link.
ACCESS_BKW	integer	Accessibility according to the bit mask against digitization direction on the link.
LENGTH	float	Length of the link in meters.
FRC	integer	Functional street meaning.
LANES_TOW	integer	Number of lanes for flow traffic in the direction of digitization.
LANES_BKW	integer	Number of lanes for flow traffic against digitization direction.
FORMOFWAY	integer	Constructional form of the link.
MAXHEIGHT	float	Height restriction in meters.
MAXWIDTH	float	Width restriction in meters.
MAXPRESS	float	Tonnage restriction in tons.
ABUTTERCAR	integer	Driving ban for vehicles other than residents.
URBAN	integer	Indicates whether the link is ”urban” or ”extra urban”. This does not affect the STVO measure ”local area”, but is a general indication of whether a link is urban or outdoor.
WIDTH	float	Width of the road in meters. If there is no lane, -1.

TOLL	integer	Links with TOLL = 1 are toll roads or temporary toll roads.
BAUSTATUS	integer	Construction status of the link. Only links with status "active" (5) are relevant for routing.
SUBNET_ID	integer	Subnet of the link. Each link in the GIP is assigned to a subnet that identifies its organizational affiliation.
ONEWAY_CAR	integer	Redundant attribute, which characterizes the vehicle trafficability. -1 ban on driving0 one way against digitization direction1 one-way in the direction of digitization2 released on both sides
ONEWAY_BK	integer	Redundant attribute, which characterizes the wheel trafficability. -1 ban on driving0 one way against digitization direction1 one-way in the direction of digitization2 released on both sides
ONEWAY_BUS	integer	Redundant attribute, which identifies the bus trafficability .-1 ban on driving0 one way against digitization direction1 one-way in the direction of digitization2 released on both sides
EDGE_ID	long	Section ID of the GIP.
EDGECAT	string	Road category.
REGCODE	string	The regional code reflects the regional administrative assignment of the link.
SUSTAINER	string	Maintainer of the link.
DBCON	integer	Database connector (1) or not (0).

Table A.2: Overview about air quality indices (Ramos et al., 2018, p.5)

Index	**Pollutants Considered**	**Number of Categories**	**Ranges of Categories**	**Symbolisation**	**General Health Recommendations**
US EPA, AQI	CO, NO_2, O_3, PM2.5, PM10, SO_2	6	0-500	Colours	✓
Canada, AQHI	O_3, NO_2, PM2.5	4	1-10+	Colours	✓
Common Air Quality Index, CAQI	CO, NO_2, O_3, PM2.5, PM10, SO_2	5	0-100+	Colours	×
UK Defra, DAQI	NO_2, O_3, PM2.5, PM10, SO_2	4	1-10	Colours	✓
Irish EPA, AQIH	NO_2, O_3, PM2.5, PM10, SO_2	4	1-10	Colours	✓
Spain Madrid	CO, NO_2, O_3, PM10, SO_2	4	0->150	Colours	×
France, ATMO	NO_2, O_3, PM2.5, PM10, SO_2	3	1-10	Colours	×
Singapore, PSI	CO, NO_2, O_3, PM2.5, PM10, SO_2	5	0-500	Colours	✓
Cairncross et al. 2007, API	CO, NO_2, O_3, PM2.5, PM10, SO_2	4	1-10	Giraffe and Colours	✓
Stieb et al. 2008, AQHI	NO_2, O_3, PM2.5 or PM10	4	1-10+	Colours	✓
Kyrkilis et al. 2007, Aggregate AQI	CO, NO_2, O_3, PM10, SO_2	-	-	-	-
Sicard et al. 2011, ARI	NO_2, O_3, PM2.5, PM10, SO_2	4	0-10	Colours	✓
Murena 2004, PI	CO, NO_2, O_3, PM10, SO_2	5	0-100	Clouds	×